OXIDATIVE DAMAGE IN DNA:
AN EXPLORATION OF VARIOUS DNA STRUCTURES

A Thesis
Presented to
The Academic Faculty

By

Thabisile S. Ndlebe

In Partial Fulfillment
Of the Requirements for the Degree
Doctor of Philosophy in Chemistry

Georgia Institute of Technology

August, 2006

OXIDATIVE DAMAGE IN DNA:
AN EXPLORATION OF VARIOUS DNA STRUCTURES

Approved by:

Dr. Gary B. Schuster, Advisor
School of Chemistry and
Biochemistry
Georgia Institute of Technology

Dr. Donald Doyle
School of Chemistry and
Biochemistry
Georgia Institute of Technology

Dr. Nicholas Hud
School of Chemistry and
Biochemistry
Georgia Institute of Technology

Dr. Bridgette Barry
School of Chemistry and
Biochemistry
Georgia Institute of Technology

Dr. Roger Wartell
School of Biology
Georgia Institute of Technology

Date Approved: April 24, 2006

ACKNOWLEDGEMENTS:

My journey towards the completion of this degree has been anchored by the support of lots of great people along the way. It would not have been as worthwhile without their individual contributions. My advisor, Dr. Schuster, has been a wonderful guide through the whole process. His understanding through the most difficult parts of completing this goal has been instrumental to my success. My experience would not have been as enriching without the support of the members of my research group. This was especially true for the friendships I made with Edna Boone, Rochelle Bradford, Lezah Roberts, Marc Cao, Chiko Umeweni, and Gozde Guler. A lot of other friendships were added to my life during this brief period. They made Atlanta feel like a home rather than just a city I attended school in. In particular, Constance Mpofu, Sara Kravig, Monique Hite, Leonard Arthur, Susanna Moore and Ta-Tanisha Favor all made it a pleasure to live here. I am grateful for all these relationships and hope they can be sustained beyond this period of my life.

Prior to and even during the pursuit of my PhD degree, my family has always been my strongest support through everything. They made it possible to get to this point in my life by believing in me. My mother's constant encouragement and support have carried me through the toughest hurdles along the way. My brother has always been the wonderful reality check we all need in our lives. I am so grateful to have them in my life. The mere presence of certain

people in your life just makes it a life worth living. This is how I feel about my family.

All this would not have been possible without the Lord guiding me through my healing to a full recovery. This whole experience has strengthened my belief that all things are possible through Him.

TABLE OF CONTENTS

LIST OF TABLES:

LIST OF FIGURES

LIST OF SYMBOLS AND ABBREVIATIONS

A	Adenine
AQ	Anthraquinone
ATP	Adenosine triphosphate
Ba	Barium
BET	Back electron Transfer
C	Carbon
C	Cytosine
Ca	Calcium
CD	Circular Dichroism
Cl	Chlorine
Co	Cobalt
CPG	Controlled pore glass
CPM	Counts per minute
Cs	Cesium
CT DNA	Calf thymus DNA
Cy3	Indodicarbocyanine-3-1-o-(2-cyanoethyl)-(N,N-diisopropyl)-phosporamidite
dA	Deoxyadenosine
dATP	Deoxyadenosine triphosphate
dC	Deoxycytosine
dG	Deoxyguanine

dGTP	Deoxyguanine triphosphate
DMS	Dimethyl sulfate
DNA	Deoxyribonucleic acid
dsDNA	Double-stranded DNA
dT	deoxythymidine
EDTA	Ethylene Diamine Triacetic Acid
ESI	Electron spray ionization
EtBr	Ethidium Bromide
Fl	1-dimethoxytrityloxy-3-[O-(N-carboxy-(di-O-pivaloyl-fluorescein)-3-aminopropyl)]-propyl-2-O-succinoyl-long chain alkylamino-CPG
FRET	Fluorescence resonance energy transfer
G	Guanine
GG	Two consecutive guanine bases within a sequence
GGG	Three consecutive guanine bases within a sequence
H	Hydrogen
HPLC	High Pressure Liquid Chromatography
ISC	Intersystem crossing
K	Potassium
Li	Lithium
Mg	Magnesium
min	Minute
N	Nitrogen

Na	Sodium
NaCaco	Sodium cacodylate buffer
NH_4	Ammonium
Ni	Nickel
nm	Nanomole
NMM	N-methylmesoporphyrin
O	Oxygen
^oC	Degrees celsius
^oC/min	Degrees celsius per minute
P	Phosphate
PAGE	Polyacrylamide gel electrophoresis
PNK	Polynucleotide Kinase
Rb	Rubidium
RCF	Relative centrifugal force
RNA	Ribonucleic acid
SDS	Sodium dodecyl sulfate
Sr	Strontium
ssDNA	Single-stranded DNA
T	Thymine
TdT	Terminal deoxynucleotidyl transferase
Tel01	N,N'-Bis(3-(4-morpholino)propyl)-3,4,9,10–perylenetetracarboxylic acid diimide
T_m	Melting temperature

TTF-TCNQ	Tetrathiofulvalene-tetracyanoquinodimethane
u	micro
UV	Ultra violet
UV-Vis	Ultraviolet visible spectroscopy
V	Vanadium
Zn	Zinc
α	Alpha
γ	Gamma
μ	micro
μL	Microlitre
μm	Micromole

SUMMARY:

Research efforts to determine the causes, effects and locations of mutations within the human genome have been widely pursued due to their role in the development of various diseases. The main cause of mutations *in vivo* is oxidative damage to DNA via oxidants and free radical species. Numerous studies have been performed *in vitro* to determine how oxidative damage is induced in DNA. Most of these *in vitro* studies require photosensitizers to initiate the oxidative damage through various mechanisms. For the purposes of this research, all the photosensitizers that were used initiated oxidative damage in DNA through the electron transfer mechanism. In the charge transport studies, an anthraquinone photosensitizer was covalently linked to the 5‘ end of DNA by a short carbon tether in order to determine the pattern of damage induced along the length of the DNA. Anthraquinone preferentially damages guanine bases. Our first work sought to determine the effects of charge transport through guanine rich quadruplex DNA dimers. The dimers were formed by the combination of two hairpins with duplex overhangs extending beyond the quadruplex region. This enabled the optimal comparison of the effects of charge transport between duplex and quadruplex DNA structures. Another area of research we pursued in this area was to determine the effects of charge transport in M-DNA (a novel DNA conformation that was reported to form in the presence of zinc ions at a pH above 8). Earlier work on M-DNA suggested that it behaved like a “molecular wire.” Our research attempted to determine the effects of charge transport on this

structure in order to show the behavior of a DNA "molecular wire" as compared to the standard studies performed in this area on normal B-DNA structures. Lastly, in collaboration with Dr. Ramaiah and colleagues we designed some viologen linked acridine photosensitizers which were tested for any ability to cleave GGG bulges. In preliminary studies, these viologen linked acridine derivatives showed preferential cleavage for guanine bases. They were not covalently bound to DNA, although they could potentially form non covalent interactions with DNA such as intercalation and/or groove binding. Our overall research goal was to determine the extent and overall effect of oxidative damage (using different photosensitizers) on the various DNA structures mentioned above.

CHAPTER 1: INTRODUCTION

1.1 General Overview of Deoxyribonucleic Acid (DNA)

1.1.1 DNA Function and Significance

Nucleic acids are the main chemical constituents found in the cell nucleus [1]. They comprise of two main classes; ribonucleic acids (RNA) and deoxyribonucleic acids (DNA). Nucleic acids are the physical agents that store and transmit information in living organisms [1]. This information ensures the normal development and functioning of an organism [2]. Significantly, DNA molecules are responsible for the uninterrupted passage of genetic information between cell generations.

1.1.2 DNA Structure

The structure of DNA plays an essential role in DNA's ability to store and transmit genetic information. This information is encoded in the sequence of their monomeric units (*nucleotides*) [3]. The helical structure of DNA packages the monomeric units in a manner that optimally insulates them from damage [4]. These units (called *nucleotides*) are comprised of the following parts: *bases, deoxyribose sugars* and *phosphodiester bonds*. Nucleotides combine together to form DNA strands, and complementary strands of DNA bind together to form a *double stranded helix* (DNA duplex). The integrity of the genetic information is maintained within this DNA structure [5]. This genetic information is converted via several processes (transcription and translation) into various structural, regulatory

and functional components *in vivo* [1]. Consequently, understanding the factors that influence the structure of DNA is significant for understanding the processes that compromise this information such as through DNA damage.

1.1.2.1 ***Primary Structure***

The primary structure of DNA consists of bases, deoxyribose sugars and phosphodiester.

Bases:

Bases are aromatic rings that serve as the primary informational elements in DNA. There are four natural bases in DNA; adenine, guanine, thymine and cytosine. These bases fall under two main groups; purines and pyrimidines [4].

A purine ring contains a six membered ring fused to a 5 membered ring with two nitrogen atoms in each respective ring (note numbering in Figure 1). The two common purine derivatives found in DNA are adenine and guanine (Figure 1). Adenine contains an amino group at the C6 position of the purine ring, while guanine contains an amino group at the C2 position and a carbonyl group at the C6 position [6].

On the other hand, a pyrimidine ring contains a six membered aromatic ring with two nitrogen atoms (note numbering in Figure 1). The two pyrimidine derivatives commonly found in DNA are cytosine and thymine (Figure 1). Cytosine contains an amino group at C4 and a hydrogen atom at the C5 position. Thymine contains carbonyl groups at C2 and C4, as well as a methyl group at C5 [6].

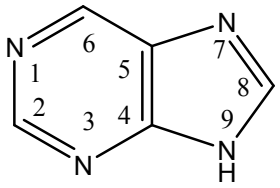

Purine

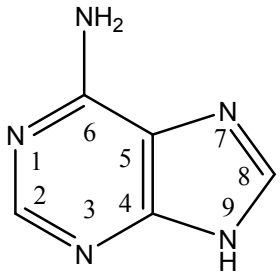

Adenine
(A)

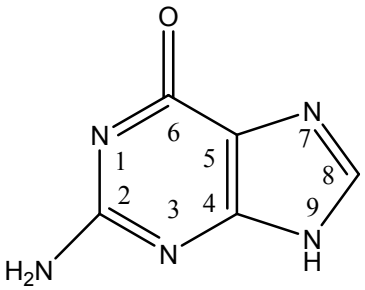

Guanine
(G)

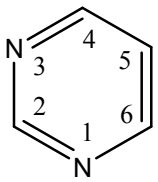

Pyrimidine

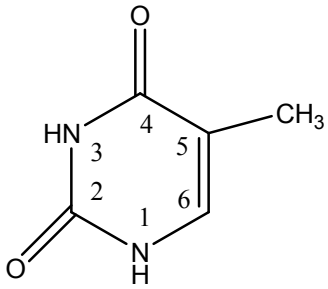

Thymine
(T)

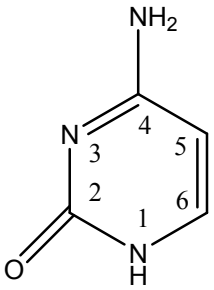

Cytosine
(C)

Figure 1: Structure of Pyrimidines and Purines

Sugars

Deoxyribose sugar molecules found in DNA are derivatives of cyclopentane groups (see Figure 2). Cyclopentane is a very flexible molecule that exists in various conformations. In order to conform to the tetrahedral arrangement of each carbon molecule, four out of the five carbons remain in the same plane while the last carbon puckers up or down in space. Likewise, the deoxyribose sugar is flexible and forms similar conformations. The conformation with a sugar pucker on the same side of the plane as the base and the C5' (see Figure 2) is commonly referred to as an endo conformation, while the conformation with the sugar pucker on the opposite side of the plane is referred to as an exo conformation. The C2' endo conformation commonly forms in DNA under normal conditions. This involves the oxygen molecule and 3 carbon molecules in the same plane while C2' carbon puckers out of the plane (see Figure 2). The exo conformation has not been found in DNA [6].

Phosphodiester Bond

Phosphodiester bonds attach the monomeric units (nucleotides) of DNA together. The nucleotides are attached together at either the 3' OH of the sugar or the 5' PO_4 group of the sugar (or at both ends). The formation of these bonds is thermodynamically favorable as they occur with the release of pyrophosphate from a triphosphate bearing nucleotide such as deoxyadenosine 5' triphosphate (see Figure 3). Due to this potential energy in the pyrophosphate bond, deoxyadenosine 5' triphosphate (dATP) and deoxyguanine 5' triphosphate (dGTP) are common energy carriers in the cell [7].

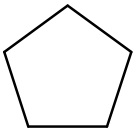

Cyclopentane

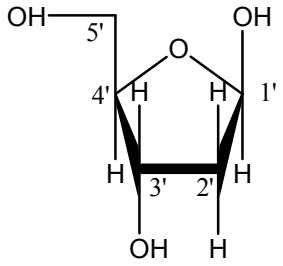

Deoxyribose

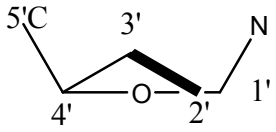

3′ Endo

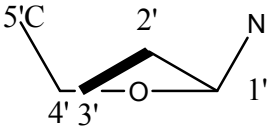

2′ Endo

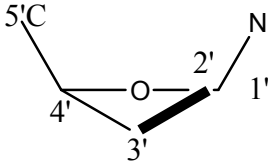

3′ Exo

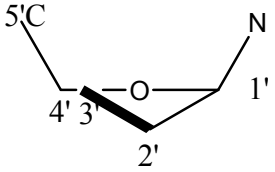

2′ Exo

Figure 2: Structure of Deoxyribose sugar and Sugar Puckers

1.1.2.2 ***Secondary Structure***

The secondary structure of DNA comprises of nucleosides and nucleotides. These are the building blocks of DNA structure.

Nucleosides

Nucleosides are made up of a deoxyribose sugar and a base (Figure 3). They are covalently bound by a glycosyl bond at the C1' of the sugar and the N9 or N1 of purines or pyrimidines respectively. Rotations about this glycosidic linkage add structural diversity to the DNA molecule. The two main conformations that are formed about the glycosyl bond are either anti or syn. The anti conformation is formed when the bulk of the base is rotated away from the sugar. This occurs when the C1'- O4' bond of the sugar is trans to the N9 – C4 bond of the purine base. In pyrimidines, the anti conformation is formed when the C2 carbonyl faces away from the sugar. This occurs when the C1' – O4' bond is trans to the N1-C2 pyrimidine bond [6].

The syn conformation is formed when the C1'-O4' bond is cis to the N9 – C4 purine bond, and cis to the N1-C2 pyrimidine. This occurs when the bulk of the purine base is facing towards the sugar or the C2 carbonyl is on top of the sugar ring [3].

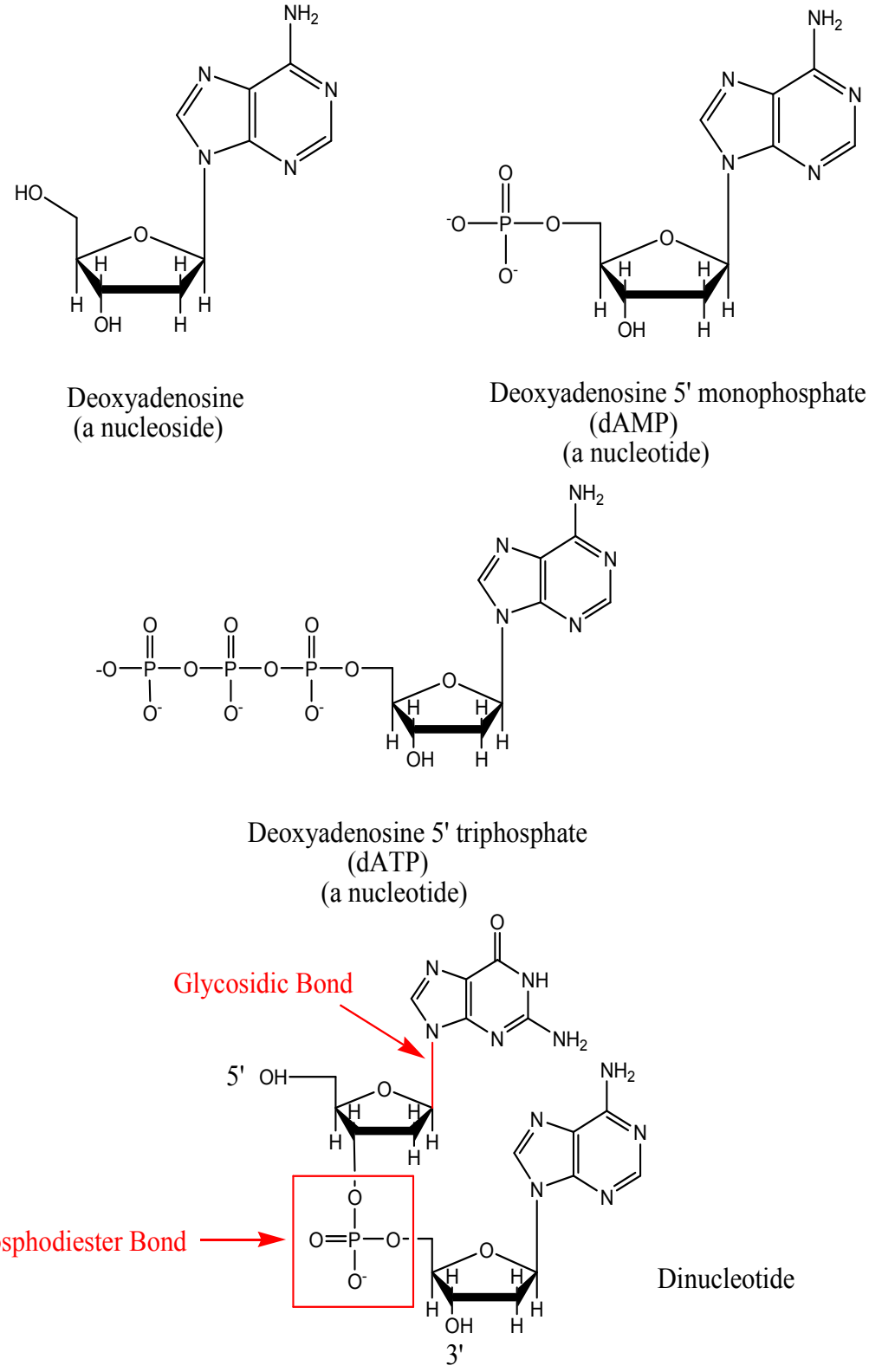

Figure 3: Structure of Nucleosides and Nucleotides

Nucleotides

As mentioned earlier, nucleotides are comprised of a deoxyribose sugar, a base and a phosphate group. The phosphate group is attached to the sugar at either the 5' end or 3' end of the sugar. This attachment lends directionality to DNA. The DNA sequence is usually read from the 5' to 3'direction (unless otherwise stated). The 5' end commonly has a phosphate group attached to it while the 3' end contains just the sugar hydroxyl. Therefore, by convention the monomeric unit of DNA contains a 5' phosphate group followed by a deoxyribose sugar with a base attached at the glycosidic bond (Figure 3) [1].

There are four naturally occurring nucleotides, namely deoxyadenosine triphosphate, deoxythymidine triphosphate, deoxyguanine triphosphate and deoxycytidine triphosphate [4]. These nucleotides are connected by phosphodiester linkages to form single-stranded DNA. The phosphodiester bond is formed by the 5' phosphate of one nucleotide attaching to the 3' hydroxyl of the next nucleotide. Oligonucleotides comprise of less than 30 deoxynucleotides, and polynucleotides contain 30 deoxynucleotides or more. A sugar-phosphate backbone is formed in the DNA polymer through the following repeat unit along the polymer: 5'P-C5'-C4'-C3'-3'O [6].

The molecules in a polynucleotide could rotate about the sugar-phosphate backbone forming numerous conformations. The combination of this rotational freedom as well as the freedom found in both the sugar ring and the glycosidic bond creates a very flexible DNA polymer. This flexibility is relatively harnessed

by fusing two single-stranded DNA (ssDNA) molecules together to form a double-stranded helix (dsDNA) [5].

1.1.2.3 ***Tertiary Structure***

Base pairs

The 4 bases found in DNA form non-covalent bond couplings called base pairs. The natural base pairs involve adenine base pairing to thymine (Figure 4a), and guanine to cytosine (Figure 4b). The base pairs are held together by hydrogen bonds. These are short, non-covalent interactions between covalently bound hydrogen atoms and negatively charged acceptor atoms such as carbonyl oxygen atoms or the lone pair electrons of nitrogen atoms [3]. Hydrogen bonds are relatively weak (3-7 kcal/mole in 2.6-3.1 angstrom range of interaction), compared to covalent bonds (80-100 kcal/mol, within same range) [4]. Adenine and thymine (A:T) base pairs are held together by two hydrogen bonds (as shown in Figure 4a), whereas guanine and cytosine (G:C) base pairs are held by 3 hydrogen bonds (see Figure 4b). As a result, G:C base pairs are stronger than A:T base pairs. The base pairing pattern shown in Figure 4 is called Watson-Crick base pairing. This pattern is the most common base pairing pattern found in DNA. It involves base pairing between the C2-N3-C4 pyrimidine face and the C2-N1-C6 purine face (see Figure 4a and 4b) [3].

Hoogsteen Base pairs

Although Watson-Crick base pairing is more commonly found in DNA, Hoogsteen base pairing has been observed in several DNA structures such as parallel, triplex and quadruplex DNA structures. Hoogsteen base pairing involves

Watson-Crick Base pairing:

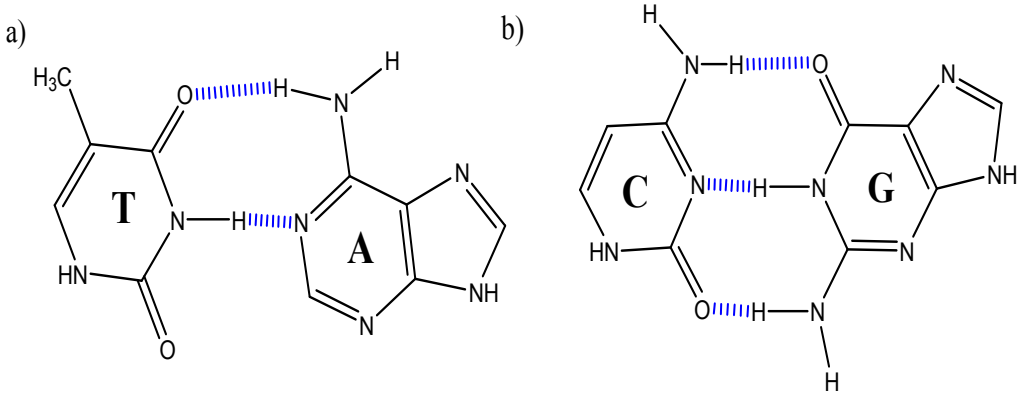

AT Base pair

GC Base pair

Hoogsteen Base pairing:

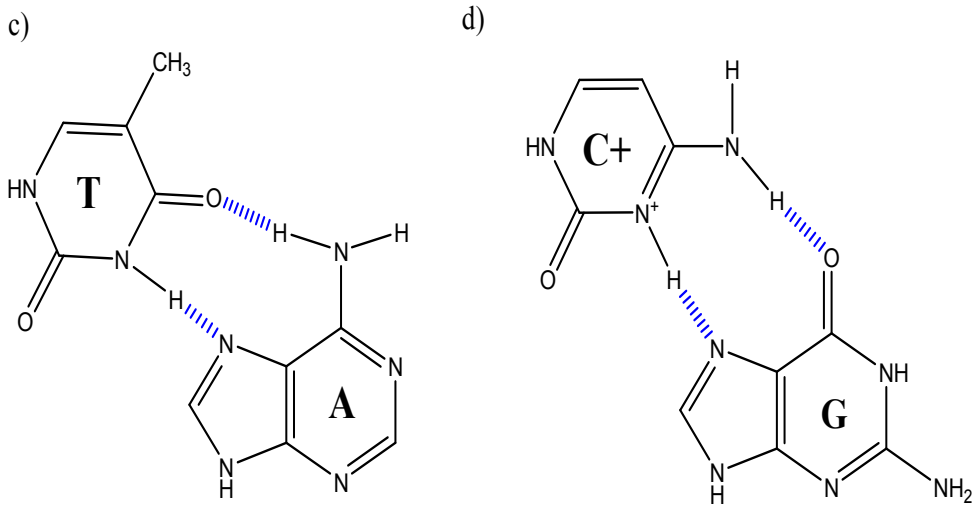

AT Base pair

GC^{+} Base pair

Figure 4: Watson-Crick base pairing (a & b) and Hoogsteen base pairing(c &d)

the N7-C5-C6 purine face pairing with the Watson-Crick C2-N3-C4 pyrimidine face (Figure 4c and 4d). Hoogsteen base pairing alters the normal base pairing pattern by base pairing through the N7 position [6].

Double stranded DNA

In order to protect the genetic information found in DNA bases from chemical modification, DNA usually assumes a double stranded helix structure. The bases are packed within the center of the helix with a sugar-phosphate back bone wrapping around them. They are held in place within the helix by hydrogen bonds that are formed between bases from complementary strands. The two strands are anti-parallel, that is, one strand is oriented in the 5' – 3' direction while the other strand is oriented in the 3' - 5' direction. This enables the complementary bases on each strand to optimally base pair. The DNA double helix has major and minor grooves within its edges due to the orientation of these base pairs [4].

The double stranded DNA helix (DNA duplex) is stabilized and held together by several different forces. Firstly, hydrogen bonding between the bases on the complementary strands stabilizes the DNA duplex. Secondly, the aromatic bases within the center of the helix further stabilize the duplex through hydrophobic interactions between the aromatic rings in adjacent bases. Thirdly, metal cations surround the negatively charged phosphate groups in the sugar-phosphate backbone adding more stability to the DNA duplex. Lastly, water molecules cooperatively bind along the major and minor groove of the DNA

adding further stability to the duplex structure. Ultimately, these relatively weak forces together form a very stable DNA helix [6].

1.1.3 **DNA Conformations**

DNA duplex structure assumes a number of different conformations namely B form, A form, Z form and other forms of DNA (see Table 1).

Table 1: Properties of various DNA conformations[4]

Parameters	B-DNA	A-DNA	Z-DNA
Helical handedness	Right	Right	Left
Residues per helical turn	10.5	11	12
Distance between base pairs (angstroms)	3.4	2.55	3.7
Rise per helical turn (angstroms)	34	28	45
Rotation per residue (degrees)	36	32.7	-30
Glycosidic bond configuration	Anti	Anti	Anti and syn
Sugar Pucker	C2' endo	C3' endo	C2' and C3' endo

1.1.3.1 ***B form DNA***

B-form DNA is the most common DNA conformation. It contains a right handed helix with both bases held within the center of the duplex, and the

phosphate backbone in the periphery. The base pairs in B form DNA (B-DNA) are relatively flat, perpendicular to the helical axis, and approximately 3.4 angstroms apart. B form DNA has 10 base pairs per helical turn which extend over approximately 34 angstroms. Its glycosidic bonds form anti conformations, while its sugar puckers form C2' endo conformations. B DNA has narrow, deep minor grooves, and wide major grooves. The bases within the groove edges are accessible from the outside of DNA, which facilitates sequence specific recognition by DNA binding proteins [2].

1.1.3.2 ***A form DNA***

A form DNA (A-DNA) is shorter and stubbier than B DNA. It is formed either under low humidity conditions or under high humidity conditions in GC rich sequences. Each helical turn in A-DNA has about 11 base pairs (28 angstroms). Its adjacent base pairs are rotated by 32.7 degrees, and are 2.55 angstroms apart. They form a slanted angle with the helical axis. The glycosidic bond of A-DNA forms the anti conformation, while its sugar puckers favor the C3' endo conformation. A-DNA has very deep, narrow major grooves, and wide, shallow minor grooves. The deep major groove pushes bases toward the edge creating an empty core [3-5].

1.1.3.3 ***Z form DNA***

Z form DNA (Z-DNA) is a tall, thin left handed helix. It is formed by poly(dG-dC).poly(dG-dC) chains under high salt conditions. It is also formed by poly(purine-pyrimidine).poly(purine-pyrimidine) chains under physiological conditions. Z-DNA has 12 base pairs per helical turn (45 angstroms long). The

distance between adjacent base pairs is approximately 3.7 angstroms. Base pairs in Z-DNA are rotated 30 degrees in the opposite direction from each other. Also, purines form the syn conformation, while pyrimidines are in anti conformation. Z-DNA forms both C3' and C2' endo sugar puckers. As a result of the alternating C2' endo conformation in pyrimidines and the C3' endo conformation in purines, the Z-DNA sugar phosphate backbone forms a zigzag patterns. Z-DNA has deep minor grooves, and a bulged convex surface for the major groove [3-6].

1.1.3.4 ***Other forms***

Various conformations of DNA are formed under specialized conditions. D-DNA is formed by poly(dA).poly(dT) runs under the least hydrated conditions. It contains 8.5 base pairs per helical turn. C-DNA forms in fibers at 57-66% humidity. It contains 9.3 bases per helical turn. T-DNA is formed from cytosine residues with a hydroxyl methyl group on the C5. It is found in bacteriophages, and contains an 8 base pair repeat [4].

1.1.4 **Other DNA Structures**

1.1.4.1 ***Triplex DNA***

Triplex DNA is formed by laying a third strand within the major groove of DNA. This strand forms Hoogsteen base pairing with the non-Watson-Crick face of the duplex. The central strand in triplex DNA must be a purine-rich strand which bonds through both of its hydrogen bonding faces (see Figure 5). Triplex formation also requires a homopurine.homopyrimidine region in order to provide a purine central strand [4, 6].

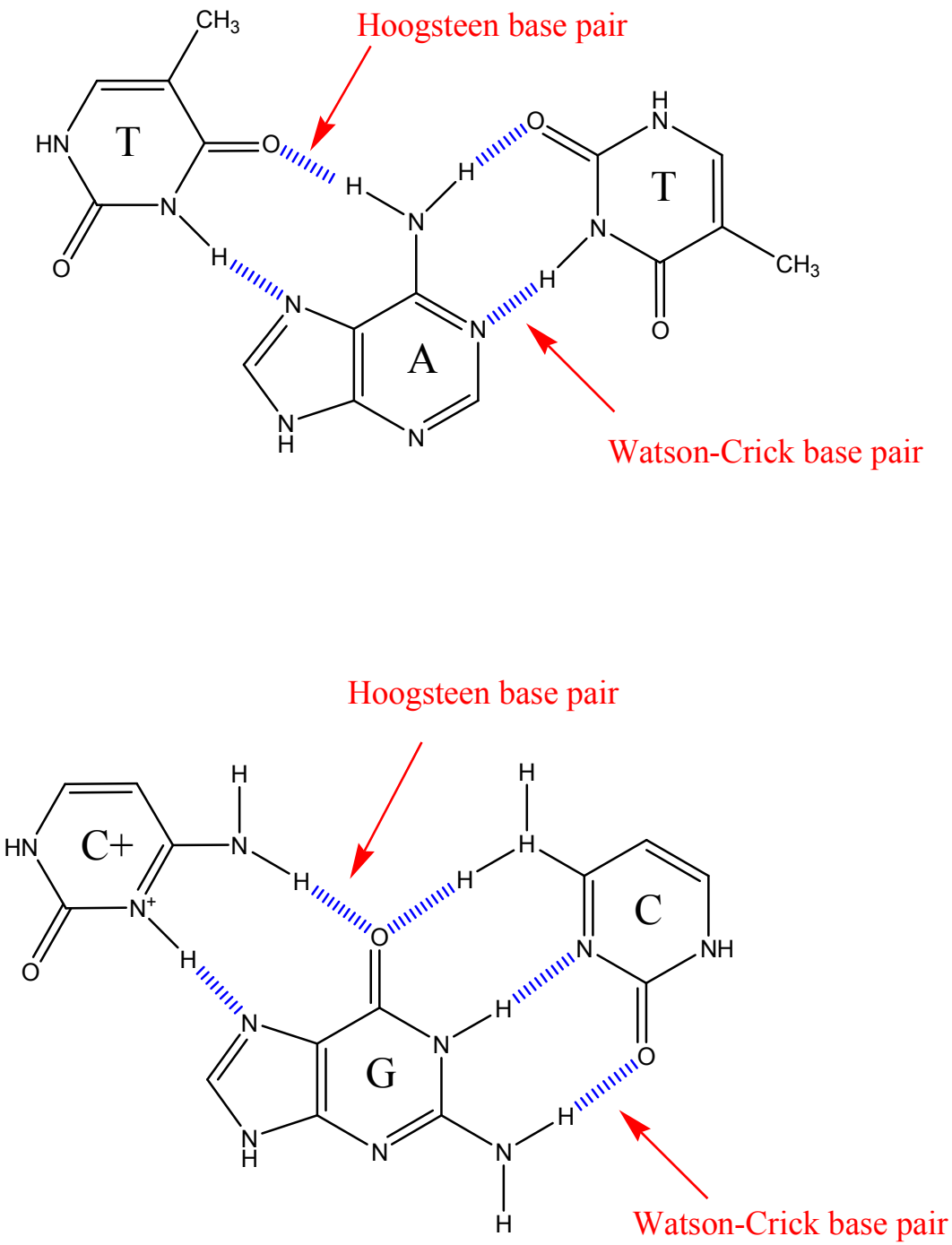

Figure 5: Triplex DNA base pairing

1.1.4.2 ***Quadruplex DNA***

G-quartets are planar structures formed by the hydrogen bonding of four guanine bases through Watson-Crick base pairing as well as Hoogsteen base pairing (Figure 6). Under the right conditions, these G-quartets stack together to form quadruplex DNA. The right conditions for quaduplex DNA formation require guanine rich sequences and high salt concentrations. Metal cations stabilize the quadruplex structure by neutralizing the repulsion between negatively charged phosphate groups in the sugar phosphate backbone of the strand. This enables the g-quartet stacks to get close enough to form quadruplex DNA. Quaduplex DNA can be formed by one strand, two strands or four strands of DNA under the appropriate conditions [3-6].

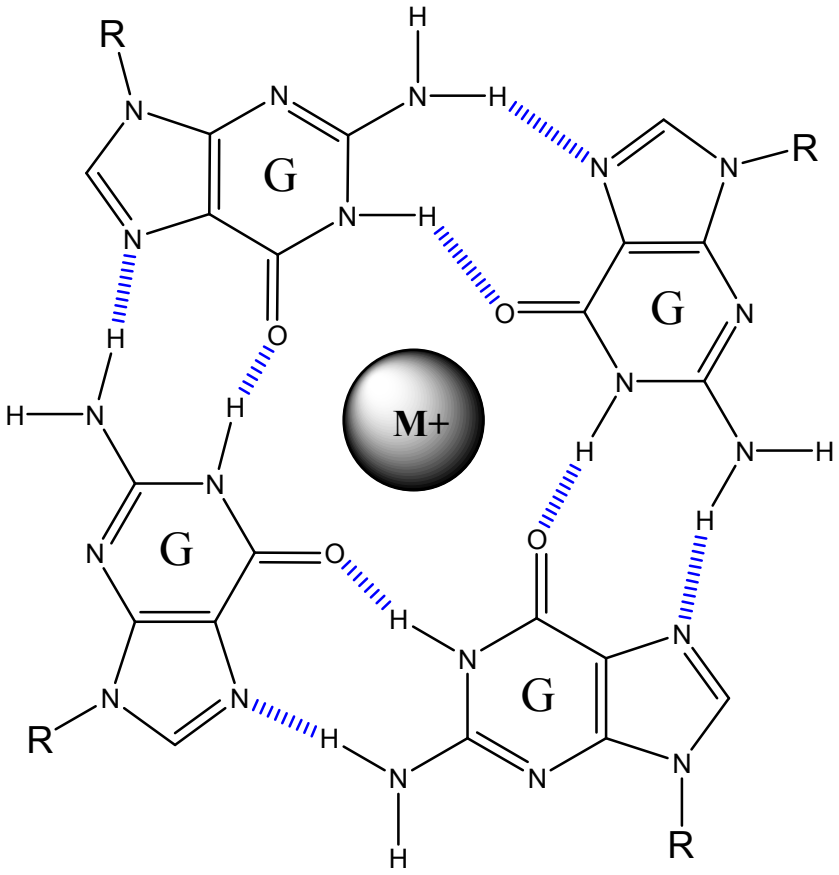

G quartet

* M+ - metal cation

Figure 6: G quartet base pairing

1.1.5 **Chemical Probes for DNA**

Although DNA is a relatively stable molecule, it is still susceptible to chemical damage. Carcinogens and mutagens react with individual bases resulting in chemical modifications that could lead to mutations. Some of these carcinogens and mutagens target very specific elements in DNA such as specific bases and sugars. This specificity is very desirable for chemical probes for DNA.

These probes can serve as research tools to investigate specific features in DNA. The following chemicals are commonly used as chemical probes in nucleic acid research.

1.1.5.1 ***Hydrazine***

Hydrazine is a highly reactive nucleophile that probes for thymine and cytosine residues in DNA. For thymine residues, it reacts with the C4 and C6 atoms resulting in the formation of a pyrazole derivative. Under high salt conditions, it displaces the C4 amino group in cytosine to form N4 aminocytosine (see Figure 7) [4].

1.1.5.2 ***Osmium Tetroxide***

Osmium tetroxide is commonly used as a chemical probe for single stranded regions containing thymine residues (see Figure 7). It reacts strongly with thymine by binding to its double bond forming osmate ester bonds. It also binds to a lesser degree with cytosine residues [4].

1.1.5.3 ***Dimethyl sulfate (DMS)***

Dimethyl sulfate is often used as a chemical probe for guanine residues (see Figure 7). It methylates the N7 position of guanine. DMS is able to penetrate the major groove of double stranded DNA to access the N7 position of guanine. It is commonly used in footprinting experiments to determine where proteins are bound to DNA [4].

Hydrazine

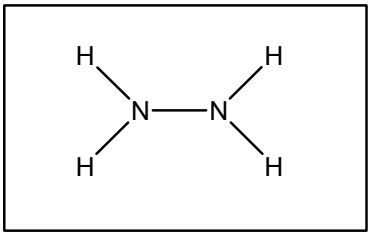

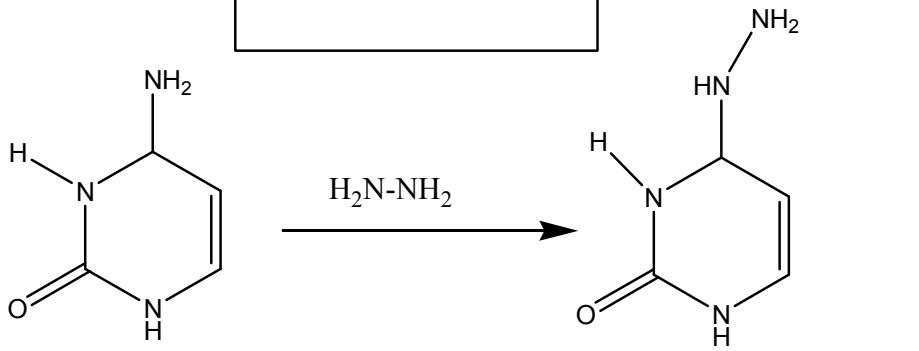

Cytidine

N4 Aminocytidine

Osmium Tetroxide

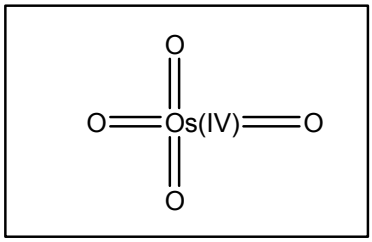

Dimethyl Sulfate

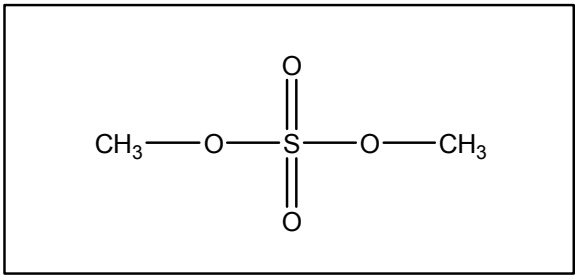

Figure 7: Chemical Probes for DNA

1.2 Introduction to Charge Transport in DNA

The main function of DNA is to store and transmit genetic information [1-7]. Therefore, maintaining the integrity of DNA is essential for its function. There has been a lot of interest in understanding the mechanisms that compromise the chemical integrity of DNA through the damage of its chemical constituents [8-17]. These modifications to DNA could possibly lead to mutations which could have severe consequences on the organism [3, 4]. The major source of mutations *in vivo* is oxidative damage [14]. Numerous studies have been performed to determine how oxidative damage is induced in DNA [13-17]. These studies have been performed using various photosensitizers to initiate oxidative damage by the following three processes, namely, *hydrogen abstraction*, *singlet oxygen generation* and *electron transfer*.

1.2.1 Hydrogen Abstraction

Hydrogen abstraction is the process where irradiation of a photosensitizer in the presence of a hydrogen donating substrate leads to the removal of the hydrogen from the donating substrate to the excited photosensitizer [18]. The immediate result of this is the formation of a radical pair. In DNA, the deoxyribose sugar moiety often behaves as the hydrogen donating substrate as it has multiple hydrogen donating sites [13]. The sugar radicals formed often rearrange, and ultimately lead to strand cleavage of DNA [14]. Hydrogen abstraction, in DNA, is generally a non-selective process due to the presence of deoxyribose sugars all along its backbone [13]. Some examples of photosensitizers

that cleave DNA through hydrogen abstraction are photoactive rhodium (III) complexes [19], cationic metal porphyrins [20], and activated bleomycin [21].

1.2.2 **Singlet Oxygen Generation**

Singlet oxygen is the lowest excited state of molecular oxygen. It is highly reactive [13]. Singlet oxygen generation often occurs by energy transfer from an excited photosensitizer to ground state molecular oxygen [15]. The excited photosensitizer should have high enough triplet energy to generate singlet oxygen [13]. It preferentially modifies guanine (G) residues in DNA [22]. Singlet oxygen induces DNA damage that is either alkali labile (require further treatment in alkali conditions to be detected), or piperidine labile (require piperidine treatment to be detected), or even frank breaks (do not require further treatment to be detected) [23]. Some photosensitizers that have been found to induce oxidative damage through singlet oxygen generation are Ruthenium (III) complexes [24], porphyrins [25], and Vanadium (V) complexes [26].

1.2.3 **Electron Transfer Agents**

The transfer of an electron from one molecular entity to another is known as electron transfer. In DNA, a base donates an electron to an excited photosensitizer producing a radical cation on the base and a radical anion on the photosensitizer. Electron transfer is dependent on the reduction potential, and excited state energy of the photosensitizer, and the oxidation potential of the base [15]. Guanine has the lowest oxidation potential of the four bases [16, 28]. As a result, guanine residues often undergo the most oxidative damage. For the electron transfer process, the amount of DNA cleavage at guanine residues is highly

dependent on the sequences that flank the guanine base [16]. Both singlet oxygen and electron transfer processes exhibit selective cleavage at GG steps along the length of the DNA strand [13]. There is predominantly more DNA cleavage at guanines that are located 5' to another guanine than at any other locations in electron transfer products. This 5' G selectivity is often used to distinguish between electron transfer and singlet oxygen cleavage products. This selective GG step cleavage often varies along the DNA strand. Some examples of photosensitizers that induce oxidative damage through electron transfer are riboflavin [28] and anthraquinones [8].

For the purpose of this work, our primary focus will be on *anthraquinone* as the photosensitizer for oxidative damage in DNA through the electron transfer mechanism. It will be the sole photosensitizer used in all our charge transfer experiments throughout this work.

1.2.3.1 ***Antraquinone***

Several anthraquinone (AQ) derivatives have been developed by the Schuster group for the study of oxidative damage in DNA (see Figure 8) [9]. Although AQ can undergo both hydrogen abstraction and electron transfer, the Schuster group has shown that oxidative damage in DNA proceeds primarily through the electron transfer process [9]. Upon irradiation, the AQ is excited to the singlet state followed by electron transfer from a base to the excited singlet AQ. The radical pair formed undergoes rapid back electron transfer which reforms the starting materials (Figure 9) [13]. The excited singlet AQ also undergoes intersystem crossing (ISC) to the excited triplet AQ. The excited triplet AQ then

oxidizes a base forming a triplet radical ion pair which cannot undergo back electron transfer (BET). This gives the radical ion pair a long enough lifetime to engage in further reactions [9]. The radical AQ anion reacts with molecular oxygen to regenerates AQ and form superoxide. The base radical cation is ultimately trapped by water molecules, leading to DNA damage at these sites [13]. Prior to this, the radical cation migrates through the DNA forming various cleavage products along the DNA. This long range migration of charge through DNA has been studied extensively to determine its mechanism [9-12].

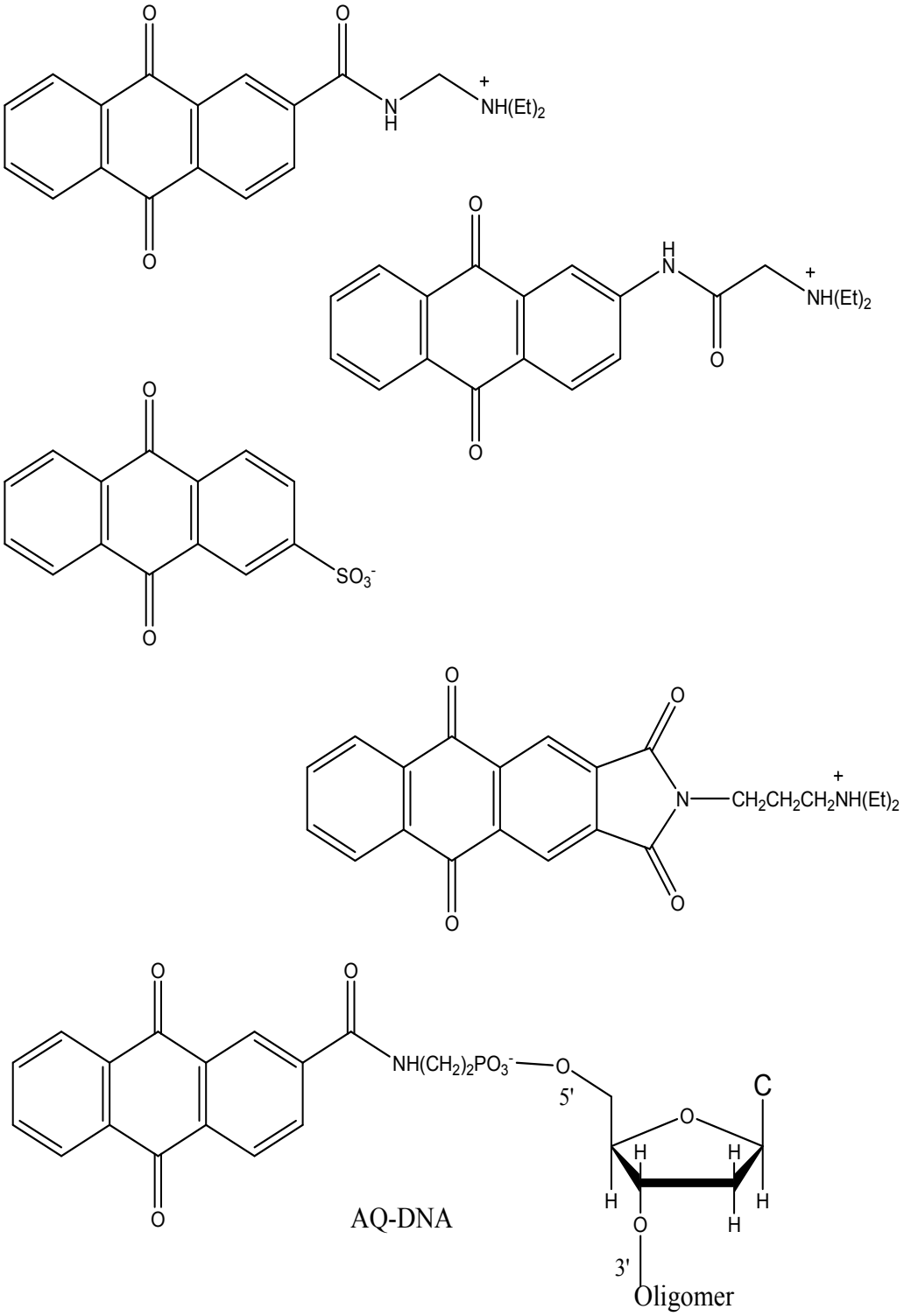

Figure 8: Anthraquinone Derivatives

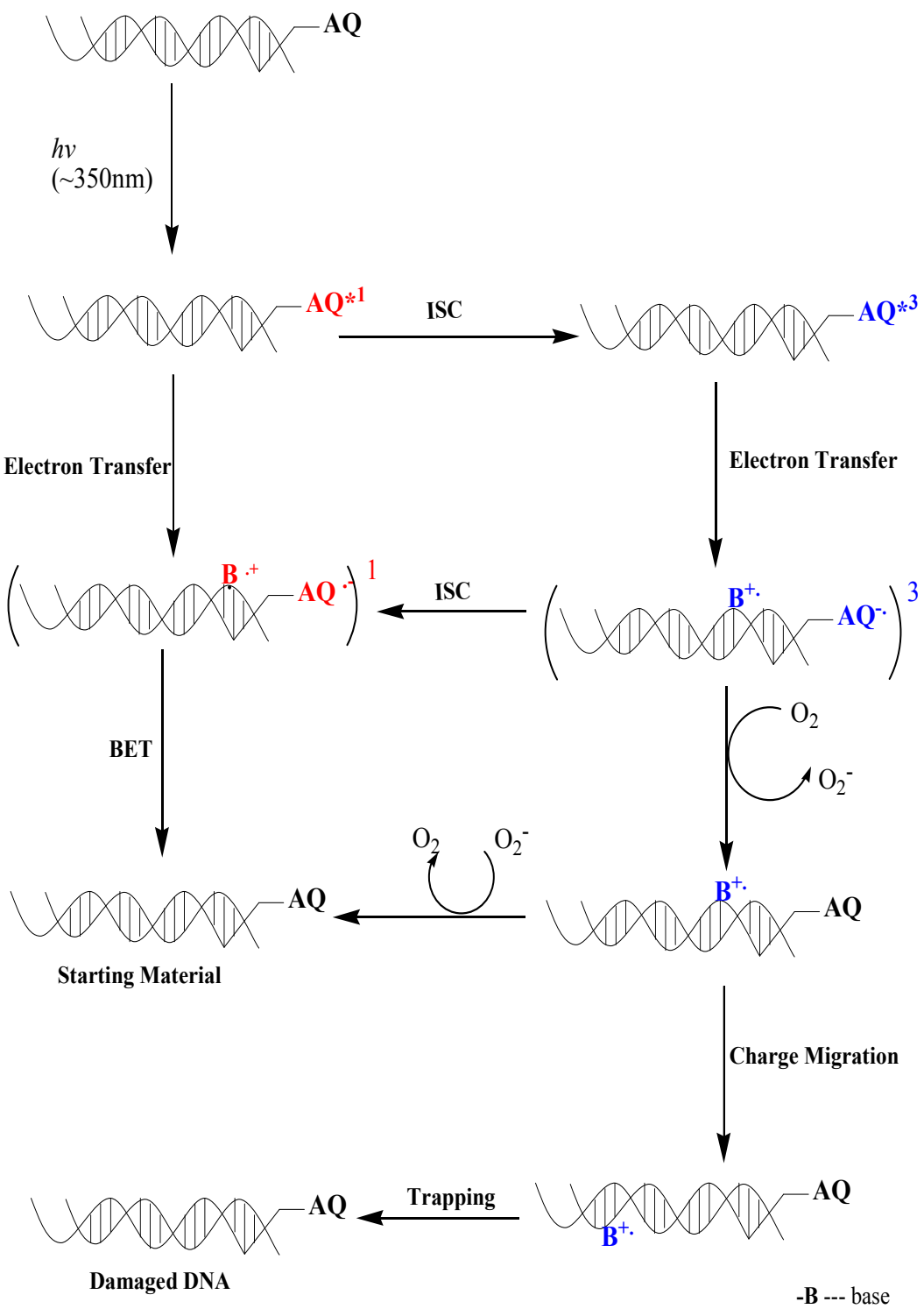

Figure 9: Electron Transfer Mechanism for AQ

1.2.4 **Long Distance Charge Migration**

A vast amount of research has been performed to determine the mechanism of long distance charge migration [9-12]. These studies found that charge migrates through a hopping mechanism as opposed to the previously proposed tunneling mechanism [29]. One of the hopping mechanisms proposed suggests that when charge is injected into DNA it is stabilized by delocalization over several bases [9]. This charge delocalization structurally distorts the DNA in order to accommodate the charge. The distortion migrates along with the charge over long stretches of DNA. The migration of the structural distortion (polaron) of DNA is enabled by thermal motions (phonon) which cause the polaron to hop over one or more bases along the DNA. This mechanism was referred to as the phonon assisted polaron hopping mechanism [9, 30]. Some other proposed hopping mechanisms were the conformation gated hopping mechanism [31], the hole resting model [32-34], and the A/G hopping mechanism [11, 35].

The observation of long distance charge migration in DNA and reports of DNA as an efficient conductor led to interest in the potential application of DNA as a quantum wire [36, 37]. The extent of DNA's ability as a conductor is still widely debated as some other studies have shown that DNA exhibits properties that are more insulator-like than conductor-like [37-42].

Due to its self annealing capability, the potential implications of DNA as a self organizing microelectronic device continue to spur interest in its conducting capability [36].

References

1. Bresler, S. E., *Introduction to Molecular Biology*, Academic Press, 1971

2. Branden, C., Tooze, J., *Introduction to Protein Structure,* 2nd Ed., Garland Publishing, 1999

3. Voet, D., Voet, J.G., *Biochemistry*, 2nd Ed., John Wiley & Sons, Inc., 1995

4. Sinden, R. R., *DNA Structure and Function*, Academic Press, 1994

5. Campbell, M. K., *Biochemistry*, 2nd Ed., Saunders College Publishers, 1995

6. Sarma, M. H.; Sarma, R. H., *DNA Double Helix and The Chemistry of Cancer*, Academic Press, 1988

7. Stryer, L., *Biochemistry*, 4th Ed., Freeman & Co., 1995

8. Breslin, D. T., Schuster, G. B., *J. Am. Chem. Soc*. **1996**, 118, 2311

9. Schuster, G. B., *Acc. Chem. Res*. **2000**, 33, 253-260

10. Nunez, M. E., Hall, D. B., Barton, J. K., *Chem. Biol*. **1999**, 6, 85-97

11. Giese, B., *Acc. Chem. Res*. **2000**, 33, 631-636

12. Lewis, F.D., Letsinger, R. L., Wasielewski, M. R., *Acc. Chem. Res*. **2001**, 34, 159-170

13. Armitage, B., *Chem. Rev.* **1998,** *98,* 1171-1200

14. Pogozelski, W. K., Tullius, T. D., *Chem. Rev*. **1998**, 98, 1089-1107

15. Kochevar, I., Dunn, D. A., *Biorg. Photochem*. **1990**, 1, 273-315

16. Burrows, C. J., Muller, J. G., *Chem. Rev.* **1998**, 98, 1109-1151

17. Paillous, N, Vincendo, P. J., *J. Photochem. Photobiol. B* **1993**, 20, 203-209

18. Turro, N. J., *Modern Molecular Photochemistry,* Benjamin/Cummings Publication Co., Inc.,California, 1978

19. Chow, C. S., Barton, J. K., *Methods Enzymol*. **1992**, 212, 219-242

20. Pratviel, G., Pitie, M., Bernadou, J, Meunier, B., *Angew. Chem. Int. Ed. Engl.* **1991**, 30, 702-704

21. Burger, R. M., *Chem. Rev.* **1998**, 98, 1153-1170

22. Lee, C. C., Rodgers, M. A., *Photochem. Photobiol*. **1987**, 45, 79-86

23. Blazek, E. R., Peak, M. J., *Photochem. Photobiol.* **1988**, 47S, 33S

24. Mei, H., Barton, J. K., *Proc. Natl. Acad. Sci. U.S.A*. **1988**, 85, 1339-1343

25. Croke, D. T., Perrouault, L., Sari, M. A., Battioni, J. P., Mansuy, D., Helene, C., Le Doan, T., *J. Photochem. Photobiol.B* **1993**, 18, 41-50

26. Hiort, C., Goodisman, J., Dabriowiak, J. C., *Biochemistry* 1996, 35, 12354-12362

27. Steenkan, S., Javanovic, S.V., *J. Am. Chem. Soc.* **1997**, 119, 617-618

28. Ito, K., Inoue, S., Yamamoto, K., Kawanishi, S., *J. Biol. Chem*. **1993**, 268, 13221-13227

29. Turro, N. J.; Barton, J. K. *Biol. Inorg. Chem.* **1998**, 3, 201-209

30. Liu, C-S; Hernandez, R.; Schuster, G. B. *J. Am. Chem. Soc.* **2004,** 126, 2877-2884

31. O'Neill, M. A., Barton, J. K., *J. Am. Chem. Soc*. **2004**, *126,* 11471-11483

32. Jortner, J. Bixon, M. Langenbacher, T., Micheal-Beyerle, M. E., *Proc. Natl. Acad. Sci. USA* **1998**, 95, 12759-12765.

33. Bixon M., Giese, B., Wessely S., Langenbacher T., Micheal-Beyerle M. E.,

Jortner J., *Proc. Natl. Acad. Sci. USA* **1999**, 96, 11713-11716

34. Bixon, M., Jortner, J., *J. Phys. Chem. B.* **2000**, 104, 3906-3913.

35. Giese B., *Top. Curr. Chem.* **2003**, 236, 27-44.

36. Di Ventra, M., Zwolak, M., *Encyclopedia of Nanoscience and Nanotechnology: DNA Electronics,* American Scientific Publishers, 2004, 2, 475-493

37. Fink, H. W., Schonenberger, C., *Nature* **1999**, 398, 407-410

38. Porath, D., Bezryadin, A., De Vries, S., Dekker, C*., Nature* **2000**, 403, 635-638

39. Cai, L. T., Tabata, H., Kawai, T., *Appl. Phys. Lett.* **2000**, 77, 3105-3106

40. Yoo, K. H., Ha, D. H., Lee, J. O.*, Phys. Rev. Lett* **2001***,* 87, 198102-198105

41. Storm, A. J., van Noort, J., de Vries, SS., Dekker, C., *Appl. Phys. Lett.* **2001**, 79, 3881-3883

42. de Pablo, P. K., Moreno-Herrero, F., Colchero, F., Gómez Herrero, J., Herrero, P., Baró, M., Ordejón, P., Soler, J. M., Artacheo, E., *Phys. Rev. Lett.* **2000**, 85, 4992-4995.

PART 1: CHARGE TRANSPORT IN QUADRUPLEX DNA

CHAPTER 2: QUADRUPLEX DNA

Over forty years ago, researchers resolved an unusual DNA structure formed by high concentrations of guanosine [1]. This unusual structure became known as a guanine tetrad or G quartet. It comprised of four coplanar guanine residues held together by Hoogsteen base pairs. These guanine tetrads were later shown to stack together to form relatively complex three dimensional structures referred to as quadruplex DNA structures [2-4]. More recently these structures have gained a lot of interest due to their potential biological significance [5-14]. Although there have been some efforts towards providing direct evidence for quadruplex structures *in vivo,* it has not been compelling. However, indirect evidence for the presence of quadruplex DNA structures *in vivo* is strong. For example, compounds that selectively bind to quadruplex DNA have been shown to selectively inhibit telomerase, an enzyme that caps telomeres (the ends of chromosomes) [5-7]. Also a number of proteins have been found that bind [8-10] and induce quadruplex DNA formation [10, 11]. In addition, some researchers have discovered some helicases that unfold quadruplex structures [12, 13]. The most compelling evidence for the presence of quadruplex structures *in vivo* was provided by the identification of a quadruplex specific nuclease [14].

Based on this evidence some potential biological roles have been presented for quadruplex structures. They have been proposed as the structures that form in guanine rich regions of the genome. Therefore, quadruplexes may form in gene promoter regions [15-17], immunoglobulin switch regions [18] or

sequences associated with some diseases [19]. Likewise, the guanine rich sequences found in telomeres are also expected to form quadruplex structures that may protect these single stranded regions from the cell's inherent DNA damage repair machinery [6, 20-23].

Numerous studies have shown quadruplex DNA to be relatively polymorphic [24-26]. This structural diversity is introduced by the various orientations of the strands, bonds and loop regions found in quadruplex DNA. The metal cations that induce its formation also contribute to this diversity. This structural diversity must be taken into account in order to aptly describe quadruplex DNA. The following segment will focus on describing the structural elements that introduce this diversity in quadruplex DNA.

2.1 General Description

Quadruplex structures can be formed by either one, two or four strands of DNA. These strands are drawn and held together by both metal cations and hydrogen bonds. The metal cations influence the stability of the quadruplex structure formed. Quadruplexes can have loop regions, which can be contain either two or more nucleotide residues. Most loop regions contain thymine residues. Loop regions enable the one or two stranded quadruplex molecules to form by enabling these strands to fold back on themselves (see Figure 10) [26].

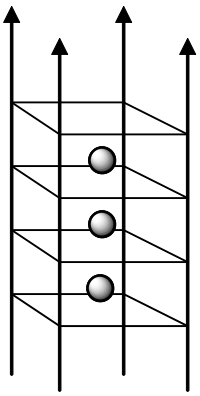

Four stranded Quadruplex (tetramer)

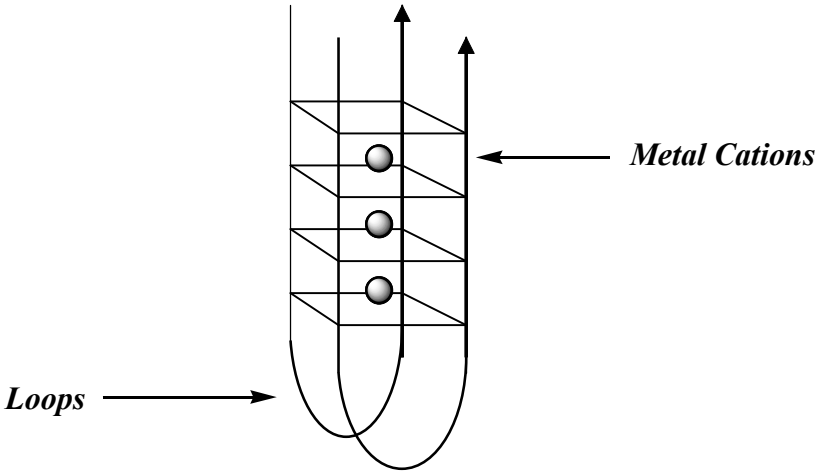

Two stranded Quadruplex (dimer)

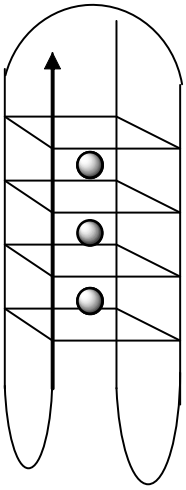

One stranded Quadruplex (monomer)

Figure 10: Quadruplex structures

2.1.1 **Strand orientation**

DNA strands combine in various ways to form quadruplex DNA structures. Dimeric and tetrameric quadruplexes can form in two ways. They may either be formed by the strands facing the same general direction or by the strands combining in different directions. Quadruplexes with strands that combine in the same direction are referred to as parallel quadruplexes (see Figure 11), whereas quadruplexes that combine in different directions are referred to as antiparallel quadruplexes. In dimeric quadruplexes, parallel structures have their loop regions on the same side of the quadruplex, while antiparallel structures have their loop regions on different sides of quadruplex. Parallel tetrameric quadruplexes have all their strands facing the same 5'-3' direction, while antiparallel tetrameric quadruplexes have some strands facing different directions form each other (see Figure 11) [24, 26].

2.1.2 **Loop Orientation**

Monomeric and dimeric quadruplexes have loops which connect the guanine tetrad stacks in various ways. Dimeric quadruplexes can either have loops that connect along the edges of the G quartet stacks or they may run over the quadruplex core to the corner of the tetrad that is not on the same edge (see Figure 12). The former loop orientation is referred to as an edgewise loop, while the latter is referred to as a diagonal loop. Edgewise loops can form on the same side of the quartet stack, however due to steric hindrance the diagonal loops do not usually form on the same side [26]. In addition, monomeric quadruplexes are generally formed by a combination of these two loop orientations (see Figure 10).

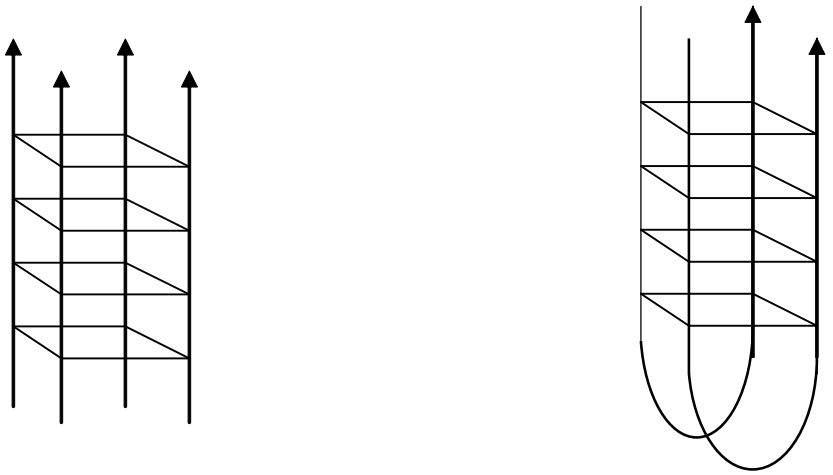

Parallel Quadruplexes

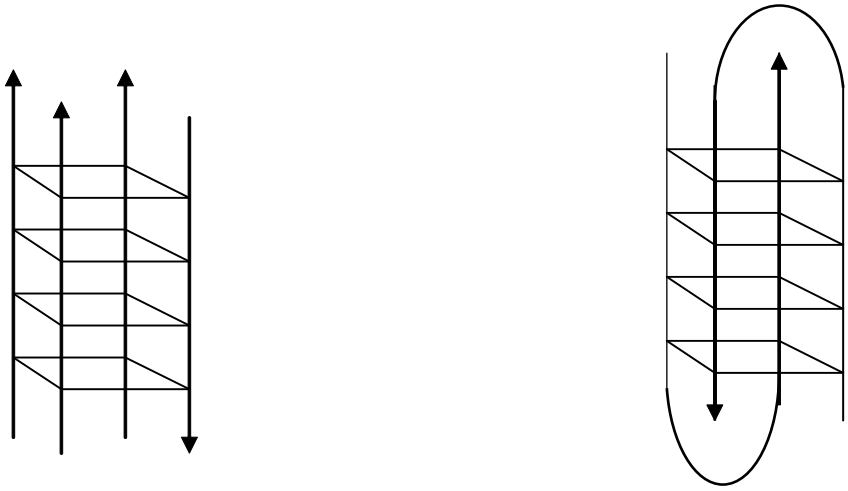

Antiparallel Quadruplexes

Figure 11: Antiparallel vs Parallel Quadruplexes

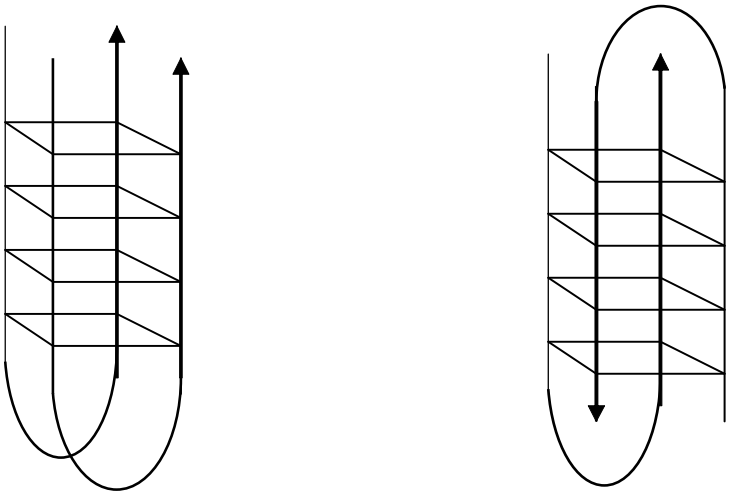

Edgewise Loop Regions

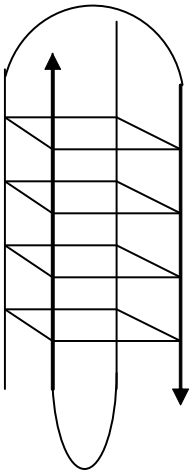

Diagonal Loop Regions

Figure 12: Loop Orientations in Quadruplex Dimers

2.1.3 **Metal Cations**

Metal cations stabilize quadruplex DNA by neutralizing the negatively charged phosphate backbone and also stabilizing the quadruplex stack [26, 27]. Metal cations stabilize the quadruplex stack by packing within the quadruplex core, and coordinating to the carbonyl oxygen atoms (O6) found on each of the guanine residues in the tetrad. It is unclear whether the metal cation between two tetrads coordinates to the oxygen atoms from both tetrad stacks (above and below the cation) or they coordinate with just one stack (either above or below the cation). Monovalent and divalent metal cations stabilize quadruplex DNA [27]. The order of stability that the metals cations induce is somewhat dependent on the size of the cation. Monovalent cations stabilize quadruplex DNA in the following order:

$$\mathbf{K^+ >> Na^+ > Rb^+ > NH_4^+ > Cs^+ >> Li^+}$$

They all have stabilizing effects except for lithium which has a destabilizing effect on quadruplex DNA. The cation size and the charge on the metal cation affect the location of ions within the quadruplex core. The smaller sodium ions line up in the central axis of the quadruplex between the tetrad stacks midway between the planes. On the other hand, the larger potassium ions pack slightly off the central axis of the quadruplex [26].

Divalent metal cations have the following stabilization order:

$$\mathbf{Sr^{2+} >> Ba^{2+} > Ca^{2+} > Mg^{2+}}$$

Although, divalent metal cations stabilize quadruplex DNA at lower concentrations, they destabilize quadruplex DNA at high concentrations [26, 27].

2.1.4 **Glycosidic bonds**

The guanines in G quartets form either anti conformations, syn conformations or both these conformations. In parallel stranded structures, the anti conformation is exclusively favored over all other possible conformations. Antiparallel structures form moderately stable structures which alternate both anti and syn sugar conformations [27].

2.2 **Potential Applications**

Interest in quadruplex structures has also stemmed from their potential applications in other areas. Upon discovering that certain ligands that stabilize quadruplex DNA also inhibited telomerase activity[31, 32], they were actively pursued for anticancer efforts [28-30] as telomerase has been shown to play a major role in tumorigenesis [33, 34]. Therefore, quadruplex molecules were used as structural targets for developing more selective molecules for telomerase inhibition [5-7].

Quadruplex structures have been shown to form DNA aptamers which are specific for ATP, proteins or other molecules [35-37]. They have also been pursued for their potential application as biomolecular nanowires [38].

CHAPTER 3: CHARGE TRANSPORT IN QUADRUPLEX DNA

Compared to studies on charge transport in duplex DNA, work on charge transport in quadruplex DNA has been limited [38-40]. The earliest published work in this area was performed on a monomeric $d(G_3T_2A)_n$ quadruplex unit [39]. They showed that quadruplex monomers are not hole traps (do not prevent charge from migrating beyond the G quartet stack). They also found that more damage occurred at the 5' and 3' guanines of the quadruplex than at the central guanine. More recent work was performed on a DNA/quadruplex conjugate which comprised of a monomeric quadruplex with an extended single stranded end which introduced a discontinuous duplex overhang region [40]. A similar pattern of DNA damage was observed for this work as they also found more damage at the 5' and 3' guanines of the quadruplex than at the central guanine. They proposed that the variations between the damage observed at the two outer guanines and the central guanine was due to the quadruplex core being inaccessible to molecular oxygen [40]. They also showed that quadruplex DNA provided a more effective electron trap than duplex DNA (more damage observed at quadruplex guanines than at 5'-GG-3' steps within duplex DNA). Both works found that the guanine tetrad stacks did not show any of the stacking effects that have been observed for GG or GGG steps in duplex DNA [41, 42].

In comparison, our research sought to determine the effects of electron transfer on a $[d(G_5T_4G_5)]_2$ quadruplex dimer. This quadruplex dimer was created from the combination of two identical hairpins (Figure 13). It contained a duplex

overhang that extended from each of the hairpin ends. The quadruplex dimer was made up of five G quartets which enabled the quadruplex core to stay intact in the presence of the two 10 base pair duplex overhangs. An anthraquinone (AQ) photosensitizer was attached to one of the hairpin ends in order to introduce charge into the quadruplex complex (see Figure 13). The dimer was designed to more effectively analyze and compare the effects of electron transfer on both quadruplex and duplex DNA.

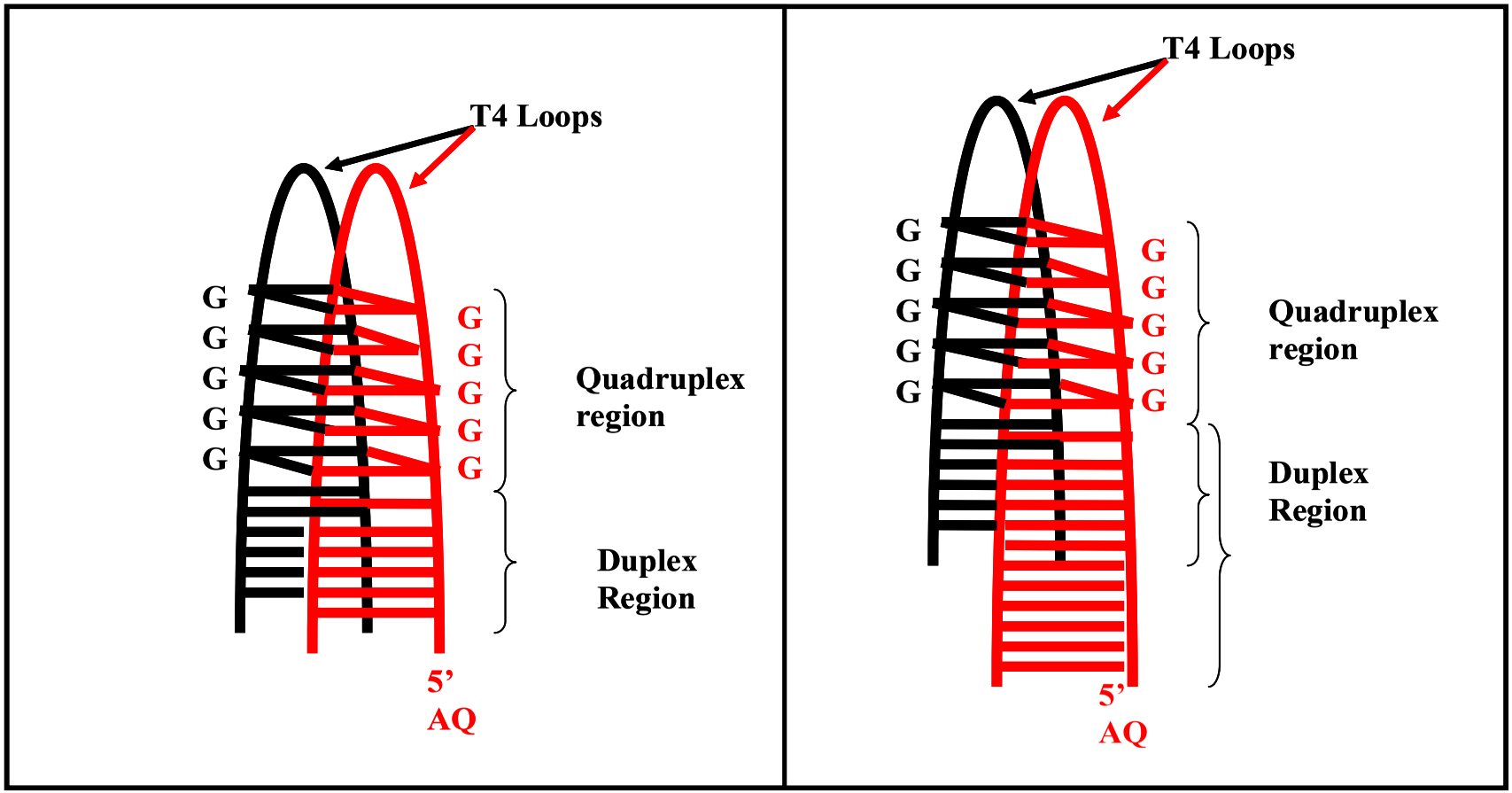

*Although figures show parallel quadruplex dimer conformations, the quadruplex structure could have an antiparallel conformation

Figure 13: Quadruplex Models

CHAPTER 4: EXPERIMENTAL

Materials: The radioactive isotopes, $^{\gamma\text{-}32}$P-ATP and $^{\gamma\text{-}32}$P-ATP, were purchased from Amersham Biosciences. The enzymes, *T4 polynucleotide kinase* (T4-PNK), *Terminal deoxynucleotidyl transferase* (TdT) and *DNase 1* were purchased from New England Biolabs and stored at -20º C. The following chemicals, 3, 4, 9, 10-Perylenetetracarboxylic Diimide and N-(3-Aminopropyl) morpholine, were purchased from TCI America. N-methyl mesoporphyrin (NMM) was purchased from Frontier Scientific, Inc. Indodicarbocyanine-3-1-o-(2-cyanoethyl)-(N,N-diisopropyl)-phosporamidite (Cy3) and 1-dimethoxytrityloxy-3-[O-(N-carboxy-(di-O-pivaloyl-fluorescein)-3-aminopropyl)]-propyl-2-O-succinoyl-long chain alkylamino-CPG (3' Fl) were purchased from Glen research and stored at –20^{o}C. The oligonucleotides were synthesized on an Applied Biosystems DNA synthesizer, and purified by reverse phase HPLC on a Dynamax C18 column. The DNA sequences that were analyzed are shown in Table 2. Electron spray ionization (ESI) mass spectrometry was used to confirm the oligomers' purity. The concentrations of the oligomers were determined on an UV spectrophotometer and monitored at an absorbance wavelength of 260nm. The extinction coefficients of the oligonucleotides were obtained from an online biopolymer calculator. UV-Vis melting and cooling experiments were performed on a Cary 1E spectrophotometer. Circular Dichroism (CD) spectra were obtained on a Jasco 720 spectropolarimeter. Fluorescence experiments were performed on a SPEX Fluorolog-2 spectrofluorometer.

Table 2: DNA Sequences Used

Name	DNA Sequence
G5A	5' AAT GGC CTA T**GG GGG** TTT T**GG GGG** ATA GGC CAT T 3'
G5C (Complementary)	5' TTA CCG GAT ACC CCC AAA ACC CCC TAT CCG GTA A 3'
G5T	5' TTT TTA AT GGC CTA T**GG GGG** TTT T**GG GGG** ATA GGC CAT T 3'
G5A-AQ	5' ***Aq*** AAT GGC CTA T**GG GGG** TTT T**GG GGG** ATA GGC CAT T 3'
G5T-AQ	5' ***Aq*** A AT GGC CTA T**GG GGG** TTT T**GG GGG** ATA GGC CAT T TTTTT3'
G5A AQ2	5' ***Aq*** AA TGG CCT ATC CGG TAT **GGG GG**T TTT **GGG GG**A TAC CGG ATA GGC CAT T 3'
5CY3-G5A	5' **Cy3** AAT GGC CTA T**GG GGG** TTT T**GG GGG** ATA GGC CAT T 3'
G5A-3FL	5' AAT AAT GGC CTA T**GG GGG** TTT T**GG GGG** ATA GGC CAT T **Fl** 3'

UV absorbance: Quadruplex DNA samples comprised of 50 μM DNA (G5A) in 10mM sodium cacodylate (NaCaco) buffer solution (pH =7) and 25 μM potassium phosphate salt. The duplex DNA samples contained 50 μM DNA (calf thymus) in 10 mM sodium cacodylate buffer. The absorbance spectra of these samples were recorded upon being placed in quartz cuvettes with 10 mm pathlengths. The absorbance spectra was also recorded for the samples after the addition of 1 μM N-methyl mesoporphrin (NMM) [43, 44] and 2 μM N, N'- Bis (3-(4-morpholino) propyl)- 3,4,9,10 – perylene tetracarboxylic acid diimide (Tel01),

respectively. The synthesis and purification of Tel01 was performed as previously specified [7].

UV Melting and Cooling Experiments: Quadruplex DNA samples (same composition as mentioned above) were hybridized by being heated for 5 minutes at 90^{o}C, then allowed to equilibrate to room temperature. The samples were then placed in cuvettes with 10 mm pathlengths, and monitored at absorbance wavelengths of 295 nm (quadruplex DNA absorbance). The duplex samples were prepared for hybridization by adding 25 μM DNA (G5A), 25 μM of its complementary sequence (G5C), and 10 mM sodium cacodylate buffer. The samples were ramped twice from 15 – 90 ^{o}C, and 90 -15 ^{o}C, and the absorbance was recorded every 0.5 ^{o}C/min. The melting temperature (T_m) was obtained from the maxima of the first derivative plot of absorbance versus temperature.

Circular Dichroism (CD): The formation of the quadruplex DNA structure was probed by CD spectroscopy. Each quadruplex sample was prepared in a 10 mM sodium cacodylate buffer solution (pH=7) with a 50 μM DNA oligomer concentration, and 25. μM potassium phosphate salt concentration. The duplex samples were prepared as mentioned for the melting experiments. They were hybridized prior to CD analysis. An additional 6 μM NMM was added to the samples. All CD experiments were performed at room temperature, and the CD scans were recorded at 200 nm/min.

Photo-cleavage Analysis by PAGE: Quadruplex samples with the label on the non-AQ containing strand were radiolabeled by incubating 2 μL T4 PNK, 2 μL T4 PNK buffer, 1 μL $^{\gamma-32}$P- ATP, and 25μM G5T DNA at 37°C for 45 minutes. On the other hand, quadruplex samples with the label on AQ containing strand were radiolabeled by incubating 2 μL TdT enzyme, 2 μL Phor-all buffer, 1 μL $^{\alpha-32}$P- ATP, and 25μM G5T-AQ DNA at 37°C for 45 minutes. The labeling samples were suspended in 10μL of loading dye, and then loaded onto a purification gel which was run for 1.5 hours at 400 watts. Purified DNA was removed from the gel by placing it in 750μL elution buffer (1mM EDTA, 0.5M sodium acetate, 10mM magnesium acetate, 0.1% SDS), and incubating the solution at 37°C overnight. The DNA was precipitated by the addition of 750μL of 100% ethanol and 1μL glycogen to the vials, and stored at -80°C for 4 hours. The vials were then centrifuged at 13000 RCF for 30 minutes. After decanting the eluent, 100μL of 80% ethanol was added to the vials and centrifuged for 5 minutes. The 80% ethanol wash was repeated, and the samples were dried. Quadruplex samples with the γ^{-32}P radiolabel on the non anthraquinone containing strand of DNA (G5T sequence) were prepared for hybridization by adding 6μL of labeled G5T to 50μM unlabeled G5T-AQ, 25 μM potassium phosphate salt, and 10mM sodium cacodylate buffer. The quadruplex samples with the α^{-32}P radiolabel on the AQ containing strand of DNA (G5T-AQ sequence) were prepared by adding 6μL of labeled G5T-AQ to 50μM unlabeled G5T, 25 μM potassium phosphate salt, and 10mM sodium cacodylate buffer. The experimental samples for the analysis of intermolecular electron transfer

comprised of 6μL of labeled G5T to 25 μM potassium phosphate salt, 10mM sodium cacodylate buffer and 50μM unlabeled G5A-AQ quadruplex DNA for analysis of the non –AQ containing strand. All these samples were hybridized. Irradiation of hybridized samples was performed for 10 minutes for the non AQ containing strand and 15 minutes for the AQ containing strand using a Rayonet photoreactor with eight 360nm lamps. The precipitated samples were treated with 1M piperidine for 30 minutes at 90^{o}C. After evaporating the piperidine, the samples were suspended in loading buffer. Samples with 4000 CPM were analyzed on a 20% polyacrylamide gel. The gels were dried, and the cleavage was revealed by an autoradiograph and quantified by a Fuji phosphorimager.

FRET Experiments: The control samples for the fluorescence resonance energy transfer (FRET) experiments contained 25 μM quadruplex samples (prepared as stated for UV absorbance) that were labeled with either 5' Cy3 or 3'Fl, respectively, and 25 μM unlabeled quadruplex DNA in 10mM sodium phosphate buffer with 25 μM potassium phosphate salt. . The experimental samples contained one equivalent of 25 μM 5Cy3-G5A DNA and 25 μM G5A-3Fl DNA in 10mM sodium phosphate buffer with 25 μM potassium phosphate salt. The fluorescence spectra were measured with the excitation at 450 nm (where Cy3 is least excited). The spectra were recorded at 25^{o}C with 0.5 mm slits on both the emission and excitation monochromators.

DNase 1 assay Experiment: Duplex and quadruplex DNA samples were prepared and hybridized as mentioned earlier for the PAGE experiments. In addition, a single stranded DNA sample was prepared with 6 μL of γ^{-32} P radiolabeled DNA (G5T sequence), 50 μM DNA (G5A) and 10 mM sodium cacodylate buffer. The DNase 1 solution was freshly prepared with 20 units /mL of DNase 1, 100mM Tris buffer, 25mM $MgCl_2$, and 5mM $CaCl_2$ salt solution [45]. A formamide/EDTA dye solution was prepared with 10mM EDTA solution, bromophenol blue dye and a 4:1 ratio of formamide to water. The samples were stirred and incubated for 5 minutes at room temperature after 2 μL of DNase 1 solution was added. Then, 10 μL of the formamide/EDTA dye solution was added to each sample prior to heating the samples for 3 minutes at 90°C. Each sample (8 μL) was then loaded onto a 20% polyacrylamide gel. The gel was then dried, and the cleavage was revealed by autoradiography.

DMS Methylation Experiment: The samples were prepared as stated earlier for the DNase 1 experiment. Each sample was incubated with 2.5 μL of the 10% (v/v) DMS for 10 minutes at room temperature. The reaction was quenched by the addition of 1M 2-mercaptoethanol, and 1.5 M sodium acetate, pH = 7. The samples were precipitated by adding 750 mL ethanol and 1μL glycogen, then storing the samples at –80°C for 4 hours before decanting the eluent and drying samples. The samples were then piperidine treated and analyzed on 20% PAGE. The gel was then dried, and the cleavage was revealed by autoradiography.

CHAPTER 5: RESULTS

5.1 Structural Characterization of Quadruplex DNA

5.1.1 UV Melting Temperature and Circular Dichroism (CD) experiments

Earlier work on quadruplex DNA has shown that quadruplex molecules are generally much more stable duplex DNA molecules [27-29]. The melting temperature experiments were performed in order to determine whether our quadruplex complex exhibited similar behavior. These experiments were monitored at a wavelength of 295nm (where quadruplex DNA absorbs). The duplex DNA had a melting temperature transition at 57^{o}C, which was about 15^{o}C lower than the quadruplex DNA transition which was observed at 72 ^{o}C (see Figure 14). Therefore, the quadruplex DNA was thermally more stable than the duplex DNA.

The formation of the quadruplex DNA structure was probed by CD spectroscopy [46]. The CD analysis could confirm the presence of all the structural components (duplex region, quadruplex region, hairpin orientation) within our quadruplex complex. It enabled us to probe both the quadruplex and the duplex overhang regions. Both CD spectra for duplex DNA and quadruplex DNA showed a strong positive peak at approximately 280nm. The duplex DNA spectrum had a negative peak at approximately 250nm (see Figure 15), while the quadruplex DNA spectrum showed a negative peak at approximately 240nm (see Figure 16). The quadruplex DNA spectrum had an additional positive CD peak at approximately 260nm. Parallel quadruplex dimers have characteristic CD

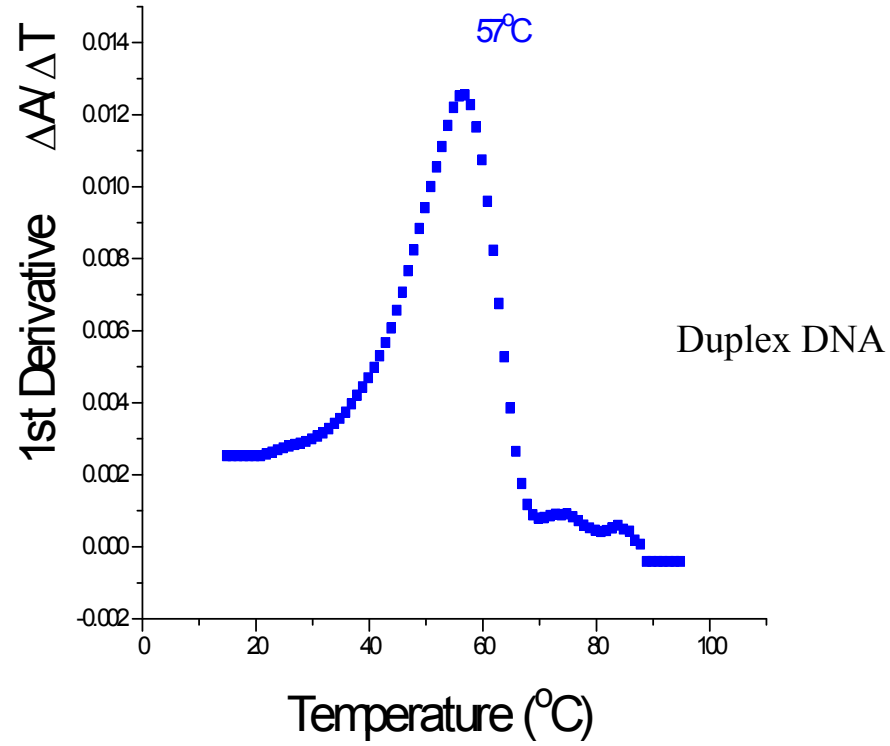

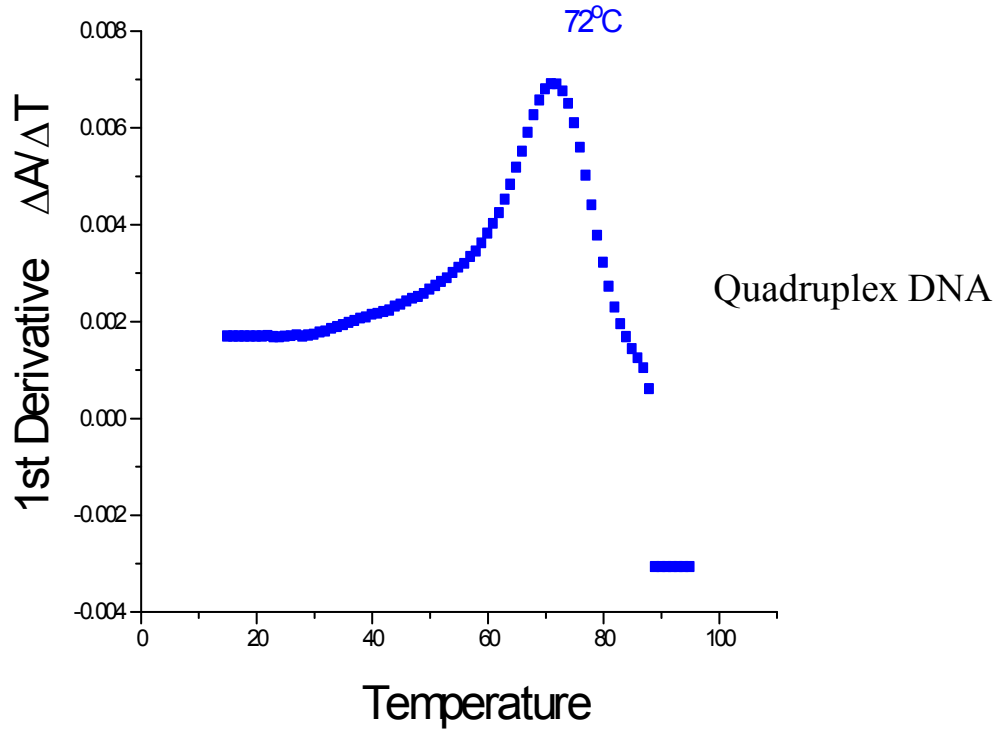

Figure 14: Melting Temperature Curves

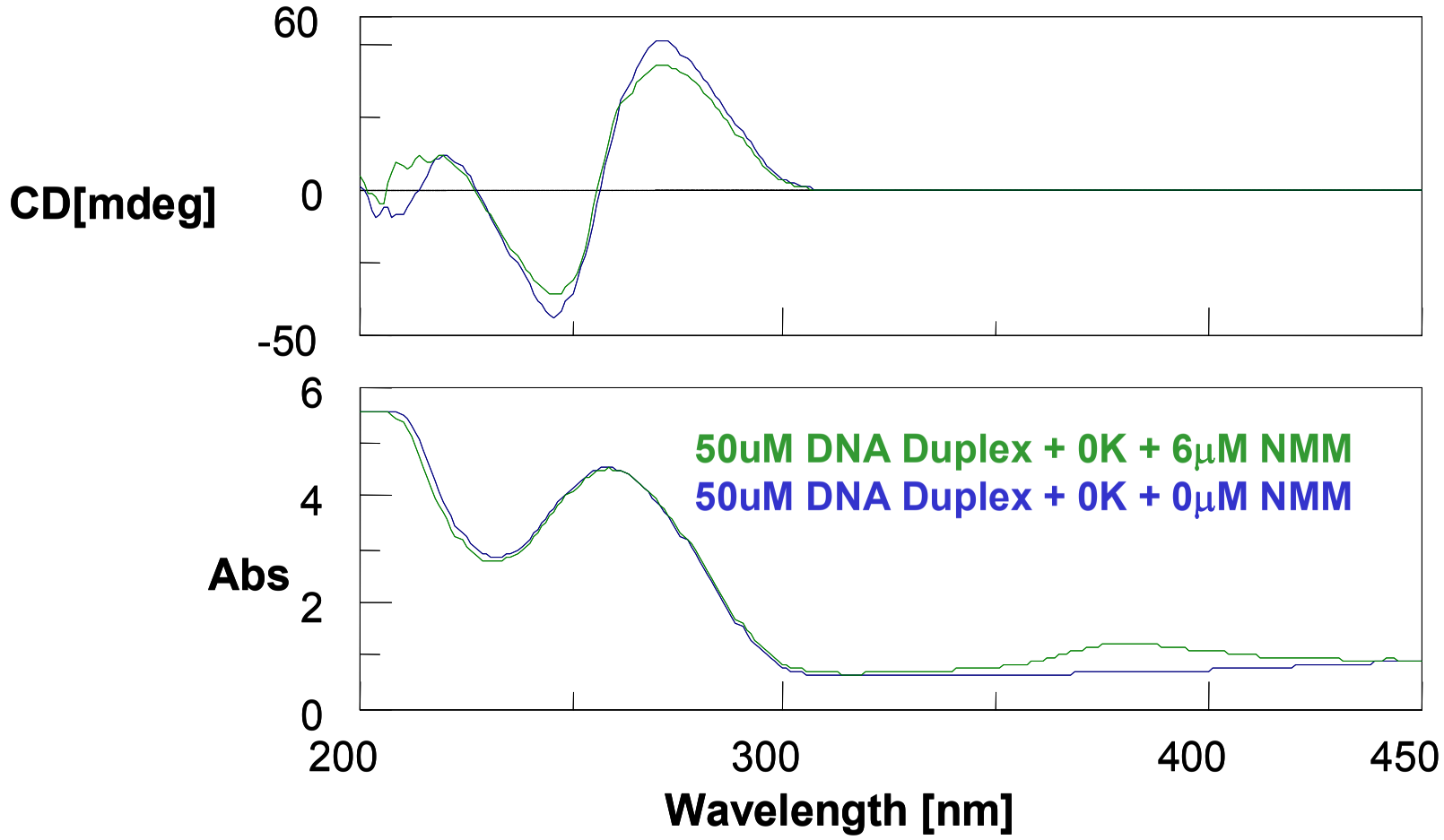

Figure 15: CD Spectra for Duplex DNA

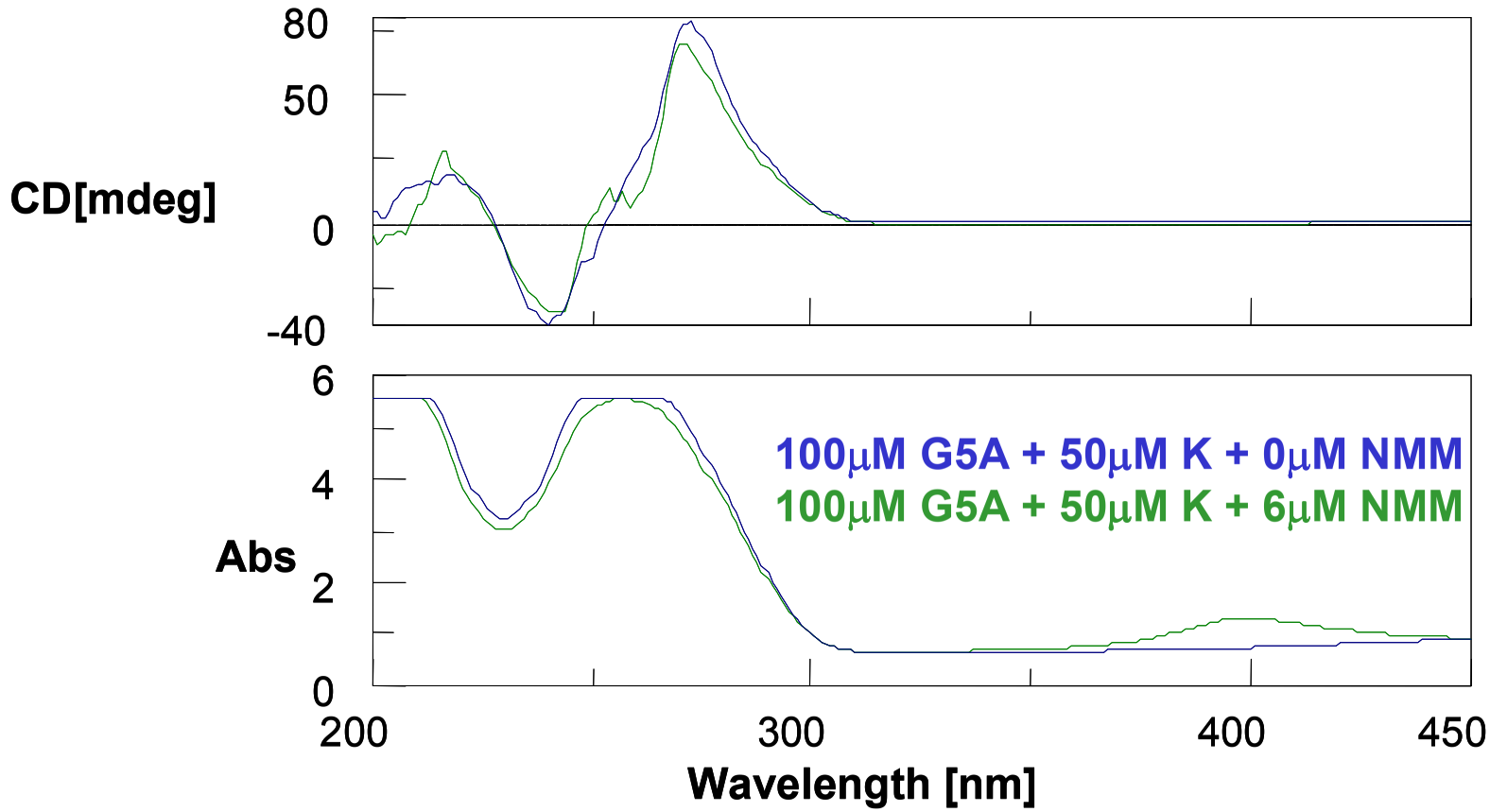

Figure 16: CD Spectra for Quadruplex DNA

peaks at 260nm (positive CD peak) and 240nm (negative CD peak), while antiparallel quadruplex dimers have characteristic CD peaks at 295nm (positive CD peak) and 260nm (negative CD peak) [46]. This suggests that the peak observed at 260nm may be from a parallel quadruplex structure. Also, the fact the peak at 260nm was enhanced in the presence of N- methyl mesoporphyrin (NMM) further confirms that this peak was from quadruplex DNA formation.

5.1.2 Confirmation of Quadruplex Formation by Dye Analysis

The fluorescent dye, N- methyl mesoporphyrin (NMM), selectively binds to quadruplex DNA [44]. Therefore, in efforts to confirm the formation of quadruplex DNA under these experimental conditions, NMM was used as a chemical indicator. The UV spectroscopy experiments show that the addition of NMM to quadruplex DNA resulted in an absorbance peak that was red shifted from the absorbance peak of NMM alone (see Figure 17). Also, adding an equivalent amount of NMM to calf thymus DNA had no effect on the absorbance of NMM (no observed shift) (see Figure 17).

In addition, some CD experiments were performed to show that NMM specifically bound to the quadruplex DNA samples (see Figure 15 and Figure 16). The observation of a negative CD at 400nm (wavelength where NMM absorbs) in the presence of G5 quadruplex DNA and NMM showed that the dye actually binds to quadruplex DNA (Figure 18). The absence of a CD (neither negative nor positive) at the same wavelength for duplex DNA in the presence of the same amount of NMM ligand showed that NMM did not bind to duplex DNA (Figure 19). This confirmed the results obtained from the UV spectroscopy experiments.

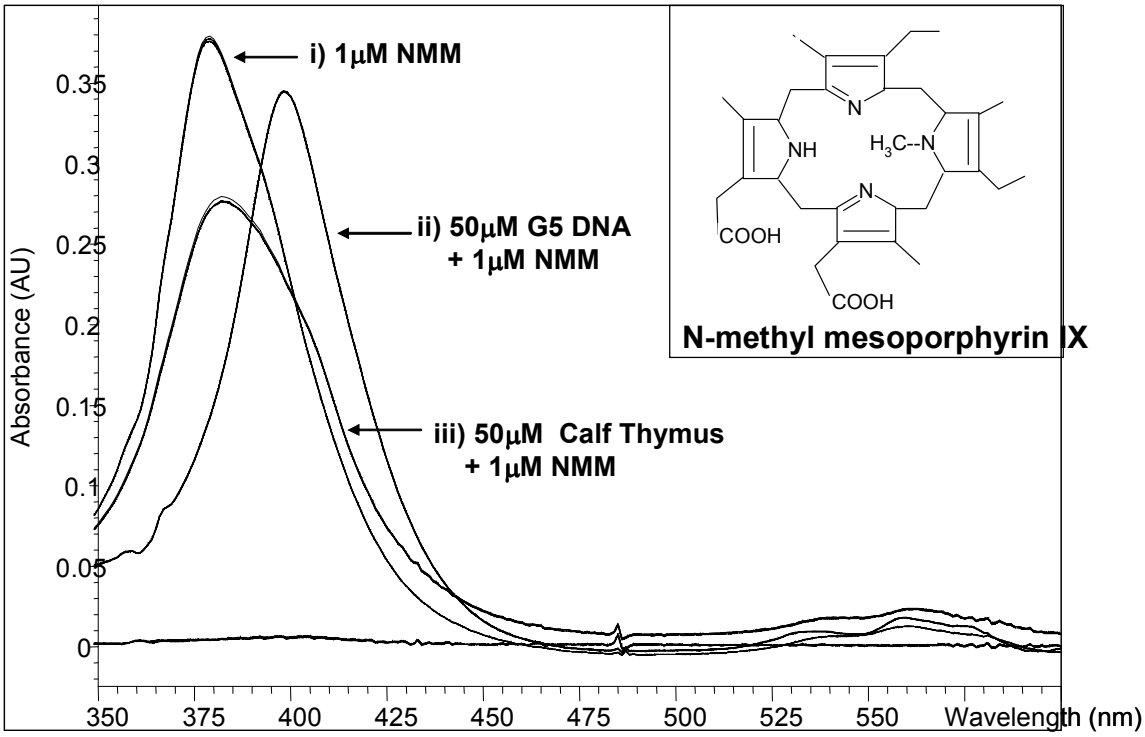

Figure 17: Quadruplex Detection by NMM Absorption

Another quadruplex binding dye was also used to confirm the formation of quadruplex DNA under these conditions. Earlier publications showed that N, N'-Bis(3-(4-morpholino)propyl)-3,4,9,10–perylenetetracarboxylic acid diimide (Tel01) specifically binds to quadruplex DNA [7, 47]. The UV absorption spectrum for Tel01 alone was similar to the UV absorption spectrum that was observed for the sample with both Tel01 and calf thymus DNA (Figure 20). This suggests that there was no interaction between the ligand and duplex DNA. However, when

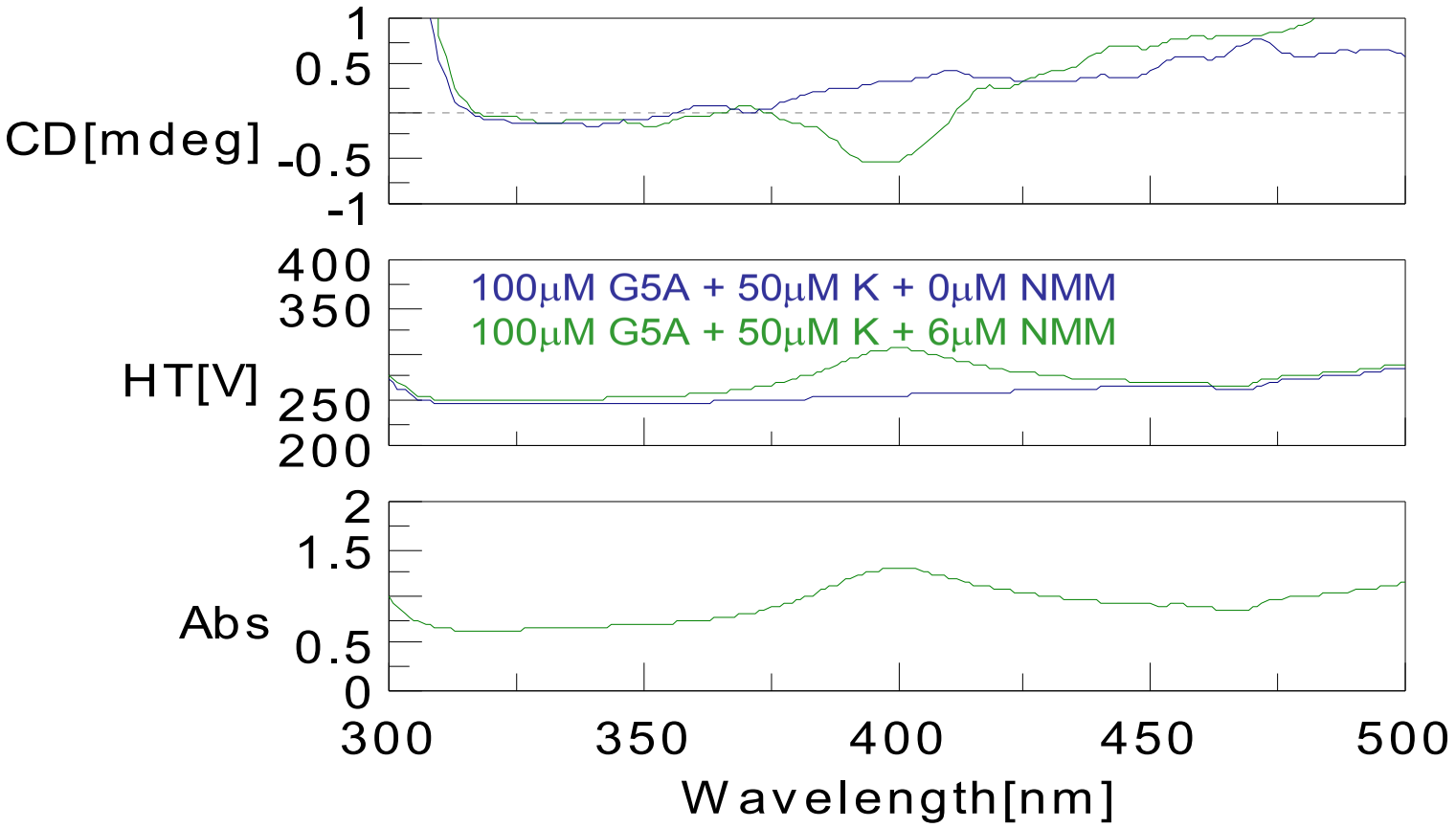

Figure 18: CD Analysis of NMM Binding to Quadruplex DNA

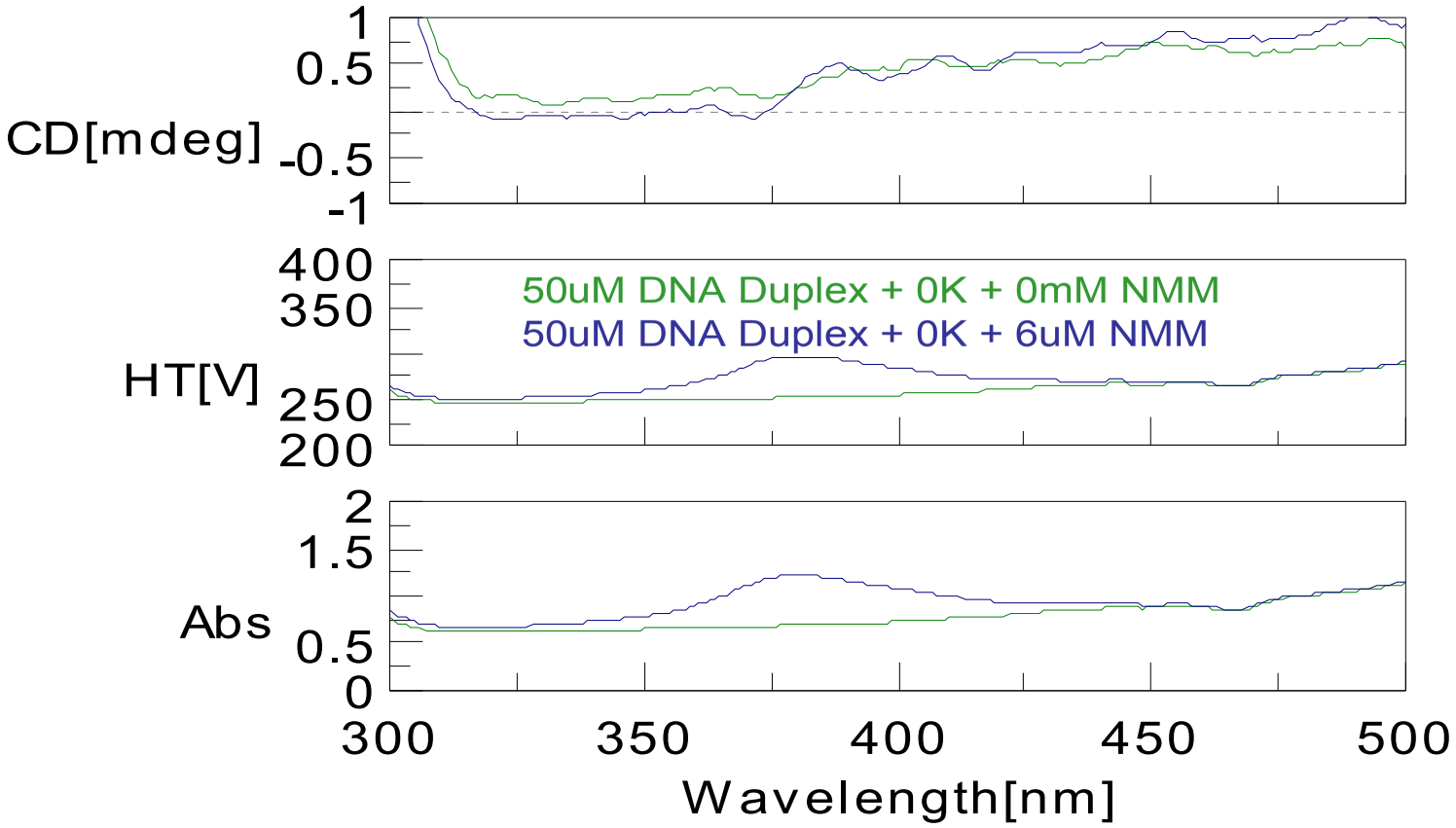

Figure 19: CD Analysis of NMM binding to Duplex DNA

Tel01 was added to G5 quadruplex DNA there was a red shift in the UV absorption spectrum as well as a transformation of the general nature of the saddle peaks observed for Tel01 dye (see Figure 20). This observation suggests that Tel01 dye selectively binds to G5 quadruplex DNA.

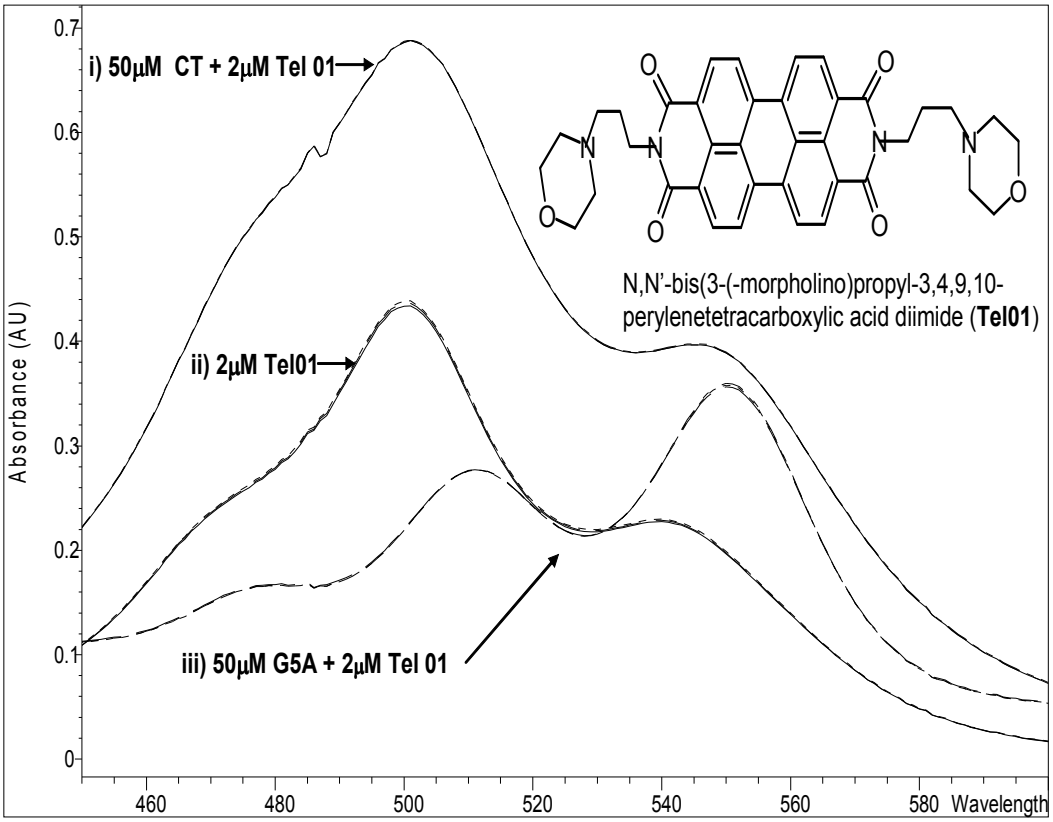

Figure 20 Quadruplex Detection by Tel01 Absorption

5.1.3 **DNase 1 Assay**

The formation of G5 quadruplex DNA was further characterized by a DNase 1 assay. The DNase 1 enzyme cleaves both single stranded and double stranded DNA into mono-, di- or tri- nucleotides. It more efficiently cleaves double stranded DNA. However, DNase 1 enzyme is unable to efficiently cleave quadruplex DNA [45]. These features enabled us to probe the formation of both the quadruplex and duplex regions within the complex. The DNase 1 analysis confirmed the formation of quadruplex DNA under these conditions. This was shown by the inability of DNase 1 enzyme to cleave the DNA in the quadruplex region of the G5 DNA (see Figure IV-8). The DNase 1 was able to cleave duplex DNA and the experimental samples that had the quadruplex forming DNA in the absence of the high concentration of salt (see Figure IV-8). The presence of damage at the 5' G steps in the duplex region of the quadruplex complex confirmed the formation of both regions (quadruplex and duplex) in the quadruplex complex.

5.1.4 **Dimethyl Sulfate (DMS) Methylation Assay**

The DMS methylation assay sought to detect quadruplex DNA formation. DMS methylates the N7 position of guanine and the N3 position of adenine, and upon further treatment, DNA strand cleavage occurs at these modified locations. The guanine base methylation is five times more efficient than adenine base methylation. Guanine residues remain unbound (free) in duplex DNA, making them susceptible to DMS methylation and subsequent cleavage [51].

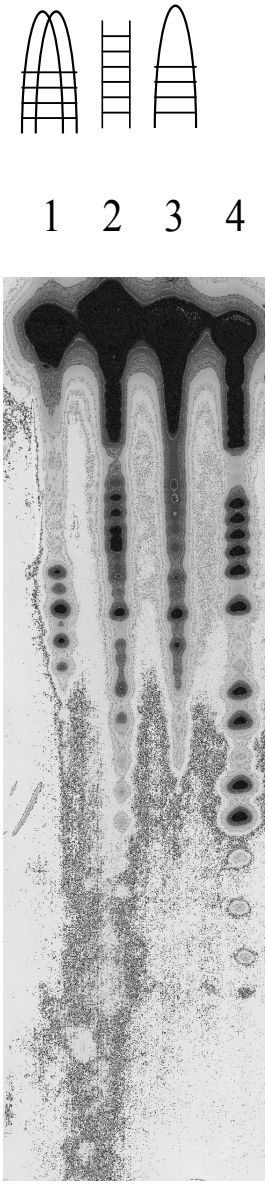

Figure 21: DNase I Analysis of Quadruplex Formation

Lane 1 - Quadruplex sample containing 50 μM G5A, 25μM K+ and 10mM NaCaco buffer;
Lane 2 - Duplex sample containing 25 μM duplex DNA, and 10mM NaCaco buffer,
Lane 3 - Control sample containing 50 μM G5A and 10mM NaCaco buffer,and no K present
Lane 4 - A/G sequencing lane

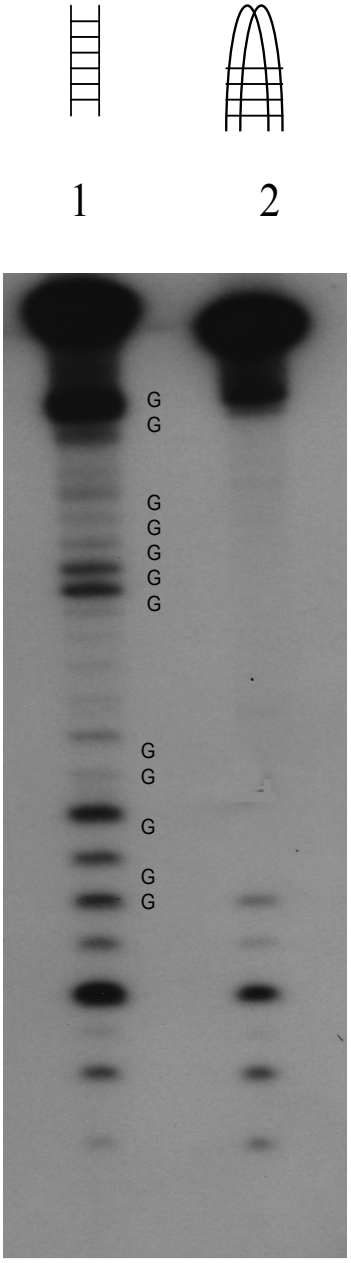

Figure 22: Analysis of Quadruplex Formation by DMS Methylation

Lane 1 - Duplex sample containing 25μM duplex DNA, and 10mM NaCaco buffer,

Lane 2 - Quadruplex sample containing 50μM G5, 25μM K+ and 10mM NaCaco buffer;

However, guanine residues in quadruplex DNA are bound (not free). They are hydrogen bonded by Hoogsteen base pairing to an adjacent guanine. As a result, the guanine residues in quadruplex DNA are protected from DMS methylation. This also enabled us to distinguish the quadruplex region from the duplex overhang region. Our results showed that while the guanines in duplex DNA were methylated, the guanines in the quadruplex region of G5 DNA were not (see Figure 22).

5.1.5 **Fluorescence Resonance Energy Transfer (FRET) Experiments**

FRET experiments have become popular tools for the structural analysis of biomolecules. They primarily yield the distances between fluorescent dyes which have been attached to structural elements within the moiety being studied. We sought to use the FRET analysis to indicate which conformation (parallel or anti-parallel) the quadruplex complex formed. The fluorescein (Fl) donor was attached to the 3' end of G5 DNA. The cyanine dye, Cy3, was used as the acceptor in this system. It was labeled to the 5' end of G5 DNA. The control experiment with a 1:1 ratio of the 3' Fl and unlabelled G5 DNA showed the maximum fluorescence possible in this system prior to quenching by Cy3 (see Figure 23). The other control experiment with a 1:1 ratio of the 5' Cy3 and unlabelled DNA showed the characteristic fluorescence curve of the Cy3 dye. The experimental sample contained a 1:1 ratio of 3'Fl and 5' Cy3 that showed the quenching of fluorescein fluorescence by Cy3 dye in the G5 quadruplex. The efficiency for energy transfer was calculated from the following equation (1);

$$E = 1 - F_{DA}/F_D \quad (1)$$

where E is the energy efficiency, F_{DA} is the fluorescence intensity for both the donor and the acceptor, and F_D is the fluorescence intensity of the donor at the donor maxima (approximately 520nm). The FRET efficiency was calculated to be 75 % for this quadruplex complex. The distance (R) between the donor and the acceptor was determined from the following equation derived from the Forster equation (2);

$$R = R_o (E^{-1} - 1)^{1/6} \quad (2)$$

Using the Forster distance (R_o) value of 56 angstroms [48], the actual distance (R) was calculated to be 46 angstroms. Therefore, the FRET experiments suggest that G5 quadruplex forms a parallel quadruplex structure (see Figure 24).

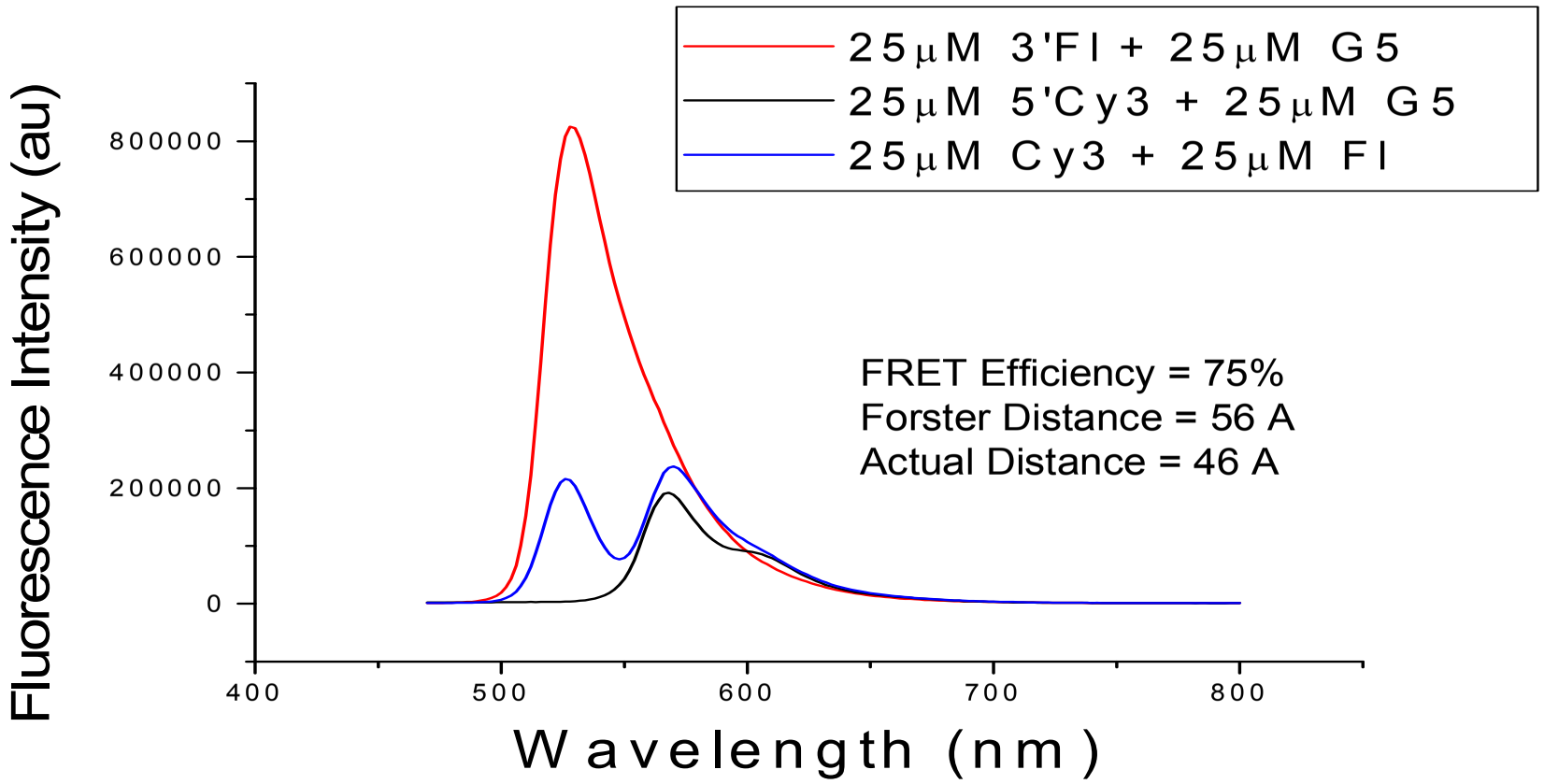

Figure 23: FRET Structural Analysis

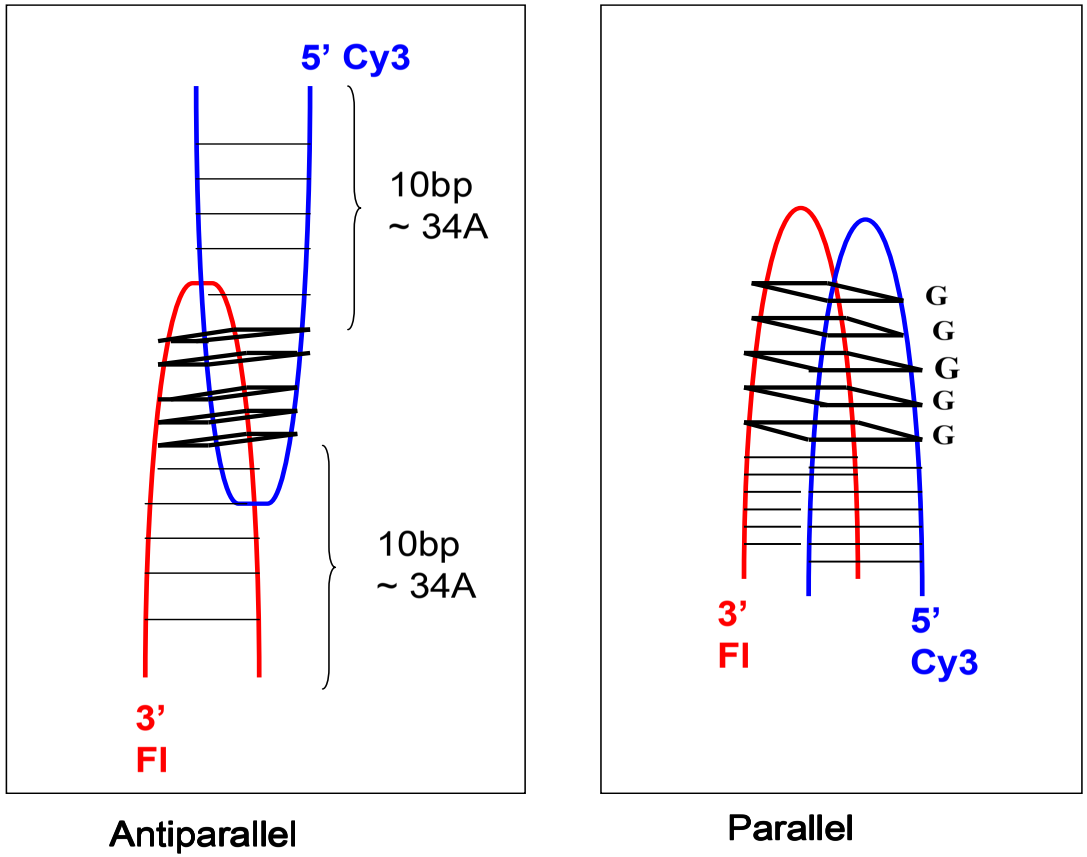

Figure 24: Possible Conformations for Quadruplex

FRET analysis suggests G5 quadruplex forms a parallel dimer as opposed to an antiparallel dimer because the fluorophores would be further apart for an antiparallelcomplex (see above).

5.2 **Effects of Electron Transfer on Quadruplex DNA**

Previous studies on the oxidation of duplex DNA have shown that oxidation of a base generates a radical cation that migrates along the length of the DNA until it is quenched most often at a guanine or G_n step by either H_2O or O_2. An interesting expansion to this would be to determine the behavior of the radical cation as it migrates along the length of the DNA through both duplex and quadruplex DNA regions. We sought to analyze this behavior by comparing the effects of charge transport on quadruplex and duplex DNA regions within a continuous quadruplex complex.

5.2.1 **Quadruplex DNA damage**

In efforts to characterize the pattern of DNA damage observed for a quadruplex dimer, the radioactive label was placed on either the non-AQ containing strand or the AQ containing strand. In order to determine whether charge migrated over to the non-AQ containing strand (G5T), a 5' $^{\alpha-32}$P label was attached to the non-AQ containing strand of G5 quadruplex (see Figure 25). This strand showed damage at both the quadruplex region and the duplex region (see Figure 25: Lane 1b). It had more damage at the external guanines of the G5 tetrad stack than at the interior guanine residues. The AQ containing strand (G5A-AQ) was characterized by placing a $^{\gamma-32}$P label on its 3' end (see Figure 25). Similar to the non-AQ containing strand, the AQ containing strand had damage at both the quadruplex and duplex regions of the quadruplex complex (see Figure 25: Lane 2b). However, in the AQ containing strand all the guanines within the quadruplex tetrad stack showed relatively similar amounts of damage.

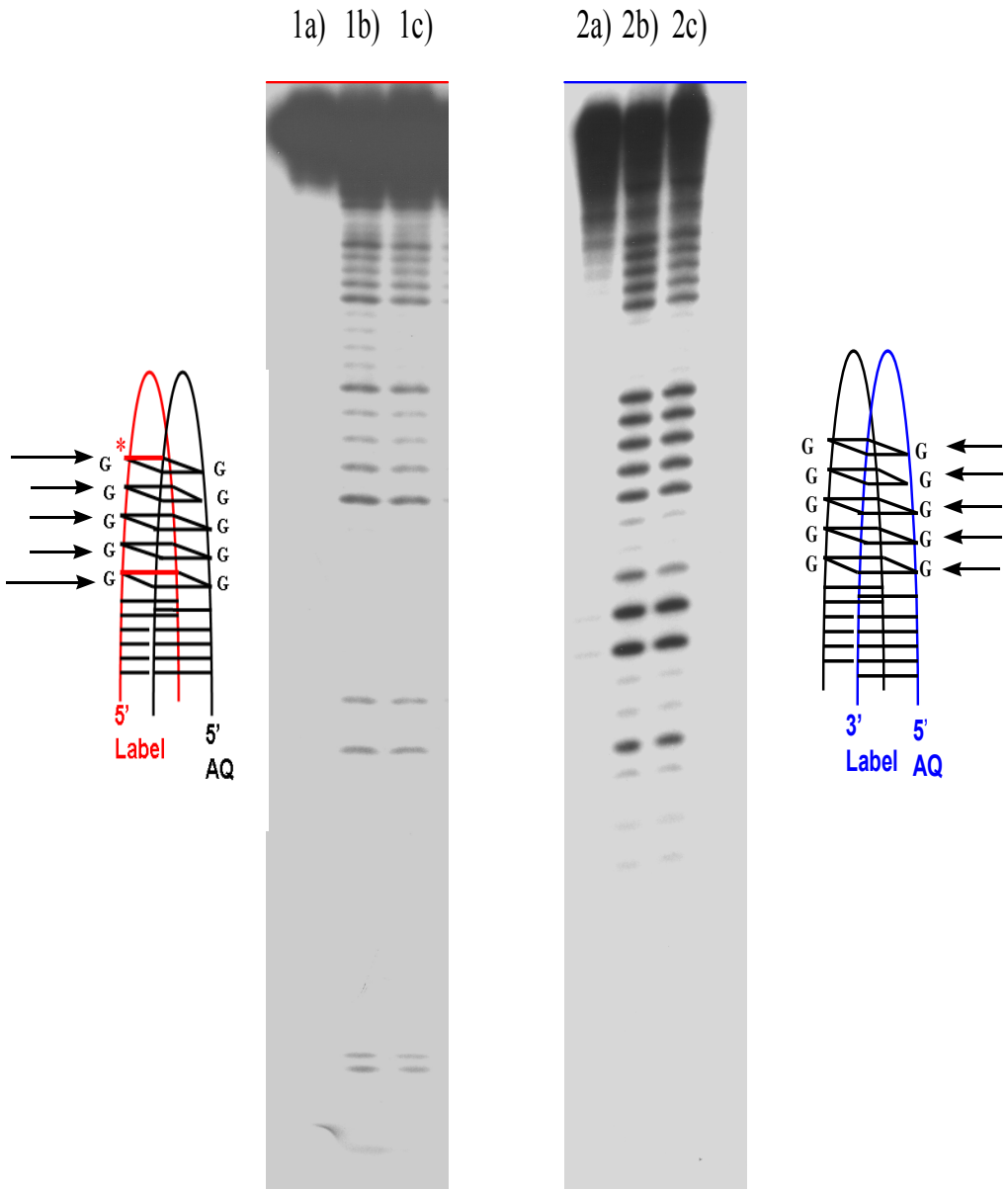

**Red lines signify guanines with most damage within the quadruplex region*
Arrows show the relative proportion of damage at the guanines within the quadruplex

Figure 25:
Quadruplex DNA Damage Analysis

All samples contained 25µM K+ and 10mM NaCaco buffer. Lane 1a - Dark control (no irradiation) containing labeled 50 µM G5T; Lane 1b - Quadruplex sample containing labeled 50 µM G5T; Lane 1c - Quadruplex sample containing labeled 50 µM G5T plus additional 25 µM duplex DNA; Lane 2a - Dark control (no irradiation) containing labeled 50 µM G5T-AQ; Lane 2b - Quadruplex sample containing labeled 50 µM G5T-AQ; Lane 2c - Quadruplex sample containing labeled 50 µM G5TAQ plus additional 25 µ M duplex DNA.

Comparison of the DNA damage in the duplex and quadruplex regions showed that the average amount of damage in the two regions was similar for both the non-AQ containing and the AQ containing strands (see Figure 25).

5.2.2 **Characterization of Cross Strand charge transfer**

Although the quadruplex DNA damage results appeared conclusive, there was still a possibility that the quadruplex damage observed for the non-AQ containing strand was from intermolecular electron transfer from an AQ containing strand to a non-AQ containing strand in another quadruplex molecule. In order to determine if this was the case, a large amount of unlabeled duplex DNA was added to the quadruplex samples. The damage observed for these experiments was similar to the experimental samples without the additional DNA (see Figure 25: Lanes 1c and 2c). This suggested that the damage observed in the non-AQ containing strand was not from intermolecular electron transfer.

5.2.3 **Anthraquinone (AQ) Cross-Intercalation charge transfer**

Another possibility for the damage observed in the non-AQ containing strand was that the AQ from one hairpin strand in the quadruplex was intercalating into the non-AQ strand in the same complex. This was analyzed by creating an extended hairpin which would contain the AQ and prevent it from intercalating the other strand (see Figure 26). The results showed that the non-AQ containing strand showed the same pattern of damage as in the shorter model of the quadruplex.

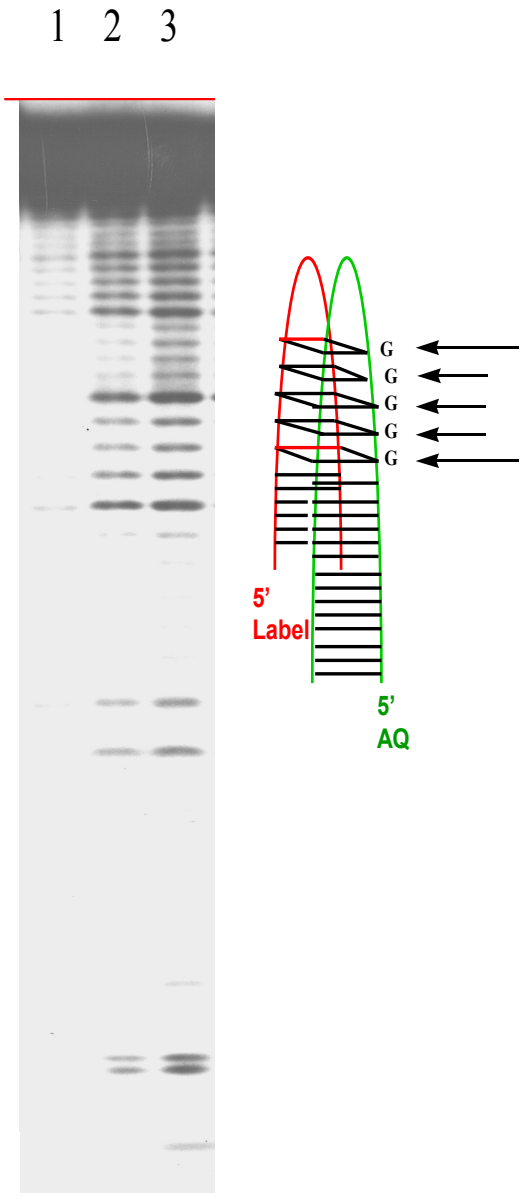

**Red lines signify guanines with most damage within the quadruplex region*
Arrows show the relative proportion of damage at the guanines within the quadruplex

Figure 26: Anthraquinone Cross Intercalation Analysis

All samples contained 25µM K^+ and 10mM NaCaco buffer. Lane 1 - Dark control (no irradiation) containing labeled 50 µM G5T; Lane 2 - Quadruplex sample containing labeled 50 µM G5T (Irradiated for 10mins); Lane 3 - Quadruplex sample containing labeled 50 µM G5T (Irradiated for 15mins)

CHAPTER 6: CONCLUSION

The characterization of the quadruplex complex formed was crucial for the fidelity of the charge transport studies. It was important to prove that both the quadruplex region and the duplex overhang regions were forming as proposed in our experimental model. The formation of the quadruplex region was confirmed by the selective binding of quadruplex DNA binders, NMM and Tel01. These dyes both showed that they selectively bound to the quadruplex structures within the complex (Figures 15 to 20). The DNase 1 and DMS methylation assays confirmed the formation of both the quadruplex region and the duplex overhang regions of the quadruplex complex. Both assays showed that the quadruplex region was formed by the absence of DNA damage in this region of the gels (see Figures 17 and 20). They also showed that the duplex overhang regions were formed by the presence of DNA damage surrounding the quadruplex region of the gels (see Figures 17 and 20). These gel assays also confirmed that the quadruplex complex could be effectively analyzed by gel electrophoresis.

Another attribute of the quadruplex complex that was important to understand was the conformation of the quadruplex dimer. As explained earlier, the quadruplex dimer could either form a parallel or antiparallel quadruplex (see Figure 24). The FRET and CD analyses support the formation of parallel quadruplex dimers. The calculated distance (46 angstroms) between the fluorophores suggests that the duplex overhangs are on the same side of the quadruplex region. An antiparallel quadruplex dimer would be expected to

exhibit a calculated distance that exceeds the length of the contributing duplex overhangs (above 68 angstroms). Therefore, the FRET analysis shows that the complex forms a parallel dimer. The circular dichroism experiments (see Figures 15 and Figure 16) showed CD peaks that are characteristic of parallel quadruplex dimers (positive CD peak at 260nm) for the quadruplex sample. There was no evidence of antiparallel dimer formation (characteristic positive peak at 295 nm). This conformational evidence was important for the accurate interpretation of the overall data.

Similar to the results in duplex DNA studies, the pattern of DNA damage observed for the quadruplex complex was sequence dependent. The non AQ containing strand showed quadruplex damage that was similar to the damage observed for quadruplex monomers. It showed more damage on the guanines at the exterior of the G quartet stack than at the interior guanines. This suggested that these exterior guanines were in a more solvent accessible environment than the interior guanines. On the other hand, the AQ containing strand showed similar amounts of damage at all the guanines in the quadruplex region of the complex. As earlier experiments showed that quadruplex DNA was being formed under these conditions, this sequence variation was probably introduced by the quadruplex dimer.

The quadruplex complex was developed to allow for the effective comparison of quadruplex and duplex regions. The charge transport studies on this complex showed that the amount of damage at the guanines in the quadruplex region was similar to the amount of damage observed for the guanines in the

duplex region. This suggests that the guanines in quadruplex region in a dimer do not provide a more effective hole trap than guanines in the GG steps of duplex DNA.

The evidence of damage in the non-AQ containing strand suggests that charge is able to somehow migrate across the quadruplex. This could possibly occur through various ways such as across the core, through the loops or through the quadruplex-duplex DNA junctions. Further studies could be performed to verify how the charge migrates across the quadruplex.

CHAPTER 7: CHALLENGES

The pursuit of the effects of charge transport on quadruplex DNA ensued with its own challenges. The most challenging aspect of this work was determining the appropriate conditions for the formation of the designed quadruplex structure. The following section will outline these challenges in an effort to complete the discussion of this work

7.1 Formation of Quadruplex DNA

Quadruplex DNA is particularly challenging to form because of the various factors that are necessary for its formation. It requires the appropriate salt, buffer and DNA concentrations to form. The various configurations of quadruplex DNA require different conditions for formations. For example, monomeric quadruplex structures require less salt concentrations than the other two configurations (dimer and tetrameric) [25]. This is due to the other configurations requiring extra salt in order to bring the separate DNA strands in close proximity to each other in order to bond. The salt minimizes the inherent repulsion between the negatively charged phosphate backbones in the DNA strands. This enables the strands to draw close enough for the quadruplex structure to form. Also, higher DNA concentrations appear to further induce the formation of quadruplex structures.

In light of this, our initial attempts at forming the quadruplex structure were performed at high DNA (greater than 100μM) and salt concentrations (millimolar concentrations). Other quadruplex dimers that had been formed in

literature were formed within these concentration ranges [49, 50]. Although we were able to initially induce its formation at 100μM DNA concentration and 50mM salt concentration, this concentration was high for the charge transport experiments we were planning to perform on the complex. Therefore, we sought to form the complex at much lower concentrations. Normal charge transport experiments using anthraquinone are performed using 2.5μM concentration of DNA. We attempted to form the complex at concentrations that were as low as 10 μM DNA, however the lowest concentration we were able to observe complex formation (by melting temperature and UV spectroscopy with NMM) was at 30μM DNA concentration (see Figure 27 and 28). In spite of this, the complex was unstable at this concentration. We were able to form the structure at 40μM DNA concentration (see Figure 29 and 30). However, similar to the 30μM complex, it was still unstable. The lowest concentration we were able to form a stable complex was at 50μM DNA concentration. This was ultimately the concentration that all the experiments were performed at.

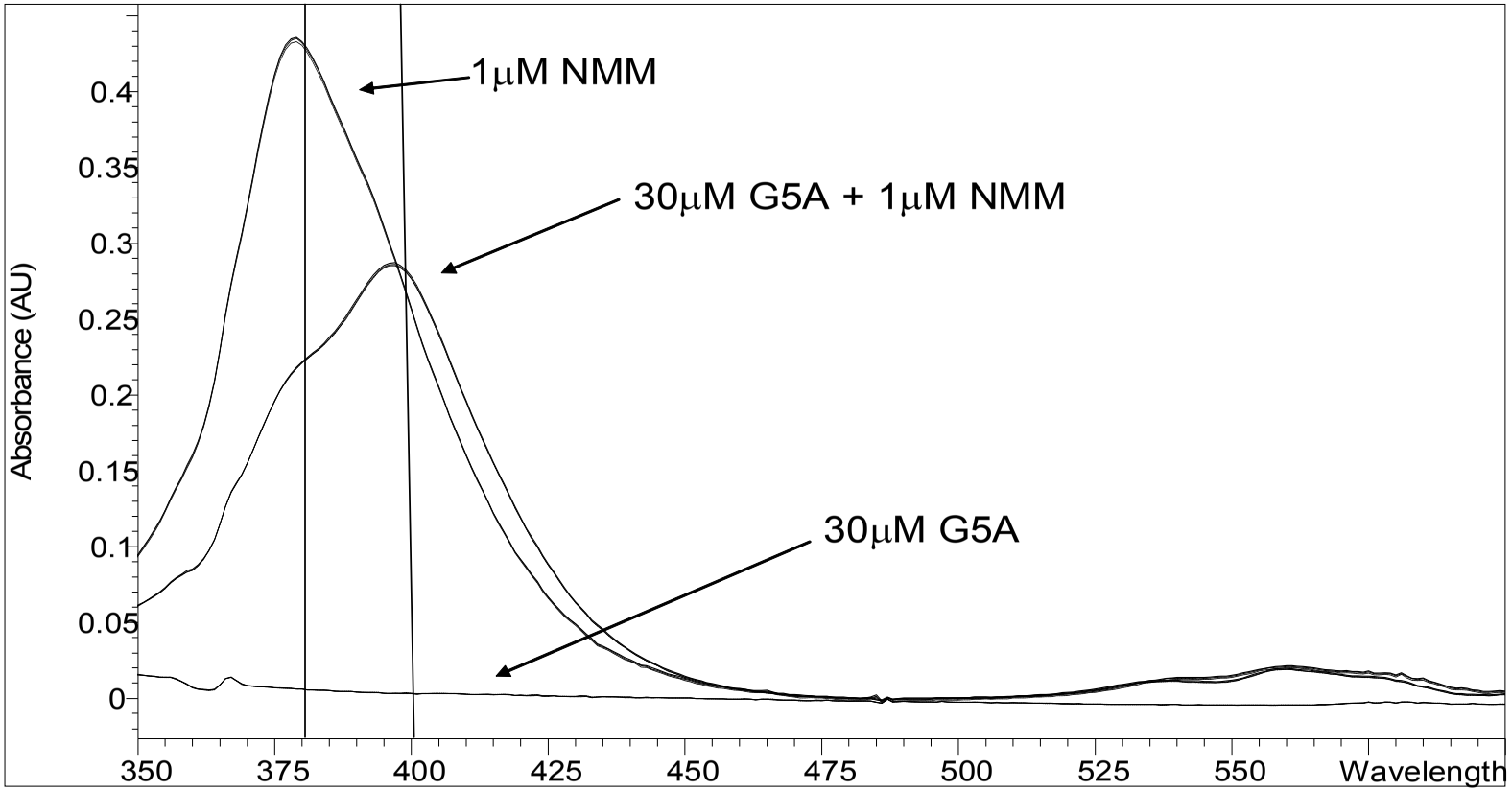

Figure 27: Detection of Quadruplex formation at 30μM DNA concentration

Quadruplex samples contained 30 μM DNA + 15μM Potassium phosphate salt + 3 mM NaCaco Buffer

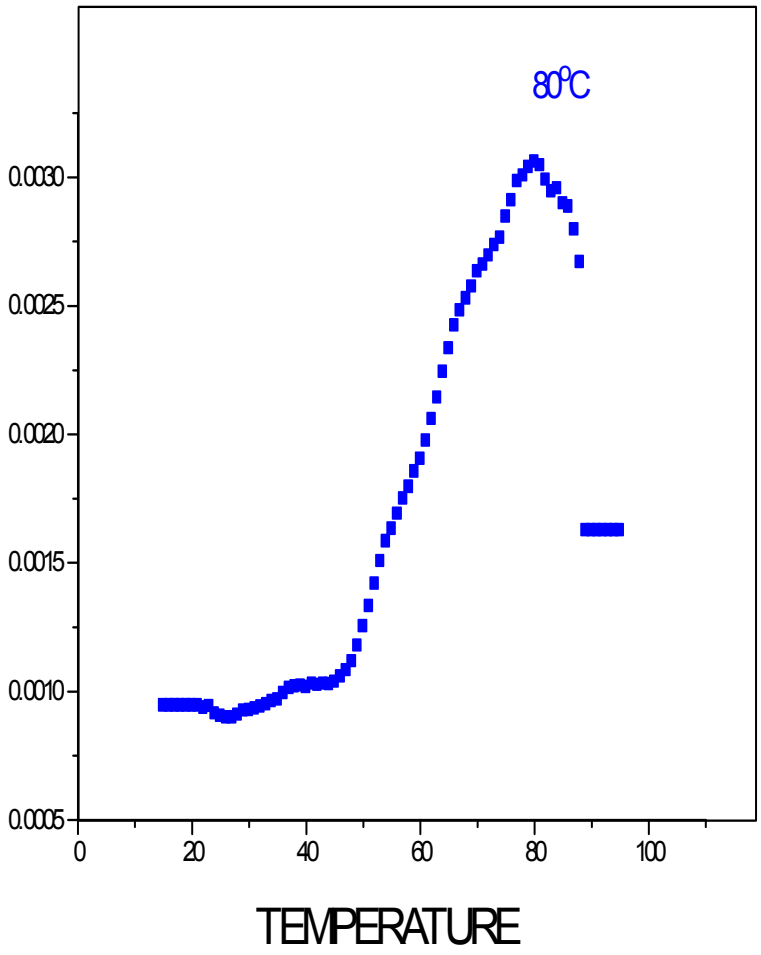

Figure 28: Melting Temperature Curve for 30μM DNA

Sample prepared with 30 μM G5A + 15μM K^+ + 3mM Sodium Cacodylate Buffer; λ = 295nm

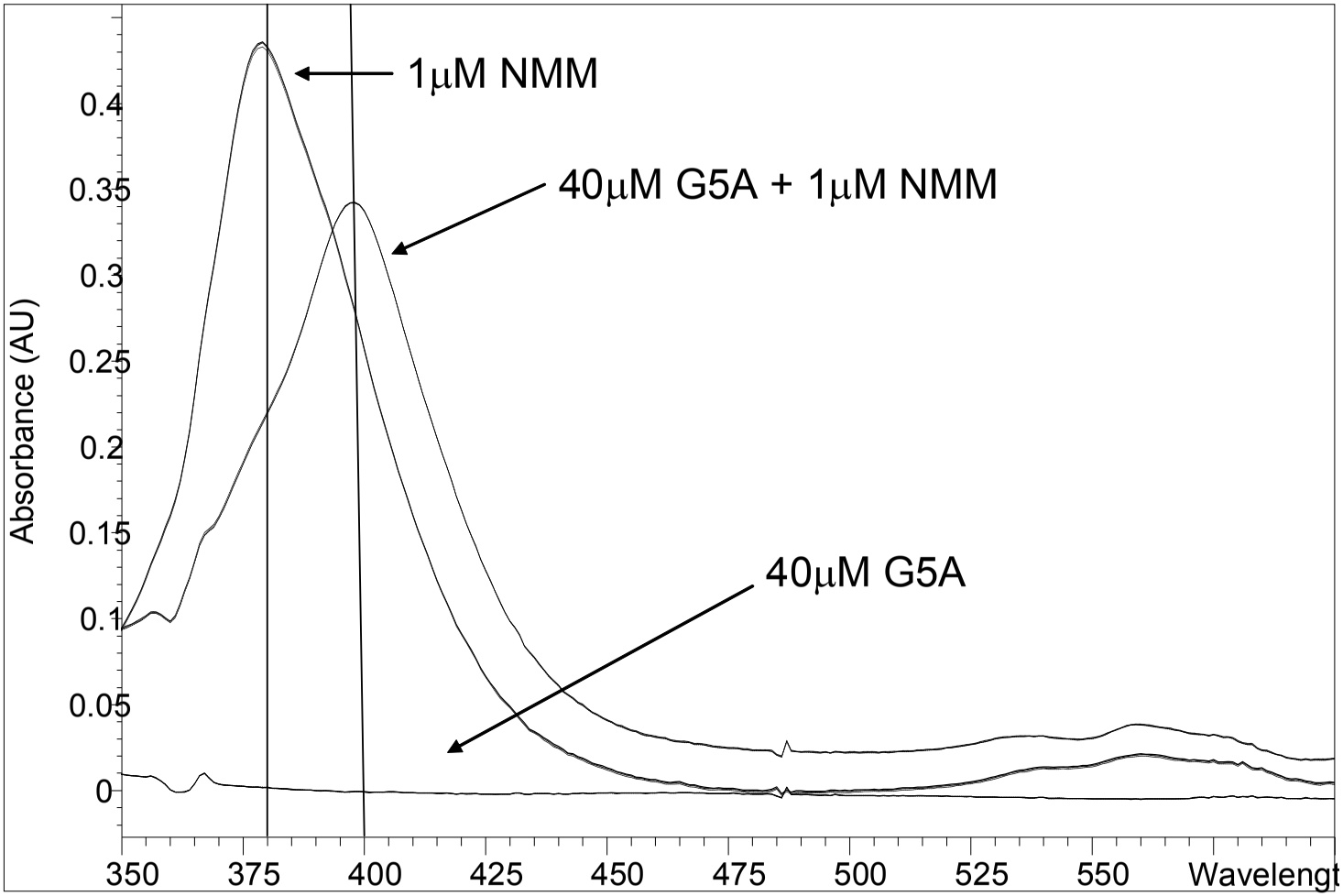

Figure 29: Detection of Quadruplex formation at 40μM DNA concentration

Quadruplex samples contained 40 μM DNA + 20 μM K^+ + 4 mM NaCaco Buffer

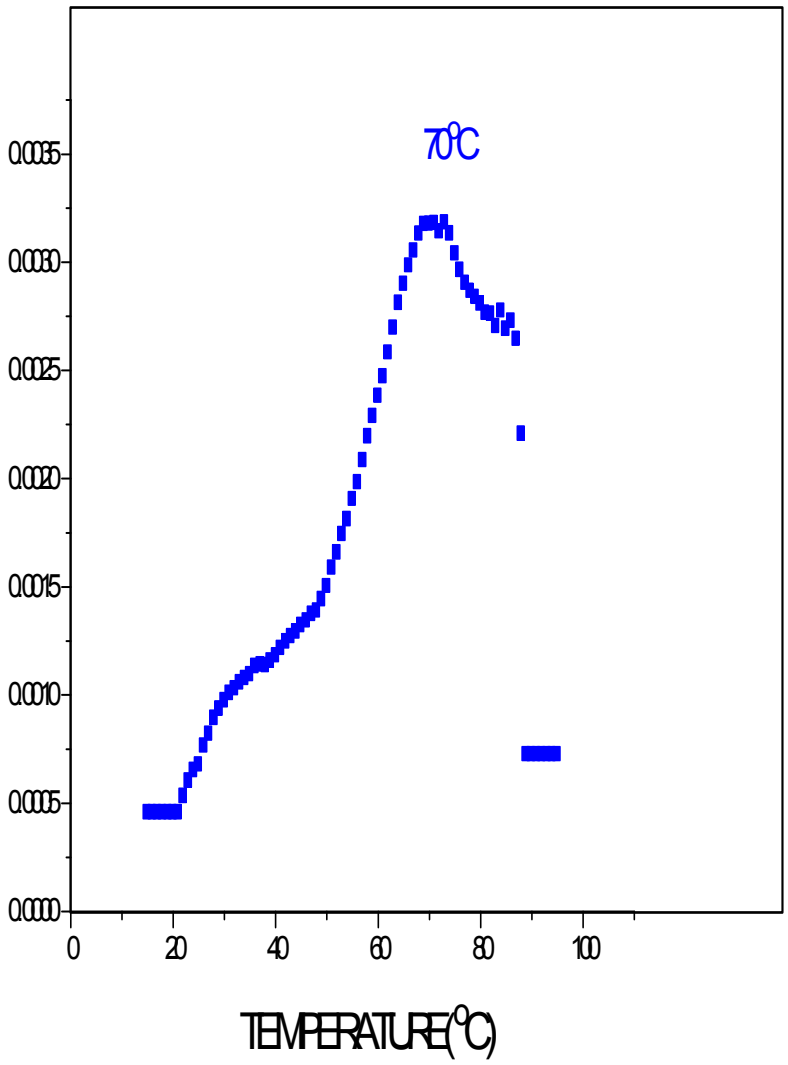

Figure 30: Melting Temperature Curve for 40µM Quadruplex DNA

Sample prepared with 40µM G5A + 20µM K^+ + 4mM Sodium Cacodylate Buffer; λ = 295nm

7.2 **PAGE analysis**

Once the complex was formed, the next big challenge we faced was with the resolution of the gels for the charge transport experiments. It was particularly challenging to get charge transport gels that clearly showed the damage closest to the labeled end. Most of the gels did not give good resolution between the guanines in the first GG step. They also did not show good resolution between the first GG step and the uncut DNA. This posed problems with the analysis of the duplex DNA regions of the complex.

References

1. Gellert, M., Lipsett, M.N., Davies, D. R., *Proc. Natl. Acad. Sci. USA* **1962**, 48, 2013-2018

2. Arnott, S., Chandrasekaran, R., Marttila, C. M., *Biochem. J.* **1974**, 141, 537-543

3. Zimmerman, S. B., *Biopolymers* **1975**, 14, 889-890

4. Zimmerman, S.B., Cohen, G.H., Davies, D.R., *J. Mol. Biol.* **1975**, 92, 181-192

5. Sun, D. B., Thompson, B., Cathers, B. E., Salazar, M., Kerwin, S. M., Trent, J. O., Jenkins, T. C., Neidle, S., Hurley, L. H., *J. Med. Chem*. **1997**, 40, 2113-2116

6. Chang, C., Kuo, I., Ling, I., Chen, C., Chen, H., Lou, P., Lin, J., Chang, T., *Anal. Chem.* **2004**, 76, 4490- 4494

7. Kerwin, S.M., Thomas, P.W., Kern, J.T., *Biochemistry* **2002**, 41, 11379-11389

8. Erlitzki, R., Fry, M., *J. Biol. Chem*. **1997**, 272, 15881-15890

9. Dempsey, L. A., *J. Biol. Chem.* **1999**, 274, 4474-4482

10. Fang, G., Cech, T.R., *Cell* **1993**, 74, 875-885

11. Giraldo, R., Rhodes, D., *EMBO J.* **1994**, 13, 2411-2420

12. Sun, H., Karow, J. K., Hickson, I. D., Maizels, N., *J. Biol. Chem.* **1998**, 273, 27587-27592

13. Fry, M., Loeb, L. A., *J. Biol. Chem.* **1999**, 274, 12797-12802

14. Liu, Z., Frantz, J. D., Gilbert, W., Tye, B. K., *Proc. Natl. Acad. Sci. USA* **1993**, 90, 3157-3161

15. Murchie, A. I., Lilley, D. M., *Nucleic Acids Res*. **1992**, 20, 49-53

16. Pecinka, P., Kubista, M., Simmonson, T., *Nucleic Acids Res.* **1998**, 26, 1167-1172

17. Sjoback, R., Simonsson, T., *J. Biol. Chem.* **1999**, 274, 17379-17383

18. Sen, D., Gilbert, W. *Nature* **1988**, 334, 364-366

19. Caskey, C. T., Pizzuti, A. Fu, Y. H., Fenwick Jr., R. G., Nelson, D. L., *Science* **1992**, 256, 784-789

20. Williamson, J. R., *Annu. Rev. Biophys. Biomol. Struct*. **1994**, 23, 703-730

21. Blackburn, E. H., *Cell* **1994**, 77, 621-623

22. Williamson, J.R., Raghuraman, M. K., Cech, R. T., *Cell* **1989**, 59, 871-880

23. Sundquist, W. I., Klug, A., *Nature* **1989**, 342, 825-829

24. Davis, J. T., *Angew. Chem. Int. Ed.* **2004**, 43, 668-698

25. Keniry, M., *Biopolymers* **2001**, 56, 123-146

26. Simonsson, T., *Biol. Chem.* **2001**, 382, 621-628

27. Hardin, C. C., Perry, A. G., White, K., *Biopolymers* **2001**, 147-194

28. Mergny, J. L., Helene, C., *Nature Med.* **1998**, 4, 1366-1367

29. Mergny, J. L., Mailliet, P., Lavelle, F., Riou, J. F., Laoui, A., Helene, C., *Anticancer Drug Des.* **1999**, 14, 327-339

30. Han, H., Hurley, L. H., *Trends Pharm. Sci*. **2000**, 21, 136-142

31. Zahler, A.M., Williamson, J.R., Cech, T.R., Prescott, D.M., *Nature* **1991**, 350, 718-720

32. Neidle, S., Reid, M. A., *Biopolymers* **2001**, 56, 195-208

33. Kim, N. W., Piatyszek, M. A., Prowse, K. R., Harley, C. B., West, M. D., Ho, P. L. C., Coviello, G. M., Wright, W. E., Weinrich, R. Shay, J. W., *Science* **1994**, 266, 2011-2015

34. Counter, C. M., Hirte, H. W., Bacchetti, S., Harley, C. M., *Proc. Natl. Acad. Sci USA* **1994**, 91, 2900-2904

35. Hermann, T., Patel, D. J., *Science* **2000**, 287, 820-825

36. Famulok, M., *Curr. Opin. Struct. Biol.* **1999**, 9, 324-329

37. Huizenga, D. E., Szostak, J. W., *Biochemistry* **1995**, 34, 656-665

38. Calzolari, A., Di Felice, R., Molinari, E., *App. Phys. Lett*. **2002**, 80, 3331-3333

39. Thorp, H. H. and Szalai, V. A., *J. Am. Chem. Soc.* **2000**, 122, 4524-4525

40. Delaney, S., Barton, J. K., *Biochemistry* **2003,** *42,* 14159-14165.

41. Prat, F., Houk, K. N., Foote, C. S., *J. Am. Chem. Soc.* **1998**, 120, 845-846

42. Takayama, M., Sugiyama, H., Nakatani, K., Tsuchida, A., Yamamoto, M., Saito, I., *J. Am. Chem. Soc.* **1995**, 117, 6406-6407

43. Arthanari, H., Basu, S., Kawano, T. L., Bolton, P. H., *Nucleic Acids Res.* **1998**, 26, 3724-3728

44. Reng, J., Chaires, J. B., *Biochemistry* **1999**, 38, 16067-16075

45. Fox, K. R., Risitano, A., *Org. Biomol. Chem*. **2003**, 1, 1852-1855

46. Zhang, X., Cao, E., Sun, X., Bai, C., *Chin. Sci. Bull.* **2000**, 45, 1959-1963

47. David, W. M., Brodbelt, J., Kerwin, S. M., Thomas, P. W., *Analytical Chemistry* **2002**, 74, 2029-2033.

48. Norman, D.G., Grainger, R.J., Uhrin, D., Lilley, D.M.J., *Biochemistry* **2000**, 39, 6317-6324

49. Bouaziz, S., Kettani, A., Gorin, H., Zhao, R., Jones, D. J., Patel, D., *J. Mol. Biol*. **1998**, 282, 619-636

50. Bouaziz, S., Kettani, A., Patel, D., *J. Mol. Biol*. **1998**, 282, 637-652

51. Voet, D., Voet, J.G., *Biochemistry*, 2nd Ed., John Wiley & Sons, Inc., 1995

PART 2: DNA PHOTOCLEAVAGE: VIOLOGEN LINKED ACRIDINIUM DERIVATIVES

CHAPTER 8: DNA PHOTOCLEAVAGE

The practical potential of compounds that can site specifically cleave DNA has generated a lot of efforts towards their development [1-15]. These compounds can be used as molecular probes for the detection of specific bases [16-18], sequences [1, 23] or structures [2-4] in DNA. Molecules that are photoactivated to cleave DNA (photocleavers) have been of particular interest due to their ability to initiate DNA cleavage at a distance and at a particular point in time [1-14]. These attributes make them desirable in nucleic acid diagnostics as compounds that have potential significance for antitumor and antiviral therapeutic endeavors [5, 6]. Photocleaving molecules have also been utilized as bioanalytical tools [7].

Photocleavers are defined as compounds that upon irradiation at a particular wavelength react with DNA in an electronically excited state resulting in DNA strand cleavage [8]. The cleavage could be direct or through a series of chemical reactions that ultimately lead to strand cleavage. Most photocleavers fall under the latter category [8]. In light of the larger work, it is important to clarify the difference between DNA cleavage and DNA damage. DNA cleavage refers to any alteration of DNA that leads to a distinguishable break in the DNA. While DNA damage refers to any alteration of DNA that can ultimately lead to mutations. This term is more inclusive as it includes DNA cleavage as well as other modifications such as altering the base pairing properties of bases.

As mentioned early, the main mechanisms for the initiation of DNA damage are hydrogen abstraction, singlet oxygen generation and electron transfer

[8, 19]. The desire for the development of site specific DNA photocleavers renders the hydrogen abstraction process an unfavorable choice due to its being a non specific process in DNA [8, 20].

Photocleaving agents predominantly utilize the either singlet oxygen mechanism or the electron transfer [21]. A lot of photocleavers formed from metal complexes and porphyrins are singlet oxygen generators because they tend to have sufficiently high triplex energy to generate singlet oxygen [8, 21]. Electron transfer agents have been shown to have some base selectivity [19]. The main challenges facing the development of photocleavers that use the electron transfer mechanism have been finding compounds that show both good cleavage efficiency, as well as selective DNA cleavage [22].

There are certain attributes that are desirable for a good photocleaving agent. For example, it must show specific DNA cleavage [9]. This limits the occurrence of potentially hazardous side effects from cleavage at sites other than the desired site of cleavage. Although most photocleavers have been shown to have either preferential damage for certain DNA structures [2-4] or base selective damage [16-18], they have not shown much sequence specificity. Photocleavers that show sequence specificity would be desirable for drug design efforts. Another important feature that a good DNA photocleavage agent should have is good cleavage efficiency [22]. Its excitation wavelength should exceed 300nm to avoid ubiquitous damage of DNA and proteins which absorb below this wavelength [23]. Furthermore, the photocleaver should not be consumed in the cleavage process [8].

Numerous photocleaving agents have been designed in attempts to develop good photocleaving agents that have most of these features [1-14]. For example, Sessler and colleagues invented oligonucleotide-texaphyrin conjugates that site specifically cleave both single stranded and double stranded DNA [1]. The oligonucleotide in the oligonucleotide-texaphyrin conjugates introduces sequence specificity by binding to its complementary sequence in the DNA. Also, Amino-p-quinacridine compounds specifically bind and photocleave triplex DNA structures by direct electron transfer between the quinacridine and guanine bases [3]. Some porphyrins effectively photocleave non duplex structures such as three way junctions [3, 10], and quadruplex DNA structures [11]. Also, anthraquinone derivatives have been developed that selectively cleave the bulge regions of hairpins [4].

As mentioned earlier, photocleaving agents that utilize the electron transfer mechanism offer their own challenges. They are also often inhibited by fast BET between the reduced photocleaver and the oxidized base [24]. This strongly competes with the forward photocleaving reaction in DNA leading to low DNA cleavage efficiency. In attempts to circumvent this problem, the co-sensitization method was developed [24]. This method involves covalently binding a co-sensitizer (electron acceptor) to a photocleaving agent (sensitizer). Upon excitation, the photocleaving agent transfers an electron to the co-sensitizer and then oxidizes an adjacent base. This creates a charge separated complex between the oxidized base and the reduced co-sensitizer, which should preferably exist long enough for DNA to undergo the reactions that ultimately lead to strand

cleavage. Therefore, the charge separated complex inhibits BET long enough to enable more DNA cleavage to occur.

Another problem associated with electron transfer agents is the relative absence of cleavage selectivity. Although electron transfer agents show selectivity for guanine bases, it has been challenging to develop photocleavers that show cleavage selectivity that goes beyond this using this mechanism [8].

CHAPTER 9: VIOLOGEN LINKED ACRIDINE DERIVATIVES

Our research in this area sought to develop a DNA photocleaving agent that overcame the problems associated with photocleaving agents that use the electron transfer mechanism. In order to do so, a sensitizer and a co-sensitizer pair were chosen. Acridine, a compound that is best known for its antibacterial, antiprotozoal and anticancer attributes was selected as the sensitizer [25, 26]. It was chosen due to its good DNA intercalating ability and its electron donating ability. Viologen was selected as the co-sensitizer. It is often used for electrochemistry experiments due to its ability to color upon reduction and bleach upon oxidation [27]. Viologen is also a widely used electron acceptor in photochemical experiments, and is therefore well characterized in this role [28-30]. Viologen linked acridine derivatives were designed in order to optimize their DNA binding and DNA photocleaving capabilities. This was achieved by linking the electron donor, acridine, to the electron acceptor, viologen (see Figure 31). The acridine moiety served as the photocleaving agent which upon excitation could transfer an electron to the viologen moiety. The resultant radical cation of acridine would then oxidize the DNA bases subsequently leading to DNA cleavage. Alternatively, electron transfer could occur from the DNA base to the excited acridine, resulting in a radical anion of the acridine. This moiety could then transfer an electron to the viologen leading to the formation of a charge separated radical cation of viologen. The spacer length between the two moieties was varied to determine the optimal length for the most efficient DNA cleavage.

Monofunctional Derivatives

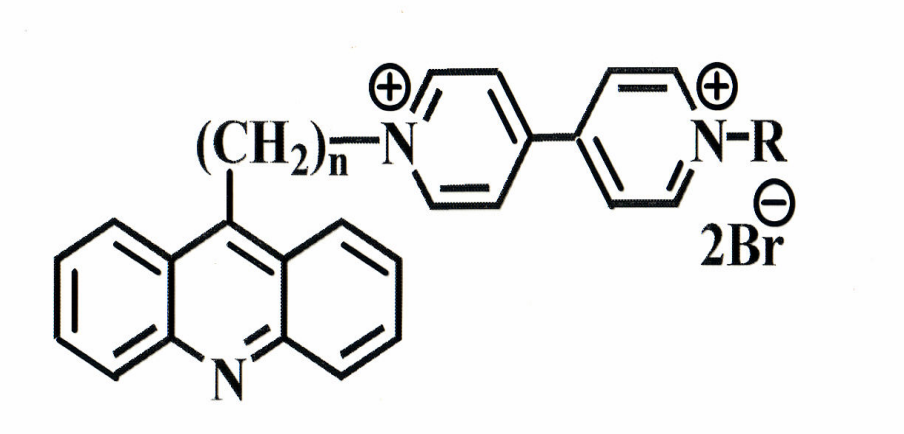

n*	Monofunctional	Bifunctional
1	M1	B1
3	M3	B3
11	M11	B11

** n = number of carbons*

Bifunctional Derivatives

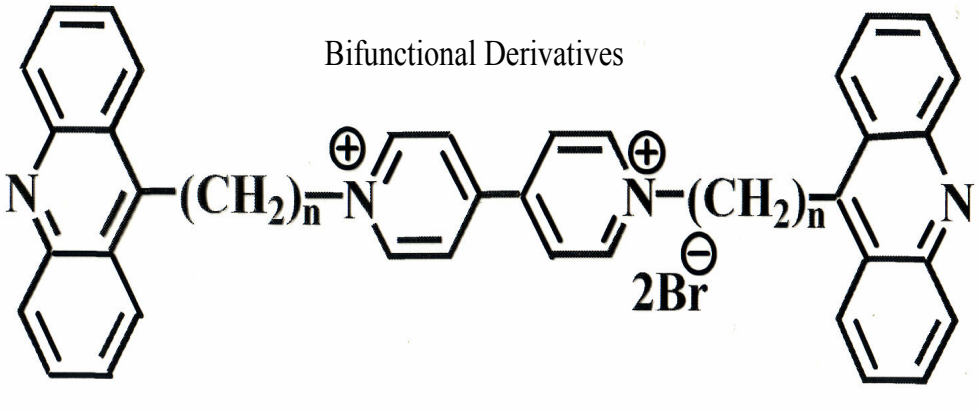

Figure 31: Viologen linked Acridine Derivatives

Ramaiah and colleagues performed the photophysical characterization of the viologen linked acridine derivatives [31]. They were unable to observe the reduced viologen radical cation in the absence of an external donor (such as DNA) due to rapid BET. However, in the presence of DNA, they observed its formation which suggested they were able to prolong the lifetime of the charge separated species through the co-sensitization method. They also found that the viologen linked derivatives (ligands) induced modifications to the DNA that were from guanosine oxidation. This selectivity for guanine is common in electron transfer mechanisms as guanine has the lowest oxidation potential of the four bases [32, 33] and is therefore most easily oxidized (see Table 3).

In light of this, our research sought to determine whether any of the viologen linked derivatives showed any specificity for GGG bulge regions over GG regions in duplex DNA.

Table 3: Oxidation Potentials of DNA bases[33]

Base	Oxidation Potential (V) vs. NHE
Thymidine	1.7
Cytidine	1.6
Adenosine	1.42
Guanosine	1.29

CHAPTER 10: EXPERIMENTAL

General: The oligonucleotides were synthesized on an Applied Biosystems DNA synthesizer, and purified by reverse phase HPLC on a Dynamax C18 column. The DNA sequences that were analyzed are shown in Table 4. The DNA sequences were labeled with radioactive isotope [$^{\gamma-32}$P- ATP] using *T4 polynucleotide kinase* (T4-PNK). Electron spray ionization (ESI) mass spectrometry was used to confirm the oligomers' purity. The concentrations of the oligomers were determined on an UV spectrophotometer and monitored at an absorbance wavelength of 260nm. The extinction coefficients of the oligonucleotides were obtained from an online biopolymer calculator. UV-Vis melting and cooling experiments were performed on a Cary 1E spectrophotometer. Circular Dichroism (CD) spectra were obtained on a Jasco 720 spectropolarimeter. The viologen linked acridine derivatives that were used are shown in Figure 31. They were synthesized and purified by Ramaiah and colleagues [31].

Table 4: DNA Sequences Used

	Sequence
Duplex	5’ CAC TGG CTT TTC GGT GCA T 3’ 5’ ATG CAC CGA AAA GCC AGT G 3’
GGG Bulge	5’ CAC TGG CTT **GGG** TTC GGT GCA T 3’ 5’ ATG CAC CGA AAA GCC AGT G 3’

Circular Dichroism (CD): The formation of the proper molecular structure of the DNA in the presence of the ligands was monitored by CD spectroscopy. Each sample was prepared in a 10 mM sodium phosphate buffer solution (pH=7) with a 2.5 μM DNA oligomer concentration, and 7.5 μM concentration of one of the ligands (3:1 ligand to DNA duplex ratio). The CD experiments were performed at room temperature. Five CD scans were averaged to obtain the average spectra at a recording rate of 200nm/min.

UV Melting Experiments: Samples with lower ligand concentrations comprised of 2.5 μM DNA oligomers in 10mM sodium phosphate buffer solution (pH =7) with 7.5 μM ligand concentrations (3:1 ligand to DNA duplex ratio), while samples with higher ligand concentrations comprised of 2 μM DNA oligomers in 10mM sodium phosphate buffer solution (pH =7) with 15 μM ligand concentrations (7.5:1 ligand to DNA duplex ratio). They were placed in cuvettes with 10 mm pathlengths, and monitored at absorbance wavelengths of 260 nm (DNA absorbance) and 360 nm (ligand absorbance). The samples were ramped twice from 15 – 90 ^{o}C, and 90 -15 ^{o}C, and the UV-Vis absorbance was recorded every 0.5 ^{o}C/min. The melting temperature (T_m) was obtained from the maxima of the first derivative plot of absorbance versus temperature.

DNA Photo-cleavage Analysis by PAGE: Samples were radiolabeled by incubating T4 PNK, [$^{\gamma - 32}$ P- ATP], and 25μM DNA at 37^{o}C for 45 minutes. The samples were suspended in 10μL of loading dye, then loaded onto a 20%

purification gel. The gel was run for 1.5 hours at 400 watts. Purified DNA was cut from the gel and placed in 750μL elution buffer, and incubated overnight at 37^{o}C. The DNA was precipitated by the addition of 750μL of 100% ethanol and 1μL glycogen to the vials, and stored at -80^{o}C for 4 hours. The vials were then centrifuged at 13000 RCF for 30 minutes. After decanting the eluent, 100μL of 80% ethanol was added to the vials and centrifuged for 5 minutes. The 80% ethanol wash was repeated, and the samples were dried. Hybridization samples were prepared in the presence of 10mM sodium phosphate buffer with 2μl of labeled DNA and 5μM unlabelled DNA oligomer concentrations. The ligand concentration that was used was 37.5 μM (7.5:1 Ligand to DNA duplex ratio). The samples were then heated to 90^{o}C for 5 minutes and allowed to equilibrate to room temperature. Irradiation of hybridized samples was performed for 3 hours using a Rayonet photoreactor with eight 360nm lamps. The precipitated samples were then piperidine treated in the presence of 1M piperidine for 30 minutes at 90^{o}C. After evaporating the piperidine and performing two water washes, the samples were dried and suspended in loading buffer. Samples with 3000 CPM were analyzed on a 20% polyacrylamide gel. The DNA cleavage was revealed by an autoradiography and quantified by a Fuji phosphorimager.

CHAPTER 11: RESULTS

11.1 Circular Dichroism Analysis

Circular dichroism (CD) enables the structural characterization of chiral molecules. It has been widely used to structurally characterize biomolecules such as DNA, proteins and lipids. The CD spectroscopy showed that the ligands did not disrupt the duplex DNA structure. This was shown by the presence of characteristic B-form DNA peaks with ~280nm and a negative peak at ~250nm (see Figure 32) [33]. Although the ligands interacted with the DNA they caused very small perturbations to the overall DNA structure. All the ligands showed similar CD spectra as for **B3**. The GGG bulge did not disrupt the overall B form structure of the DNA (with or without the ligands).

11.2 DNA Melting Behavior in presence of Viologen linked acridine derivatives

In order to determine whether the viologen linked derivatives bound to DNA as anticipated in their design, we performed some melting temperature experiments. The melting studies enabled us to determine whether the ligands bound to DNA by the increase/decrease of the melting temperature (temperature at which half of the DNA is double stranded and other half is single stranded) upon the consecutive addition of each ligand to DNA.

Table 5: Tm Data for Viologen linked acridine derivatives

	No Ligand	M1	M3	M11	B1	B3	B11
2uM Duplex DNA (1:7.5)	53	69.4	68	65	76	71	56
GGG Bulge DNA (1:7.5)	27	39	54	56	37	49	40
2.5uM Duplex DNA (1:3)	51	52	50	54	56	55	51
GGG Bulge DNA (1:3)	29	51	51	40	53	48	39

We found that at lower ligand concentrations (1:3 DNA duplex to ligand ratio), the viologen linked derivatives had little effect on duplex DNA stability (see Table 5, and Figure 33). The most stabilizing ligand at this concentration was the bi-functional derivative **B1** which stabilized the DNA by 5 ^{o}C. However, at higher ligand concentrations (1: 7.5 DNA duplex to ligand ratio), we found that although ligand **B11** had a negligible effect, the other ligands had strongly stabilizing effects on duplex DNA (see Table 5). Similar to the results obtained at lower ligand concentration, the most stabilizing ligand was **B1** which stabilized the DNA by 23 ^{o}C. The most stabilizing mono-functional derivative was **M1** which stabilized DNA by 16 ^{o}C. The stabilizing effect appeared to correlate with the linker length as the derivatives with the longest linkers were the least stabilizing and vice versa. This trend was apparent for both

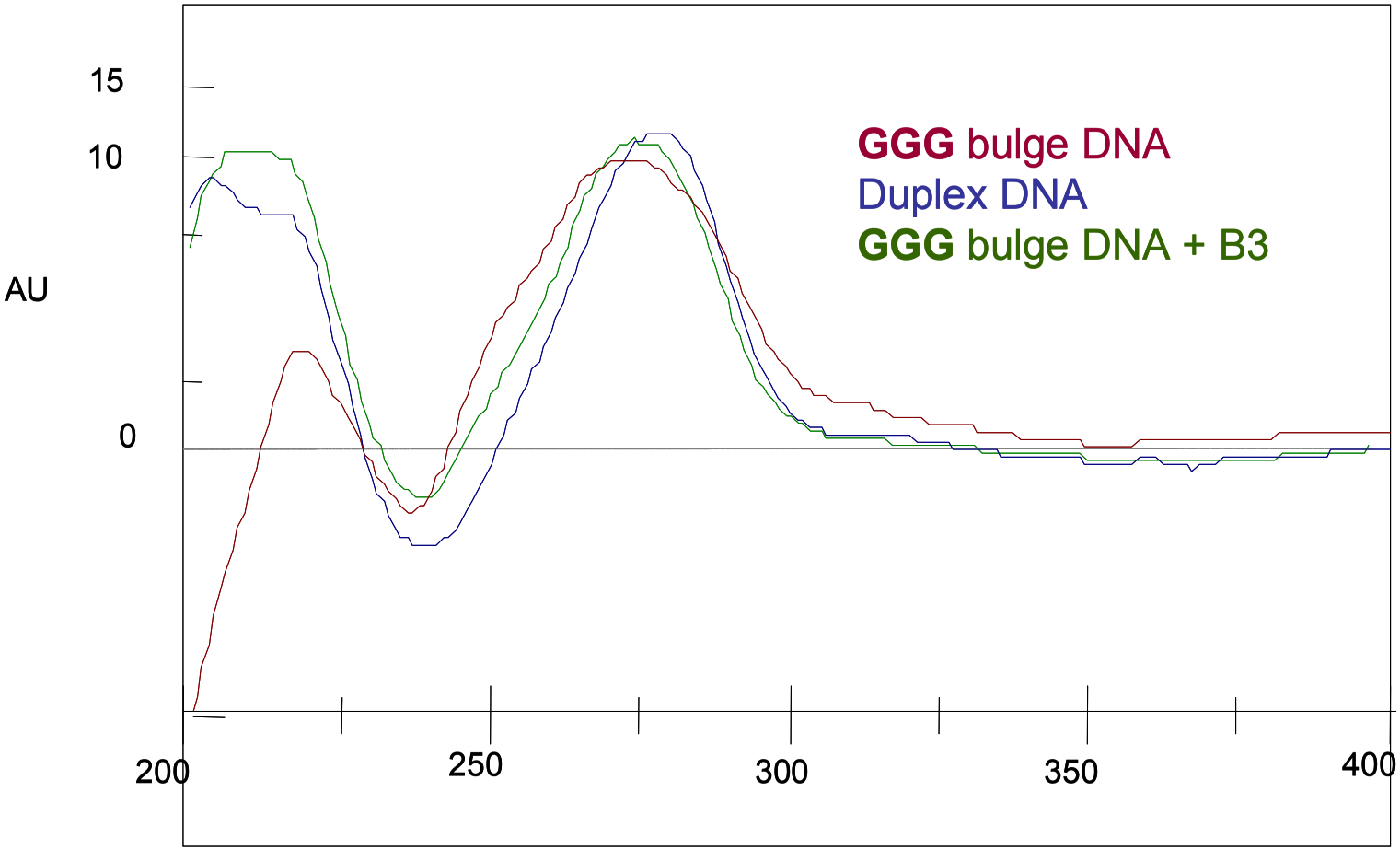

Figure 32: CD Comparison (1:7.5 DNA to Ligand ratio)

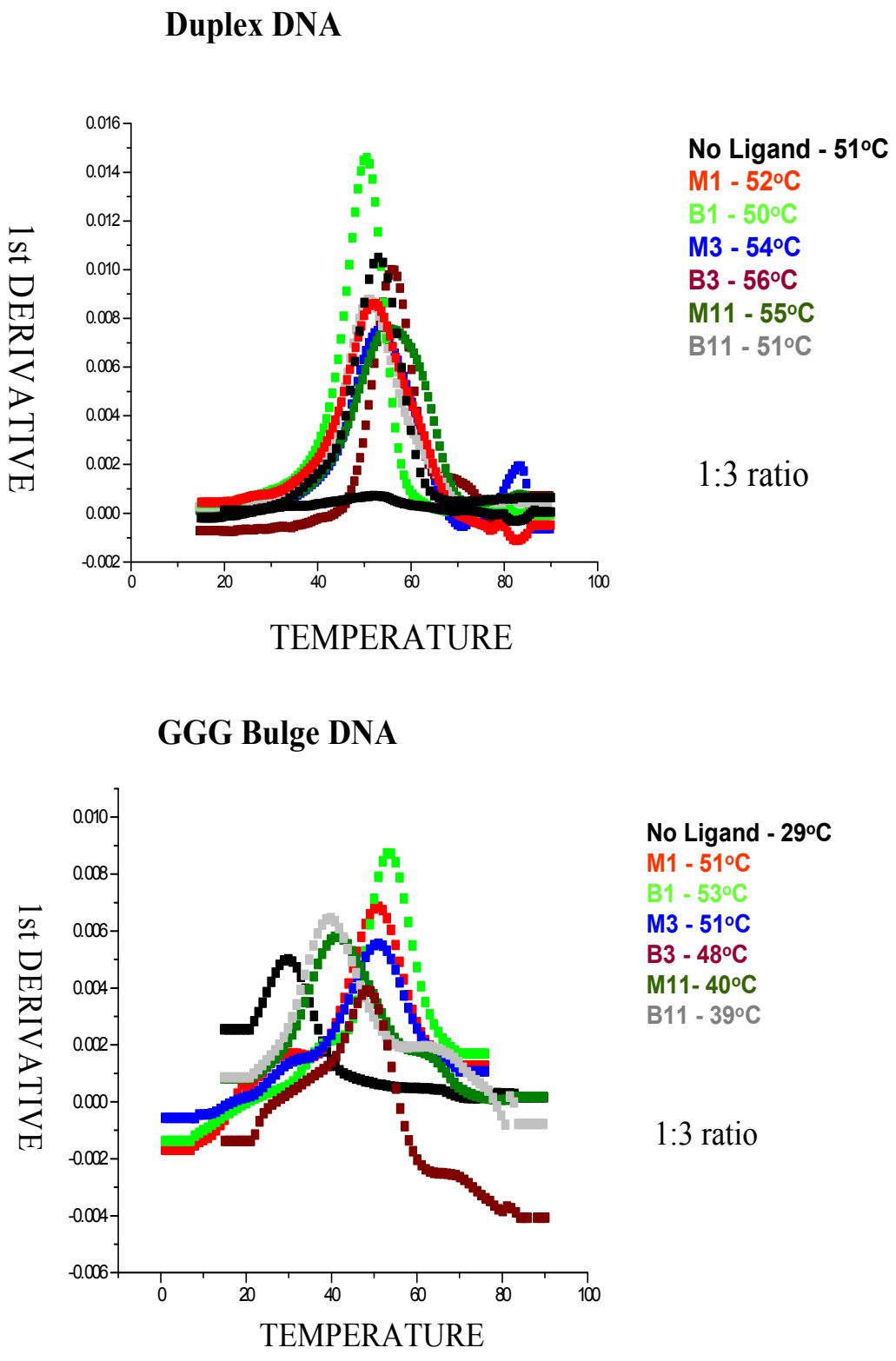

Figure 33: Tm Analysis for Viologen linked Acridine Derivatives

the mono and bi-functional derivatives at higher ligand concentrations for duplex DNA. In contrast, we found that incorporating the GGG bulge into duplex DNA destabilized the DNA by an average of 24^{o}C (see Table 5).

Further, at lower ligand concentrations (1:3), the viologen linked derivatives all showed stabilizing effects on GGG bulge DNA (see Table 5). The most stabilizing ligand was **B1** which stabilized the GGG bulge DNA by 24 ^{o}C. For the mono-functional derivatives, the most stabilizing ligands were **M1** and **M3** which both stabilized GGG bulge DNA by 22 ^{o}C. The least stabilizing ligand was **B11** which stabilized the bulge DNA by 10 ^{o}C. Generally, the derivatives with shorter linkers were the most stabilizing at this concentration. We also found that at higher ligand concentrations (1:7.5) all the ligands stabilized the GGG bulge DNA. However, the most stabilizing ligand was **M11** which stabilized the GGG bulge DNA by 29 ^{o}C, and the least stabilizing ligand, **B1**, stabilized the GGG bulge DNA by 10 ^{o}C. Unlike in the previously mentioned experiments, the derivatives with the shortest linkers were the least stabilizing at higher ligand concentrations for GGG bulge DNA.

11.3 PAGE analysis of DNA Photocleavage

Polyacrylamide gel electrophoresis (PAGE) is a popular analytical technique for the characterization of DNA cleavage. It enables the separation of the resultant DNA fragments by their relative size and charge. This reveals the cleavage points as well as the cleavage pattern formed as a result of the probe used. The analysis of the cleavage patterns illuminates the characteristic of the probe. It shows whether the probe shows any selectivity or preferential cleavage

for any of the bases or positions within the DNA. The denaturing PAGE for the ligands showed that they all induced more damage at guanine bases, than at any other bases (see Figure 34). All the guanine residues in the oligomer were cleaved irrespective of whether they were in duplex or GGG bulge regions. The ratios of average photo-damage counts between the GGG bulge domain and the 5' and 3' GG duplex DNA domains showed that there was little or no selectivity for the GGG bulge domain over the GG duplex domains (see Table 6). Therefore although the ligands preferentially cleaved guanine bases they were unable to distinguish between the guanines within the two structural environments.

Table 6: Photocleavage Analysis Data

Ligand	GGG/3' GG	GGG/5' GG
M1	1.5	1.8
M3	1.3	2.1
M11	1.4	1.4
B1	1.3	1.3
B3	1.0	1.1
B11	2.3	2.9

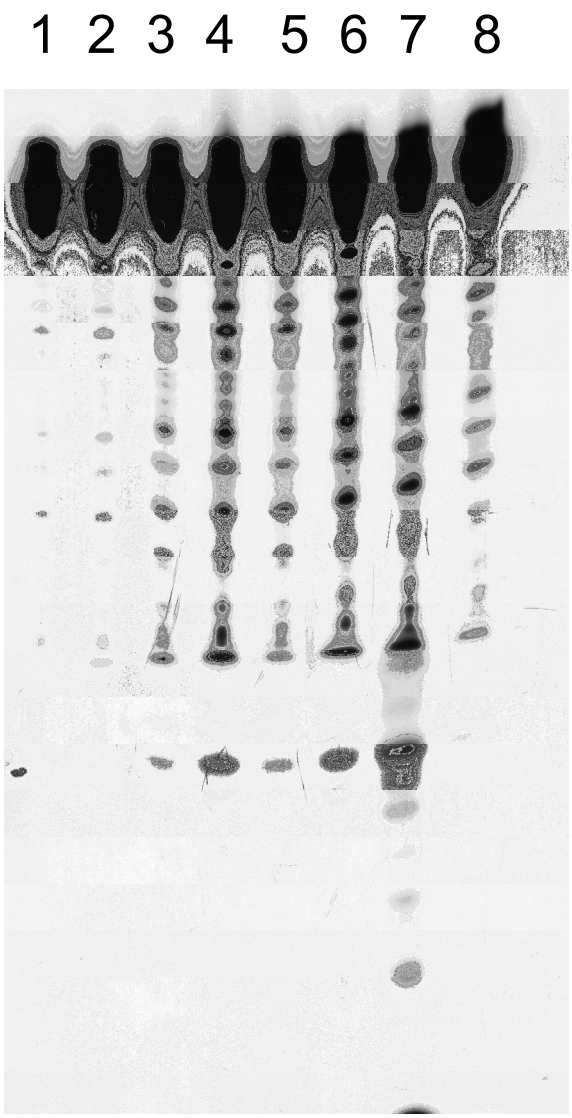

Figure 34: DNA Photocleavage analysis

All the samples were prepared with 5 μM DNA duplex in 10 mM sodium phosphate buffer. *Lane 1* – Dark control (no irradiation or ligand present); *Lane 2* - Light control (Irradiation without any ligand present); *Lane 3* –Irradiated with 37.5 μM **M1** (1: 7.5 DNA duplex to ligand ratio); *Lane 4* - Irradiated with 37.5 μM **M3** (1: 7.5 DNA duplex to ligand ratio); *Lane 5* - Irradiated with 37.5 μM **M11** (1: 7.5 DNA duplex to ligand ratio); *Lane 6* - Irradiated with 37.5 μM **B1** (1: 7.5 DNA duplex to ligand ratio); *Lane 7* - Irradiated with 37.5 μM **B3** (1: 7.5 DNA duplex to ligand ratio) ; *Lane 8* - Irradiated with 37.5 μM **B11** (1: 7.5 DNA duplex to ligand ratio)

CHAPTER 12: CONCLUSION

The introduction of different compounds to DNA has a range of effects on its overall structure. Some compounds have little or no effect on DNA structure, however, there are compounds that have disruptive effects on the DNA. These compounds distort the normally B-form conformation of DNA. The distortion could extend as far as causing the DNA to denature and lose its duplex structure. Therefore, the analysis of a ligand's interaction with DNA is an important control to perform. Circular Dichroism is one of the most effective tools for analyzing ligand interactions with DNA. Our experiments showed us that the ligands did not disrupt the B form structure of DNA. They showed that the overall DNA structure remained B form even in the presence of both the GGG bulge and each of the ligands.

It is generally accepted for electron transfer experiments that the distance between donors and acceptors affects the amount of reaction that occurs. As a result, a lot of photocleaving agents that have been developed for DNA attempt to localize the agents to the DNA by seeking to enhance their DNA binding ability. Similarly, the viologen linked derivatives were developed with their DNA binding ability in mind. Comparison of the GGG bulge DNA melting temperature data and the photocleavage results suggest that the ligands ability to bind with DNA somehow affects its cleaving ability. For example, ligand B11 had the lowest melting stability (Table 5) as well as the least photocleaving ability (see Figure 34).

Despite the fact that ligand **B11** showed the most selectivity for GGG bulge over the GG duplex region, all the viologen linked derivatives showed little selectivity for the GGG bulge over the GG duplex region (Table 6). This means that the viologen linked derivatives preferentially cleave guanines but do not have preferential preference for either single stranded bulge areas or double stranded duplex regions. Therefore these derivatives behave like other electron transfer agents used for charge transport studies in DNA. However, their relatively long irradiation times (3 hours) do not make them the most ideal photosensitizers for these studies. These long irradiation times suggest that the viologen linked acridine derivatives were not efficient photocleaving agents.

Another avenue to pursue could be to observe whether these derivatives specifically target other more structured single stranded regions such as guanine rich hairpins or stem-loops [34]. The specific binding of these derivatives to such structured regions could localize the damage to mostly one place. This could possibly introduce structural specificity for these viologen linked acridine derivatives. Furthermore, the derivatives could be covalently attached to sequences that are complementary to the targeted sequence, localizing the photosensitizer to the GGG bulge. This could further enhance the specificity of these viologen linked acridine derivatives for the certain guanine rich regions.

The challenges of developing photocleaving agents that show both DNA selectivity and efficient cleavage need to be addressed in order to harness the therapeutic potential of these molecules. Although the co-sensitization method assists with minimizing BET, this does not guarantee that the cleavage efficiency

of the ligands will be substantially enhanced. Therefore, a lot more work needs to be done to determine the best way to optimize the photocleaving ability of electron transfer agents.

References

1. Mody, T. D., Fu, L., Sessler, J. L., *Progress in Inorganic Chemistry,* John Wiley & Sons, New York, 2001, 49, 551-598

2. Martínez, L. and Chignell, C. F., *J. Photochem. Photobiol. B: Biol.* **1998**, 45, 51-59

3. Teulade-Fichou, M., Perrin, D., Boutorine, A., Polverari, D., Vigneron, J., Lehn, J., Sun, J., Garestier, T., and Helene, C., *J. Am. Chem. Soc.,* **2001**, 123, 9283-9292

4. Henderson, P. T., Armitage, B., Schuster, G. B., *Biochemistry* **1998,** 37, 2991-3000

5. Ochsner, M., *J. Photochem. Photobiol. B* **1997**, 39, 1-18

6. Sutedja, T. G., Postmus, P. E., *J. Photochem. Photobiol. B* **1996**, 36, 199-204

7. Briener, K. M., Daugherty, M. A., Oas, T. G., Thorp, H. H., *J. Am. Chem. Soc*. **1995**, 117, 11673-11679.

8. Armitage, B., *Chem. Rev.* **1998,** *98,* 1171-1200

9. Zhou, C., *J. Photochem. Photobiol. B: Biol.* **1989**, 3, 299-318

10. Klecak, G., Urbach, F., Urwyler, H., *J. Photochem. Photobiol. B: Biol.* **1997**, 37, 182-187

11. Nussbaum, J. M., Newport, M. E. A., Leontis, N.B., *Photochem. Photobiol*. **1994**, 59, 515-528

12. Morgan, A. R., *Curr. Med. Chem.*, **1995,** 2, 604-615

13. Bonnett, R., *Chem. Soc. Rev*., **1995**, 24 , 19-33

14. Armitage, B., Yu C., Devadoss, C., Schuster G. B., *J. Am. Chem. Soc.* **1994**, 116, 9847-9859

15. Kappen, L. S.; Goldberg, I. H., *Biochemistry* **1993,** 32, 13138-13145

16. Lee, S. H., Goldberg, I. H., *Biochemistry* **1989**, 28, 1019 – 1026

17. Sugiura, Y, Uesawa, Y, Takahashi, Y, Kuwahara, J., Golik, J., Doyle, T. W., *Proc. Natl. Acad. Sci*. **1989**, 86, 7672 -7676

18. Stubbe, J., Kozarich, J. W., *Chem. Rev.* **1987**, 87, 1107-1136

19. Kochevar, I., Dunn, D. A., *Biorg. Photochem*. **1990**, 1, 273-315

20. Pogozelski, W. K., Tullius, T. D., *Chem. Rev*. **1998**, 98, 1089-1107

21. Da Ros, T., Spalluto, G., Boutorine, A. S., Bensasson, R. V., Prato, M., *Curr. Pharm. Des.* **2001**, 7, 1781-1821

22. Paillous, N, Vincendo, P. J., *J. Photochem. Photobiol. B* **1993**, 20, 203-209

23. Boutorine, A. S., Brault, D., Takasugi, M., Delgado, O., Helene, C., *J. Am. Chem. Soc.* **1996**, 118, 9469-9476

24. Dunn, D. A., Lin, V. H., Kochevar, I. E., *Biochemistry* **1992**, 31, 11620-11625

25. Denny, W. A., *Curr. Med. Chem.* **2002**, 9, 1655-1665

26. Su, T., *Curr. Med. Chem.* **2002**, 9, 1677-1688

27. Martin, S., Cea, P., Gascon, I., Lopez, M. C., Royo, F.M., *J. Electrochem. Soc.* **2002**, 149, E402-E407

28. Knapp, C., Lecomte, J., Kirsh-De Mesmaeker, A., Orellana, G., *J. Photochem. Photobiol. B* **1996**, 36, 67-76

29. Udal'tsov, A. V., *J. Photochem. Photobiol. B* **1997***,* 37, 31-39

30. Kelley, S. O., Orellana, G., Barton, J. K., *J. Photochem. Photobiol. B* **2000**, 58, 72-79

31. Joseph, J., Nadukkudy, E. V., Ramaiah, D., *Chem. Eur. J*. **2003**, 9, 5926-5935

32. Burrows, C. J., Muller, J. G., *Chem. Rev.* **1998**, 98, 1109-1151

33. Vasmel, H., Greve, J., *Biopolymers* **1981**, 20, 1329-1332.

34. Mitas, M., *Nucleic Acids Res.* **1997**, *25*, 2245-2253.

PART 3: CHARGE TRANSPORT IN M-DNA

CHAPTER 13: CONDUCTING PROPERTIES OF DNA

Fifteen years after the first article re-proposing that DNA was a conducting molecular wire was published [1, 2], the question of its conducting nature remains largely unresolved. Several attempts have been made to ascertain whether DNA is a conductor [1- 4], or a semi-conductor [5, 6] or even an insulator [7]. The results of these attempts spread across the whole spectrum of possibilities. Some of the results support the initial work suggesting that DNA is a conductor, while other results suggest that DNA is a semi-conductor. The rest of the results suggest that DNA is an insulator. A lot of factors, such as differing techniques, equipment, DNA sequences and experimental setups, have contributed to this conflict. Interest in this area has been spurred on by the potential use of DNA as a molecular wire in microelectronic devices [8].

DNA has been set apart from other biomolecules and considered as a conducting molecular wire due to the overlapping electron orbitals within its structure. The planar aromatic bases stack over each other within double stranded DNA, forming ladder-like rungs. The stacks are stabilized by hydrophobic interactions between neighboring bases. These interactions involve the overlapping of the π electron orbitals from adjacent bases. In theory, these π electron stacks could potentially serve as a conduction path along DNA. This form of interaction is found in many one dimensional molecular conductors such as TTF-TCNQ [9, 10].

As a result, considerable efforts have been pursued to determine the extent of DNA's conducting nature [1-7, 11]. The work that re-ignited interest in this area fifteen years ago found that the fluorescence produced from an excited molecule was quenched when attached to a DNA molecule [2]. They suggested that the charge on the excited donor molecule moved along the length of a DNA molecule to an acceptor molecule. This implied that DNA was a conducting material. Another supporting article demonstrated that DNA was a conductor by directly measuring the resistance of thin bundles of DNA [3]. They showed that these DNA bundles had a low resistance and were ohmic conductors.

On the other hand, work performed on poly(dG).poly(dC) and poly(dA).poly(dT) DNA sequences showed that DNA had semi-conducting behavior [6]. It also showed that poly(dG).poly(dC) was a better conductor than poly(dA).poly(dT). Another research group also performed their measurements on poly(dG).poly(dC) sequences and found they were large gap semiconductors [5]. They later showed that at lengths greater than 40 nm, DNA was an insulator (no conduction was observed) [7]. Different substrate types, distances between electrodes and the contact materials were used in all these experiments.

In light of these conflicting results, questions still remain on the electronic properties of DNA. Depending on the experimental conditions used, different results were obtained. Therefore, more effective modes of analysis are necessary to address this conflict, and finally resolve the question of DNA's electronic properties.

CHAPTER 14: CHARACTERISTICS OF M-DNA

As mentioned earlier, DNA is able to form several different conformations [12-16]. These conformations are induced by sequence or environmental effects on the DNA. The most common conformation of DNA is the B form DNA which is formed under hydrated conditions. This conformation has been confirmed by both NMR [17] and x-ray crystallography [18]. Other conformations of DNA, which were addressed earlier, are variations from B-form DNA. These variations are induced by specialized conditions such as dehydration (A form), high salt concentrations (Z form), or at a particular humidity (C form). They can be subtle changes such as changes in the base pairs per turn, or global changes such as changes in the overall handedness of the DNA molecule.

Over 10 years ago, a new conformation was proposed for DNA [19]. This conformation was referred to as M-DNA. The specialized conditions for its formation were at a pH above 8 in the presence of some divalent metal cations. The metal cations that induced the formation of M-DNA were transition metals such as Zn^{2+}, Co^{2+}, Ni^{2+}. Unlike the transition metals, they found that divalent alkaline earth metals, such as Mg^{2+} and Ca^{2+}, did not induce the formation of M-DNA under basic conditions. The formation of M-DNA was easily reversed by the addition of a metal chelating agent, such as EDTA. Another distinguishing feature of M-DNA from B form DNA was its inability to bind ethidium. Based upon this feature, they monitored M-DNA's formation by monitoring the quenching of ethidium fluorescence upon M-DNA formation.

They later proposed that M-DNA behaved like a molecular wire [20]. This was based upon some fluorescence experiments that showed 95% quenching of a fluorescein donor attached to a 20 base pair duplex with a rhodamine quencher labeled to the other end of the same strand. They suggested that M-DNA containing both the π electron stacks found in B form DNA, and interchelated metal ions located between the base pairs behaved like a conductor. They performed fluorescence lifetime experiments on this conformation which showed the presence of a fast component in the decay kinetics. This component was not observed for similar experiments with B form DNA. They concluded that the fast component was from electron transfer between the donor and M-DNA.

Extensive studies on charge transport in B form DNA have been performed to determine the mechanism of long range charge transfer in DNA [21-30]. These studies have shown that DNA is able to migrate over long distances through discrete hops along the DNA. These hops involve the delocalization of charge over a distorted segment of several base pairs. A DNA molecular wire would be expected to have extensive electronic overlap that extends over much larger DNA distances. It should show very little distance dependence. Contrary to this, most of the earlier charge transport studies show distance dependence in B DNA conformations [21, 23]. Based upon these studies, most B DNA sequences do not behave as molecular wires. Therefore, we sought to characterize the effects of long range charge transport in a molecular wire (M-DNA), and compare this to the effects of long range charge transport in B DNA.

CHAPTER 15: EXPERIMENTAL

Materials: Radioactive isotope $^{\gamma\text{-}32}$P-ATP was purchased from Amersham Biosciences. The enzyme, *T4 polynucleotide kinase* (T4-PNK), was purchased from New England Biolabs and stored at -20º C. Granular zinc chloride and Tris HCL were purchased from JT Baker**.** All other chemicals were ultra pure grade from Sigma-Aldrich. The oligonucleotides were synthesized on an Applied Biosystems nucleic acid synthesizer, and purified by reverse phase HPLC on a Dynamax C18 column. The DNA sequences that were analyzed are shown in Table 7. Electron spray ionization (ESI) mass spectrometry was used to confirm the oligomers' purity. The concentrations of the oligomers were determined on an UV spectrophotometer and monitored at an absorbance wavelength of 260nm. The extinction coefficients of the oligonucleotides were obtained from an online biopolymer calculator. UV-Vis melting and cooling experiments were performed on a Cary 1E spectrophotometer. Circular Dichroism (CD) spectra were obtained on a Jasco 720 spectropolarimeter. Fluorescence experiments were performed on a SPEX Fluorolog-2 spectrofluorometer.

Table 7: DNA Sequences Used

Name	**Sequence**
A27	5’- Aq AAA TGC CGG TAC AAA CAT GGC CGT ACG -3’
A27 Complement	3’ - TTT ACG GCC ATG TTT GTA CCG GCA TGC-5’

UV Melting and Cooling Experiments: All the samples contained 2.5 μM of the DNA duplex in 5 mM Tris HCL. The M-DNA sample containing zinc chloride (150 μM) were incubated for about an hour after their pH was elevated to between 8.95 and 9.0. The samples lacking zinc were either maintained at the body pH of 7.4 or elevated to a pH between 8.95 and 9.0. The melting temperature curves were scanned through 4 ramps between 15-90 ^{o}C and 90-15 ^{o}C, with a 30 minute hold time at 15^{o}C.

Circular Dichroism (CD): All the samples were prepared in 5mM Tris HCL with 5 μM duplex DNA. One of the duplex DNA control samples was adjusted to a pH of 9, while the other control was maintained at a pH of 7. The experimental sample contained an additional 240 μM zinc chloride, and was adjusted to a pH of 9. The CD scans were recorded at 200 nm/min.

Photo-cleavage Analysis by PAGE: The complementary strand to the AQ containing strand was 5' labeled with $^{\gamma - 32}$ P- ATP. The labeling samples were suspended in 10μL of loading dye, and then loaded onto a purification gel which was run for 1.5 hours at 400 watts. Purified DNA was removed from the gel by placing it in 750μL elution buffer (1mM EDTA, 0.5M sodium acetate, 10mM magnesium acetate, 0.1% SDS), and incubating the solution at 37^{o}C overnight. The DNA was precipitated by the addition of 750μL of 100% ethanol and 1μL

glycogen to the vials, and stored at -80^{o}C for 4 hours. The vials were then centrifuged at 13000 RCF for 30 minutes. After decanting the eluent, 100μL of 80% ethanol was added to the vials and centrifuged for 5 minutes. The 80% ethanol wash was repeated, and the samples were dried. The samples were prepared as mentioned earlier for the CD experiments, except 5 mM Tris HCL buffer is replaced with 5 mM sodium phosphate buffer. The samples were hybridized by heating the samples for 5 minutes at 90 ^{o}C, then allowing them to cool down to room temperature. The samples were then irradiated using a Rayonet photoreactor with eight 360nm lamps. They were then precipitated and treated with 1M piperidine for 30 minutes at 90^{o}C. After evaporating the piperidine, the samples were suspended in loading buffer. Samples with 4000 CPM were analyzed on a 20% polyacrylamide gel. The gels cleavage was revealed by an autoradiograph and quantified by a Fuji phosphorimager.

Fluorescence Experiments: One of the three control samples just contained 5 μM DNA, 5 mM Tris HCL and 15 μM ethidium bromide, while the other contained an additional 2 mM EDTA. These samples were maintained at a pH of 7. The third control sample contained 5 μM DNA, 5 mM Tris HCL, 15 μM ethidium bromide, 2 mM EDTA and 240 μM zinc chloride. The pH for this control sample was adjusted to 9. The experimental sample contained 5 μM DNA, 5 mM Tris HCL, 15 μM ethidium bromide, and 240 μM zinc chloride. Its pH was adjusted to a pH of 9. The fluorescence spectra were recorded at 25^{o}C with 1.0 mm slits on both the emission and excitation monochromators.

CHAPTER 16: RESULTS

16.1 **Fluorescence studies**

Ethidium bromide intercalation into DNA has been widely studied [31-34]. It has been observed that the fluorescence intensity of ethidium bromide alone is much less intense than the fluorescence intensity of ethidium bromide bound to DNA. This feature of ethidium bromide has been used as an assay for the binding of different intercalators to DNA. Lee and colleagues reported that upon addition of Zn^{2+} to DNA and ethidium bromide (pH =8.5), the fluorescence intensity of ethidium bromide decreases 20 fold. They suggest that the reduction in fluorescence intensity under these experimental conditions is due to the expulsion of ethidium bromide from the DNA upon the formation of M-DNA. As expected, the fluorescence intensity of ethidium bromide intercalated in 5 μM DNA was enhanced (see Figure 35). The fluorescence intensity was substantially reduced (reduced by > 50 %) upon the addition of ethidium bromide to DNA in the presence of Zn^{2+} (see Figure 35). The addition of the chelating agent, EDTA (which chelates the zinc metal ions), resulted in the fluorescence intensity returning to the initial intensity recorded for ethidium bromide in DNA (see Figure 35).

16.2 **CD Analyses**

CD analyses have been used as structural probes for nucleic acids. They show any changes in the DNA structure that affect the global configuration of the DNA. The CD for B-DNA (pH=7) showed a characteristic positive peak at 280

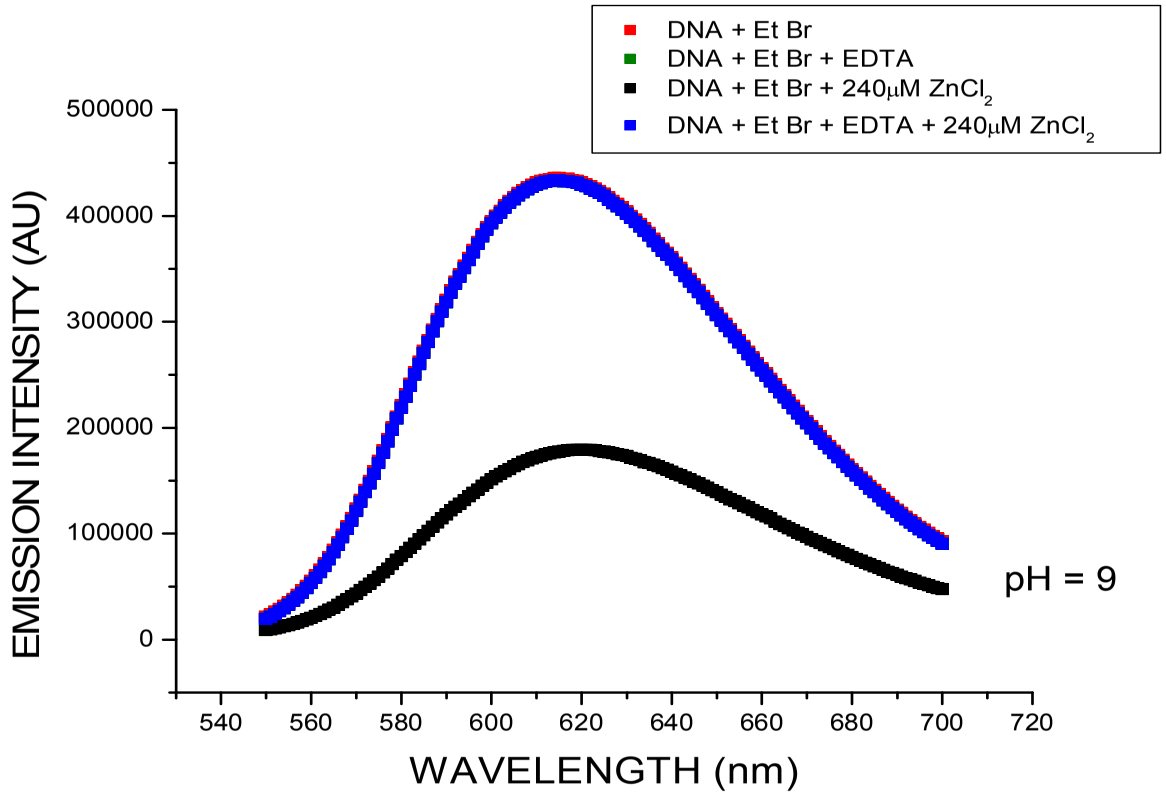

Figure 35: Ethidium Bromide Assay for M-DNA formation
All samples were prepared with 5 mM DNA and 5 mM Tris HCL buffer

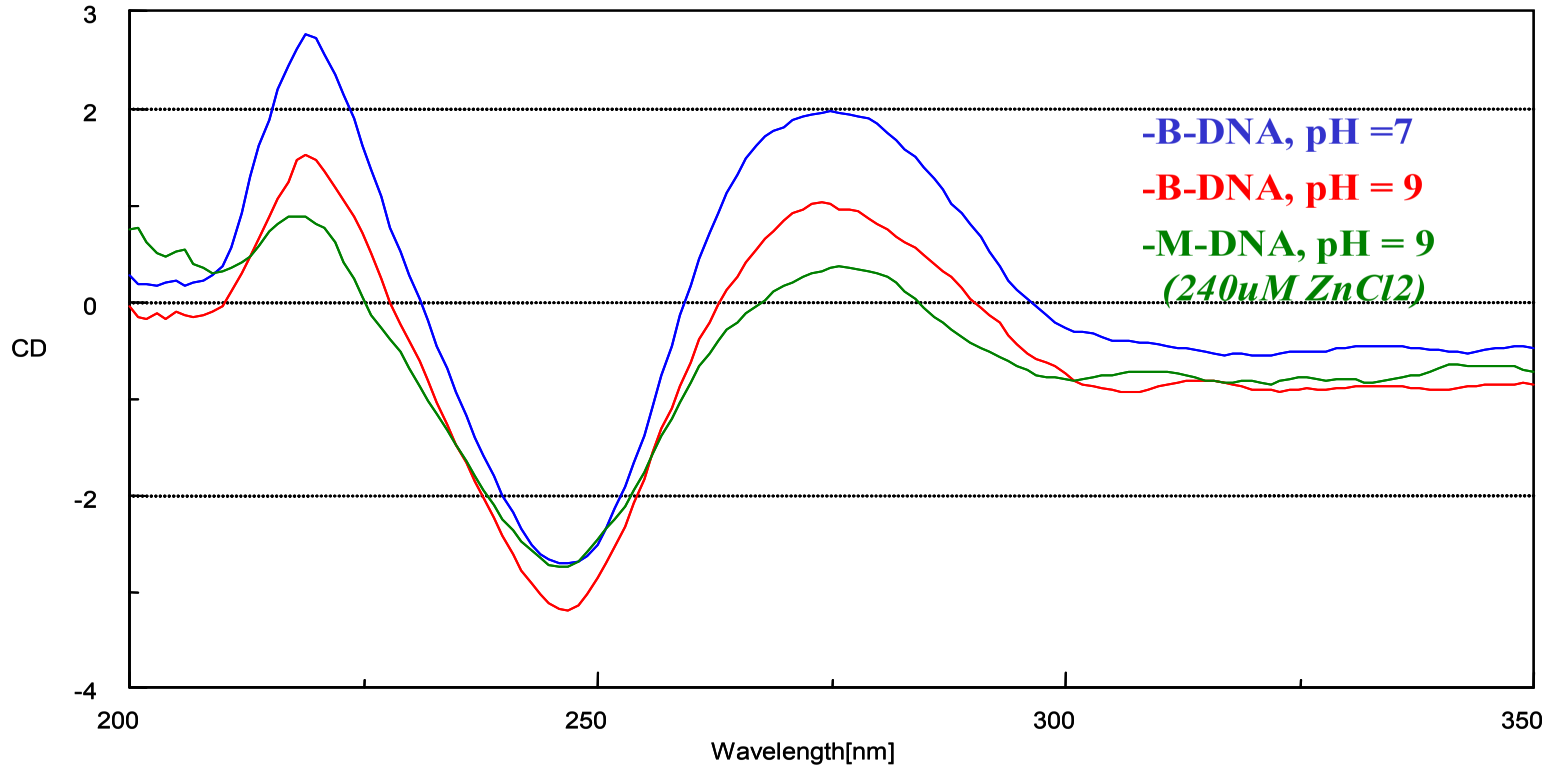

Figure 36: CD Spectra for M-DNA
Samples were prepared with 2.5 µM DNA and 5mM Tris HCL

nm, and a negative peak at 250 nm (see Figure 36). The elevation of the pH to 9 led to a decrease in the ellipticity of the CD while the peak shape and positioning remained the same (see Figure 36). The concurrent addition of zinc chloride salt and the elevation of the pH to 9 resulted in the further decrease in the ellipticity of the CD and a slight change in the peak shape (see Figure 36). The CD spectra suggest there is a slight change in the overall DNA structure upon the elevation of pH and the addition of zinc chloride salt to DNA.

16.3 **Melting temperature Studies**

Melting temperature studies were performed in order to determine the effects of both the elevated pH and the addition of zinc chloride salt on the overall stability of DNA. The melting transition for B-DNA (pH = 7.4) was observed at 55 ^{o}C (Figure 37). Upon elevating the pH from 7.4 to 9, the melting temperature decreased by 4 ^{o}C to 51 ^{o}C (see Figure 38). The addition of 150 μM zinc chloride to duplex DNA, pH = 9, resulted in a slight increase (2 ^{o}C) in the melting temperature to 53 ^{o}C (Figure 39). Overall, elevation of the pH and the addition of zinc ions did not affect the thermal stability of DNA much (change within 4 ^{o}C range).

16.4 **Long Distance Charge Transport in M-DNA**

The PAGE analysis was performed to determine whether M-DNA exhibits the behavior of a molecular wire or not. In charge transfer experiments using AQ as the sensitizer, two or more GG steps are incorporated into the sequence in order to quantify this long distance charge transport (see Figure 40). Frequently experiments performed with AQ show 5' G selective damage at GG

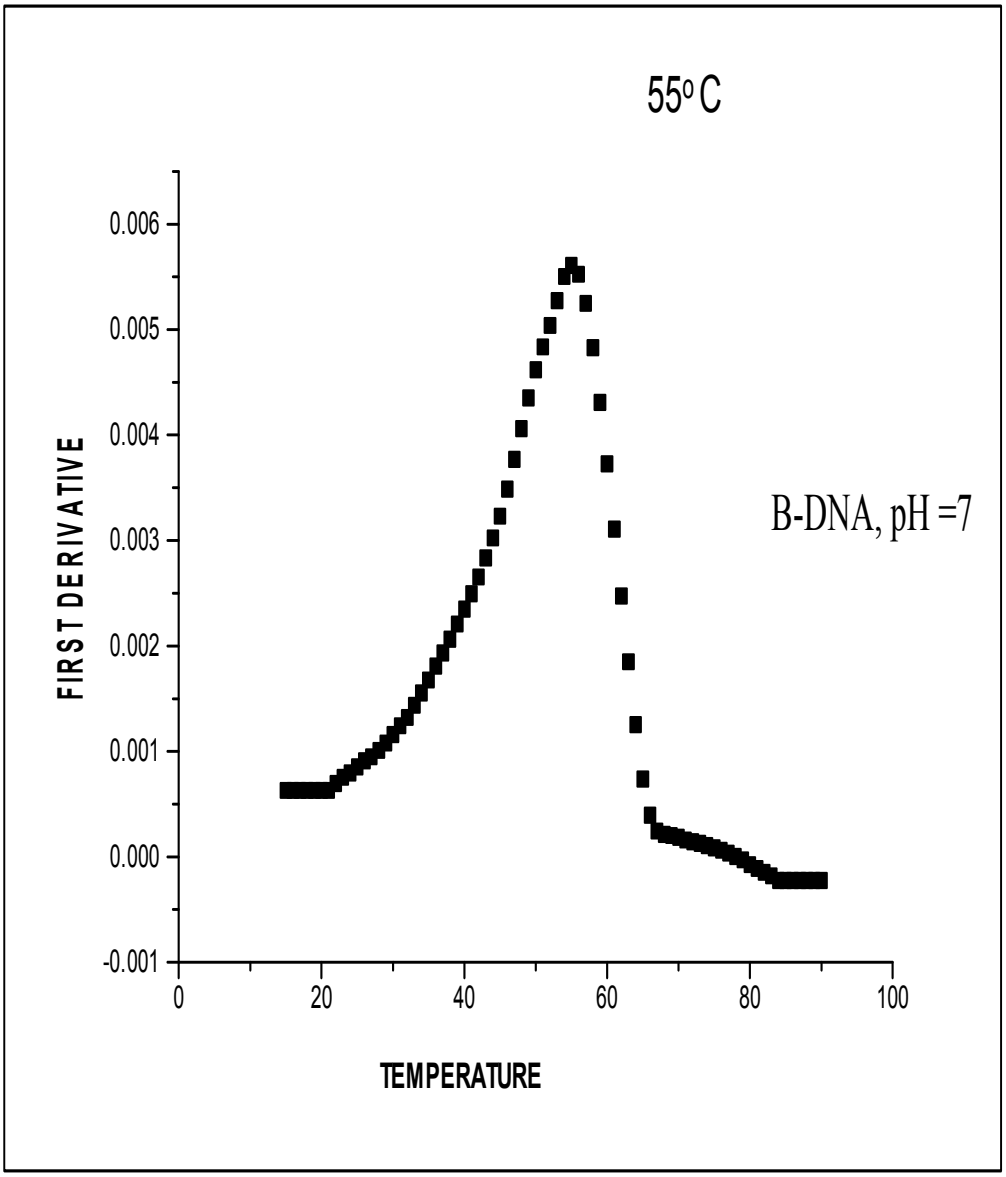

Figure 37: Tm for B-DNA (pH = 7)

Sample prepared with 2.5 μM of the DNA duplex in 5mM Tris HCL buffer solution

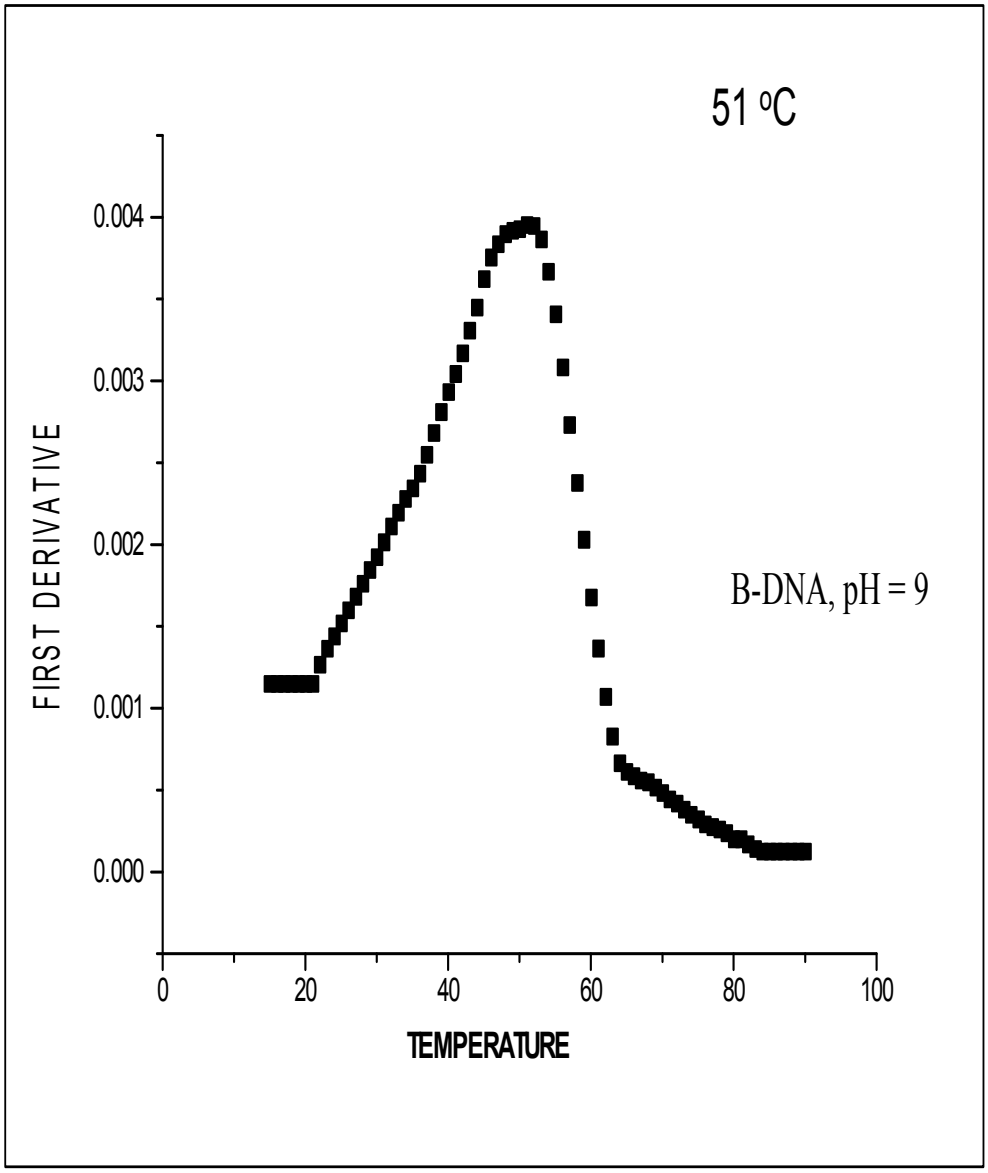

Figure 38: Tm for B-DNA (pH =9)

Sample prepared with 2.5 μM DNA and 5mM Tris HCL buffer solution

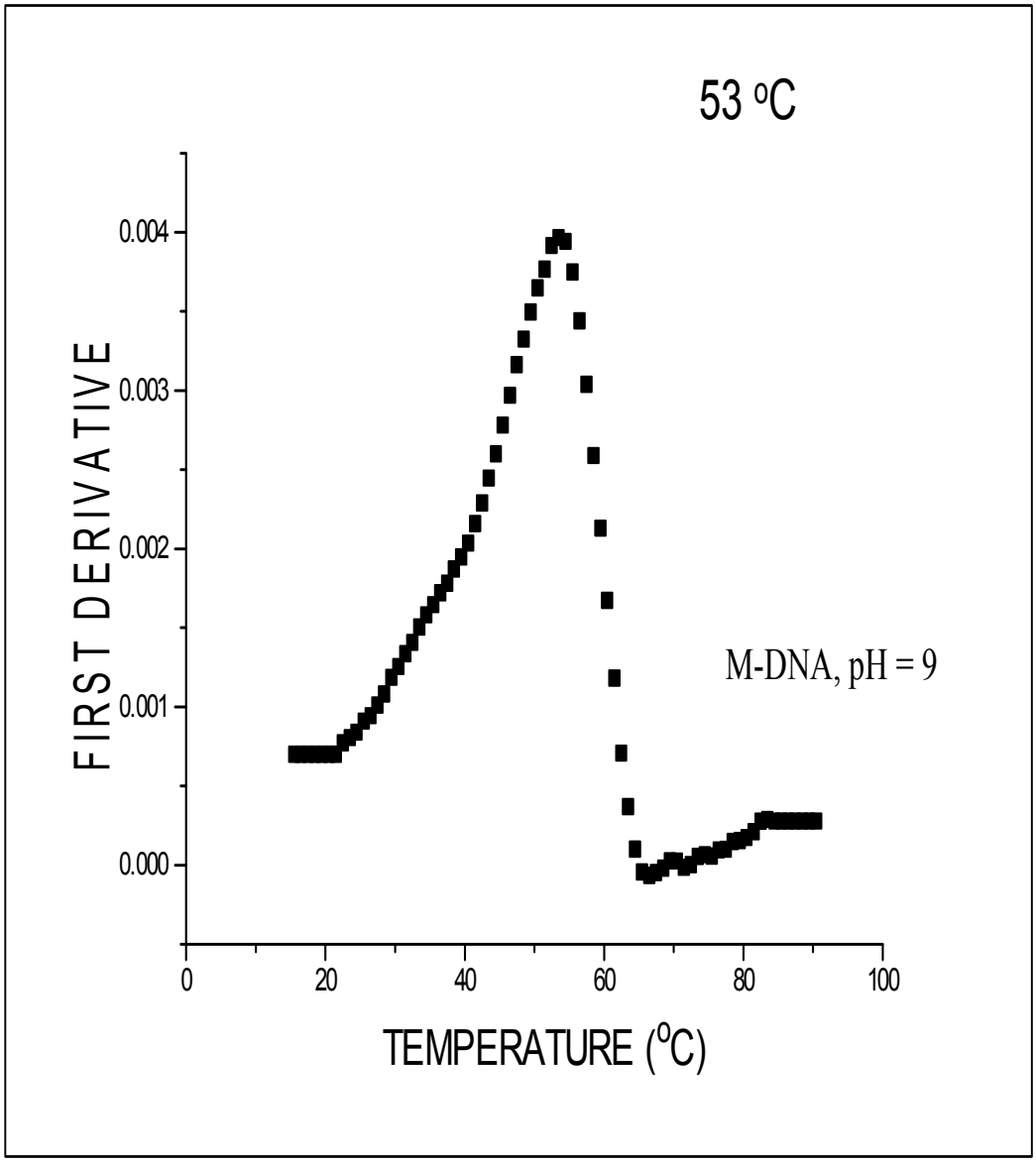

Figure 39: Tm for M-DNA (pH = 9)

Sample prepared with 2.5 μM DNA, 5mM Tris HCL buffer and 150 μM zinc chloride

steps [35]. All the samples in this experiment exhibited 5' G selectivity (see Figure 41). In fact, the damage occurred almost exclusively at the 5'G of the proximal GG step. The B-DNA control (pH = 7) showed both proximal and distal damage. As expected, the damage observed in this control was distance dependent (see Figure 41, Lanes 2 and 3). The damage observed for the DNA control (pH = 9) was also distant dependent as it did not exhibit any distal damage (see Figure 41, Lanes 5 and 6). This control sample enabled us to probe the effect of the addition of zinc chloride salt (M-DNA formation) independently from the effect of pH elevation. Upon addition of zinc chloride, there was no change. The damage observed for the M-DNA sample (240 μM $ZnCl_2$, pH =9) was distant dependent and did not exhibit any distal damage (see Figure 41, Lanes 8 and 9). In fact, the results observed for B-DNA (pH =9) and M-DNA samples were similar. Compared to normal DNA, the elevation of pH and the elevation of the pH plus the addition of the ions both appear to have similar observable effects on charge transport in DNA. This suggests that the addition of zinc ions does not enhance the ability to transport charge along the DNA. Therefore, M-DNA does not exhibit the behavior expected from a molecular wire.

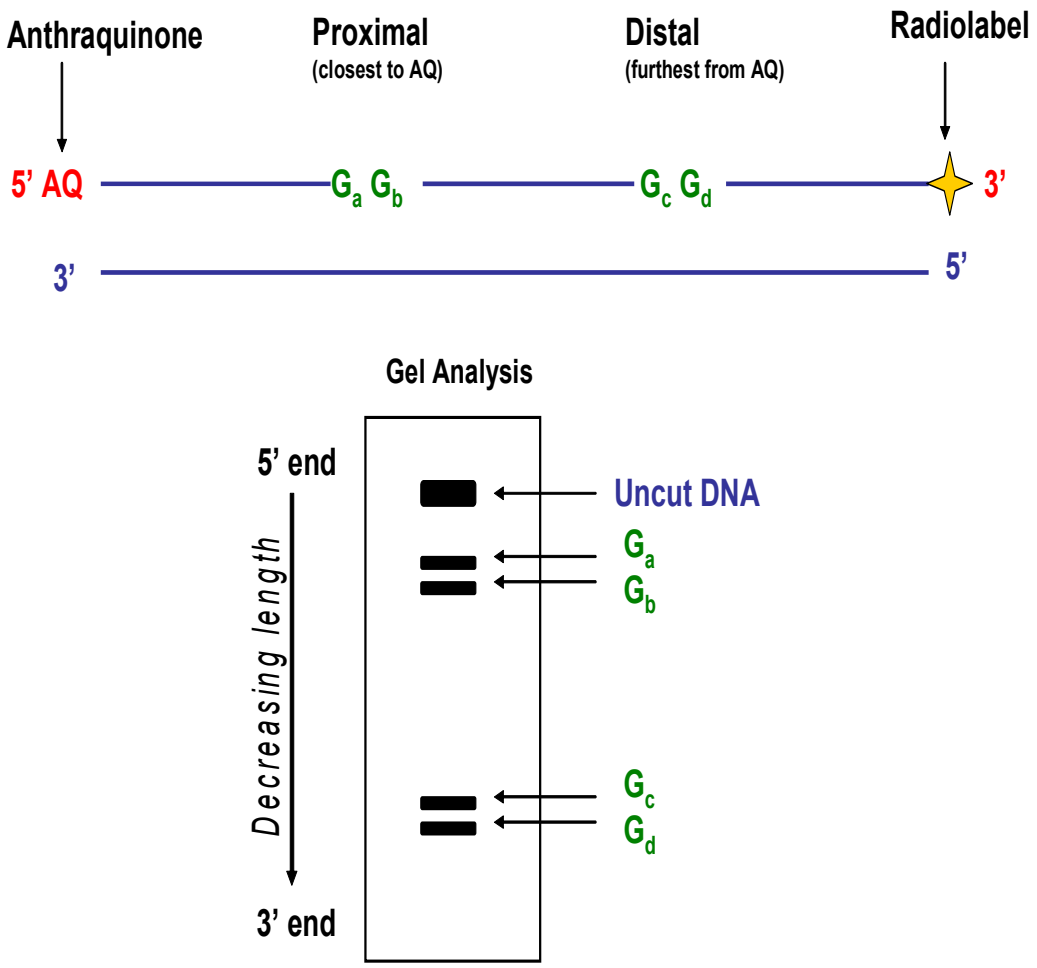

Figure 40: Illustration of PAGE Analysis

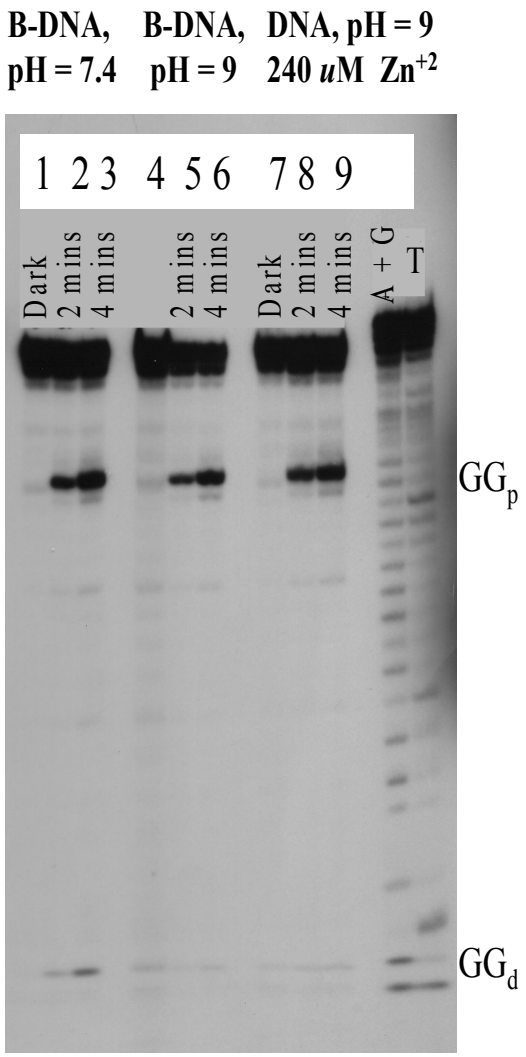

Figure 41: PAGE Comparison for B-DNA and M-DNA

All samples contain 5 μM DNA and 5 mM Sodium Phosphate buffer solution

CHAPTER 17: CONCLUSION

In efforts to determine the effects of charge transport on M-DNA, we first sought to show that we were able to form M-DNA as illustrated by Lee and colleagues. The primary feature used to characterize M-DNA was its ability to quench ethidium bromide fluorescence in the presence of DNA. In general, ethidium bromide fluorescence is enhanced in the presence of DNA [34]. However, Lee and colleagues reported that its fluorescence was significantly reduced upon M-DNA formation [19, 20]. This could possibly be explained by an increase in the exposure of ethidium bromide to water (a known ethidium bromide fluorescence quencher). It also suggests that ethidium bromide does not bind to M-DNA well. We observed similar fluorescence results as reported by Lee and colleagues. Likewise, the addition of ethidium bromide to a DNA solution resulted in the substantial enhancement of the ethidium bromide's fluorescence (see Figure 35). The addition of ethidium bromide to a M-DNA solution resulted in the quenching of its fluorescence. Despite using a different DNA sequence from their original experiments, we observed relatively similar CD spectra for DNA in the presence of Zn^{2+} ions at a pH above 8. This led us to believe we were analyzing a similar phenomenon as reported by Lee and colleagues.

The DNA structures were further characterized by melting temperature studies in order to determine their relative stability. Unlike in earlier experiments which showed that M-DNA stabilized duplex DNA (pH = 7) by up to 12 ^{o}C [19], these studies showed that B-DNA (pH = 7) and M-DNA had the same degree of

stability. In contrast, elevating the pH of B-DNA (pH = 7) to a pH of 9 was slightly destabilizing. Therefore, pH elevation alone was unfavorable, but pH elevation in the presence of zinc cations had little or no effect on the melting stability of M-DNA. This suggests that the presence of zinc cations at elevated pH did not affect the overall stability of the DNA.

A molecular wire is a conducting material that has little resistance to the transport of electrons across it [11]. Some molecular wires carry electrons through π electron orbitals within their structures [9, 10]. This involves the transfer of electrons between adjacent π orbitals along a particular direction within the material. In a similar way, DNA molecules have been speculated to exhibit a π belt which enables it to transport electrons along its length [4]. These π stacks are found stacked between aromatic groups on adjacent base pairs. In particular, based upon some experimental observations M-DNA was proposed to behave like a molecular wire [20]. This ability to efficiently transfer electrons across DNA is expected to affect long distance charge transport along DNA. A molecular wire would be expected to show very little or no distance dependence. This means there should be about equal amounts of damage at GG steps along the length of DNA. However, our charge transport studies show distance dependence for B-DNA (pH =7), B-DNA (pH = 9) as well as M-DNA (see Figure 41). That is, all these samples showed much more proximal GG damage than distal GG damage. In fact, the M-DNA and B-DNA (pH = 9) samples exhibited similar amounts of overall proximal GG damage, while the B-DNA (pH =7) samples exhibited less overall proximal damage than the other two samples. Also, the M-DNA and B-

DNA (pH = 9) samples both exhibited comparatively less overall distal GG damage than B-DNA (pH = 7). In other words, the M-DNA and B-DNA (pH = 9) samples showed enhanced distance dependence (relatively more proximal than distal damage) compared to the B-DNA (pH = 7) sample. If M-DNA behaved as a molecular wire we would expect to see virtually no distance dependence or at least some enhancement of the amount of distal damage observed for our control samples. Since we observe no enhancement in the amount of distal damage for M-DNA as opposed to the other control samples, then M-DNA does not behave as a molecular wire.

References

1. Eley, D. D.; Spivey, D. I., *Trans. Farad. Soc.* **1962**, *58*, 411-415.

2. Murphy, C. J.; Arkin, M. R.; Jenkins, Y.; Ghatlia, N. D.; Bossman, S. H.; Turro, N. J.; Barton, J. K., *Science* **1993**, *262*, 1025-1029.

3. Fink, H., Schonenberger, C., *Nature* **1999**, 398, 407-410

4. Okahata, Y., Kobayashi, T., Tanaka, K., Shimomura, M., *J. Am. Chem. Soc.* **1998**, 120, 6165-6166.

5. Porath, D., Bezryadin, A., de Vries, S., Dekker, C., *Nature* **2000**, 403, 635-637.

6. Cai, L., Tabata, H., Kawai, T., *App. Phys. Lett.* **2000**, 77, 3105-3106.

7. Storm, A. J., van Noort, J., de Vries, S., Dekker, C., *App. Phys. Lett.* **2001**, 79, 3881-3883.

8. Di Ventra, M., Zwolak, M., *Encyclopedia of Nanoscience and Nanotechnology: DNA Electronics,* American Scientific Publishers, 2004, 2, 475-493

9. Jerome, D., Schulz, H. J., *Adv. Phys*. **2002**, 51, 293-479

10. Jerome, D., *Chem. Rev.* **2004**, 104, 5565-5591.

11. Ratner, M. A., Dekker, C., *Phys. World* **2001**, 14, 29-

12. Branden, C., Tooze, J. *Introduction to Protein Structure,* 2nd Ed., Garland Publishing, 1999

13. Voet, D., Voet, J.G., *Biochemistry*, 2nd Ed., John Wiley & Sons, Inc., 1995

14. Sinden, R. R. *DNA Structure and Function*, Academic Press, 1994

15. Campbell, M. K., *Biochemistry*, 2nd Ed., Saunders College Publishers, 1995

16. Sarma, M. H.; Sarma, R. H. *DNA Double Helix and The Chemistry of Cancer*, Academic Press, 1988

17. Altona, C., *J. Mol. Struct.* **1986,** 141, 109-125.

18. Moulaei, T., Interaction of B - DNA with monovalent cations: Theory and practice in X-ray crystallography, Georgia Institute of Technology, On-line Dissertation, 2004.

19. Lee, J. S.; Latimer, L. P. J.; Reid, R. S. *Biochem. Cell. Biol.* **1993**, *71*, 162-168.

20. Aich, P.; Labiuk, S. L.; Tari, L. W.; Delbaere, L. J. T.; Roesler, W. J.; Falk, K. J.; Steer, R. P. *J. Mol. Biol.* **1999**, *294*, 477-485.

21. Schuster, G. B., *Acc. Chem. Res*. **2000**, 33, 253-260

22. Nunez, M. E., Hall, D. B., Barton, J. K., *Chem. Biol*. **1999**, 6, 85-97

23. Giese, B., *Acc. Chem. Res*. **2000**, 33, 631-636

24. Lewis, F.D., Letsinger, R. L., Wasielewski, M. R., *Acc. Chem. Res*. **2001**, 34, 159-170

25. Liu, C-S; Hernandez, R.; Schuster, G. B. *J. Am. Chem. Soc.* **2004,** 126, 2877-2884

26. O'Neill, M. A., Barton, J. K., *J. Am. Chem. Soc*. **2004**, *126,* 11471-11483

27. Jortner, J. Bixon, M. Langenbacher, T., Micheal-Beyerle, M. E., *Proc. Natl. Acad. Sci. USA* **1998**, 95, 12759-12765.

28. Bixon M., Giese, B., Wessely S., Langenbacher T., Micheal-Beyerle M. E., Jortner J., *Proc. Natl. Acad. Sci. USA* **1999**, 96, 11713-11716

29. Bixon, M., Jortner, J., *J. Phys. Chem. B.* **2000**, 104, 3906-3913.

30. Giese B., *Top. Curr. Chem.* **2003**, 236, 27-44.

31. Neidle, S.; Abraham, Z. *CRC Crit. Rev. Biochem.* **1984**, *17*, 73-121.

32. Morgan, A. R.; Lee, J. S.; Pulleyblank, D. E.; Murray, N. L.; Evans, D. H. *Nucleic Acids Res.* **1979**, *7*, 7547-7569.

33. Morgan, A. R.; Evans, D. H.; Lee, J. S.; Pulleyblank, D. E. *Nucleic Acids Res.* **1979**, *7*, 571-594.

34. Olmsted III, J.; Kearns, D. R. *Biochemistry* **1977**, *16*, 3647-3654.

35. Armitage, B., *Chem. Rev.* **1998,** *98,* 1171-1200